University of Kentucky
UKnowledge

Theses and Dissertations--Mechanical Engineering

Mechanical Engineering

2023

ANISOTROPIC MATERIAL BEHAVIOR OF 3D PRINTED FIBER COMPOSITES

Jordan Garcia
University of Kentucky, jga246@g.uky.edu
Digital Object Identifier: https://doi.org/10.13023/etd.2023.277

Right click to open a feedback form in a new tab to let us know how this document benefits you.

Recommended Citation

Garcia, Jordan, "ANISOTROPIC MATERIAL BEHAVIOR OF 3D PRINTED FIBER COMPOSITES" (2023). *Theses and Dissertations--Mechanical Engineering*. 213.
https://uknowledge.uky.edu/me_etds/213

This Doctoral Dissertation is brought to you for free and open access by the Mechanical Engineering at UKnowledge. It has been accepted for inclusion in Theses and Dissertations--Mechanical Engineering by an authorized administrator of UKnowledge. For more information, please contact UKnowledge@lsv.uky.edu.

STUDENT AGREEMENT:

I represent that my thesis or dissertation and abstract are my original work. Proper attribution has been given to all outside sources. I understand that I am solely responsible for obtaining any needed copyright permissions. I have obtained needed written permission statement(s) from the owner(s) of each third-party copyrighted matter to be included in my work, allowing electronic distribution (if such use is not permitted by the fair use doctrine) which will be submitted to UKnowledge as Additional File.

I hereby grant to The University of Kentucky and its agents the irrevocable, non-exclusive, and royalty-free license to archive and make accessible my work in whole or in part in all forms of media, now or hereafter known. I agree that the document mentioned above may be made available immediately for worldwide access unless an embargo applies.

I retain all other ownership rights to the copyright of my work. I also retain the right to use in future works (such as articles or books) all or part of my work. I understand that I am free to register the copyright to my work.

REVIEW, APPROVAL AND ACCEPTANCE

The document mentioned above has been reviewed and accepted by the student's advisor, on behalf of the advisory committee, and by the Director of Graduate Studies (DGS), on behalf of the program; we verify that this is the final, approved version of the student's thesis including all changes required by the advisory committee. The undersigned agree to abide by the statements above.

Jordan Garcia, Student

Dr. Y.Charles Lu, Major Professor

Dr. Jonathan Wenk, Director of Graduate Studies

ANISOTROPIC MATERIAL BEHAVIOR OF 3D PRINTED FIBER COMPOSITES

DISSERTATION

A dissertation submitted in partial
fulfillment of the requirements for
the degree of Doctor of Philosophy
in the College of Engineering at the
University of Kentucky

By
Jordan Garcia
Lexington, Kentucky

Director: Dr. Y.Charles Lu, Professor of Mechanical Engineering
Lexington, Kentucky
2023

Copyright© Jordan Garcia 2023

ABSTRACT OF DISSERTATION

Literature has shown that 3D printed composites may have highly anisotropic mechanical properties due to variation in microstructure as a result of filament deposition process. Laminate composite theory, which is already used for composite products, has been proposed as an effective method for quantifying these mechanical characteristics. Starting with the analysis of comparing the printing orientation of premanufactured carbon fiber reinforced filament, the mechanical properties of 3D printed objects were examined. The mechanical properties changed not only as a result of machine choice, but how the sample is oriented along the printing bed. The analysis continued with looking at the dynamic properties of 3D printed composites. Results showed that the direction of the extruded strands altered the modal frequencies even for a sample with the same geometry. With the direction of the extruded strands affecting the mechanical properties, the composition of these strands is also shown to affect the mechanical properties of 3D printed composites. For commercially available fiber reinforced filaments, it was found through microscopic analysis that the fiber content stated by the manufacturer is inaccurate. In order to apply Classical Laminate Composite Theory (CLCT) the fiber volume fraction and aspect ratio need to be known. This lead to the creation of custom filament with the desired fiber content and geometry. The Halpin-Tsai model was used to predict the mechanical behavior of short fiber reinforced composites. Finally, the mechanical properties of continuous fiber composites were examined. The continuous fiber samples showed that fiber orientation had an vast effect on mechanical properties. A well oriented composite notably outperformed other fiber orientations with a drastic drop in Young's modulus even with slight misalignment in fiber direction, but also resulted in brittle responses which may not be preferable. CLCT is applied using the simulation software ANSYS WORKBENCH. The results showed considerable correlation for each orientation and can be an accurate predictor of mechanical characteristics for 3D printed continuous fiber composites.

KEYWORDS: 3D printing, Composites, Carbon-fiber, Additive-manufacturing

Jordan Garcia

June 21, 2023

ANISOTROPIC MATERIAL BEHAVIOR OF 3D PRINTED FIBER COMPOSITES

By
Jordan Garcia

Dr. Y.Charles Lu
Director of Dissertation

Dr. Jesse Hoagg
Director of Graduate Studies

June 21, 2023
Date

I would like to dedicate this dissertation to the good God who blessed me with this opportunity, my family whom encouraged and supported me throughout the years, and my good friends who walked alongside me on this long journey. May we all meet in the next life and enjoy each others company reflecting on the path that brought us together.

ACKNOWLEDGMENTS

I would like to take this opportunity to thank my advisor Dr. Charles Lu who not only inspired me to pursue a graduate education but strive for the most of what I could become. Without his guidance and mentorship this paper would not have been possible. I would also like to give a special thanks to my committee members Dr. Haluk Karaca, Dr. Madhav Baral, Dr. Jeffrey Seay, and Dr. Alberto Corso. You have taken the time to help me along in this milestone of my life, your contribution is greatly appreciated and I could not have done this without your assistance. I would also like to thank all whom I worked alongside and motivated me to continue on the journey and complete my works. The list is long and there are not enough hours in the day to state each individual name and express how thankful I am. To each and every one of you, form the bottom of my heart, thank you.

TABLE OF CONTENTS

Acknowledgments iii

List of Tables vi

List of Figures vii

Chapter 1 INTRODUCTION 1
1.1 Background information 1
1.1.1 Additive manufacturing 1
1.1.2 Additive manufacturing of composite materials 5
1.2 Current limitations and setbacks 8
1.3 Motivation 10

Chapter 2 LITERATURE REVIEW 11
2.1 State of composite printing 12
2.1.1 Discontinuous fiber FDM 15
2.1.2 Continuous fiber FDM 18
2.1.3 Mechanical testing and models 21

Chapter 3 ANISOTROPIC BEHAVIOR OF 3D PRINTED SHORT FIBER COMPOSITES – STATIC MECHANICAL PROPERTIES 25
3.1 Introduction 25
3.2 Materials and methods 26
3.2.1 3D Printing of CF-ABS composites 27
3.2.2 Compression molding of CF-ABS composites 28
3.2.3 Mechanical testing 29
3.3 Results and discussion 29
3.3.1 Stress-strain curves of CF-ABS composites from different printers 33
3.3.2 Stress-strain curves of CF-ABS composites from compression molding 35
3.4 Perimeter/contour effect 37
3.4.1 Sample testing effects 39
3.4.2 Recorded differences in sample types 44
3.5 Theoretical analysis of mechanical properties of 3D printed fiber composites 48
3.6 Conclusion 51

Chapter 4 ANISOTROPIC BEHAVIOR OF 3D PRINTED SHORT FIBER COMPOSITES – DYNAMIC MECHANICAL PROPERTIES . . 52
4.1 Materials and procedures 54
4.1.1 Materials and samples 54

4.1.2 Experimental procedures 54
4.2 Computational procedures 58
4.3 Results and Discussion 61
4.3.1 Validation of experimental method 61
4.3.2 Experimental modal responses of composite plates 63
4.3.3 Computational modal responses of composite plates validation of FEM method 65
4.3.4 Computational model responses of composite plates 67
4.4 Comparison of experimental data and simulated results 70
4.5 Conclusion 73

Chapter 5 EFFECT OF FIBER CONTENT AND FIBER ASPECT RATIO ON ANISOTROPIC BEHAVIOR OF 3D PRINTED SHORT FIBER COMPOSITES 74
5.1 Introduction 74
5.2 Mass Produced Fiber Filaments 74
5.2.1 Microscopic analysis 75
5.3 Image processing 80
5.4 Materials and methods 82
5.4.1 Slicing settings 87
5.4.2 Sample dimensions and testing 90
5.5 Experimental results 91
5.6 Theoretical analysis (Haplin-Tsai) 108
5.7 Conclusion 113

Chapter 6 ANISOTROPIC BEHAVIOR OF 3D PRINTED CONTINUOUS FIBER COMPOSITES 115
6.1 Materials and methods 115
6.1.1 Slice settings 116
6.1.2 Sample fabrication and testing 120
6.2 Experimental results 121
6.3 Theoretical Analysis Tsai-Wu 130
6.4 ANSYS simulations 139
6.5 Conclusion 145

Chapter 7 SUMMARY AND FUTURE WORKS 146

Appendices 149

Bibliography 155

Curriculum Vitae 166

LIST OF TABLES

4.1 Summary of fundamental material properties of ABS resin and carbon-fiber ABS composite in MPa. 60

LIST OF FIGURES

1.1 Schematic of how the bulk filament material is extruded in several layers to construct the desired part. 2
1.2 The effect of the layer height and quality of a print to capture the geometry desired known as the stair stepping effect. 3
1.3 Cartesian and delta configurations. 3
1.4 G Code numerical instructions example. 4
1.5 Illustration depicting the selective composite formation manufacturing method using the resin impregnated metallic substrate 6
1.6 Modified 3D printer extruder assembly to incorporate a continuous reinforcing fiber strand from a bulk roll. 7
1.7 Comparison of filament microstructures for a pure polymer filament (transverse (a) & longitudinal (b)) and for a fiber reinforced filament (transverse (c) & longitudinal (d)). 9

2.1 Schematic depicting the co-extrsuion process with the fiber being extruded along with the polymer matrix 12
2.2 Example of 3D printing using the stereo-lithography method. 13
2.3 Example of 3D printing using the direct energy deposition method for a powder based material (With permission from Springer Nature https://www.springer.com/jour [1].) 14
2.4 Spool of short fiber reinforced polymer extruded through a heated print head (With permission from Springer Nature https://www.springer.com/journal/170/ [2].) 15
2.5 Scanning Electron Microscope (SEM) image of the micro-structure of the extruded fiber filaments. 17
2.6 Field Emission Scanning Electron Microscopy (FESEM) performed to observe the fiber-matrix interface showing with proper preparation the interface gaps can be reduced or even eliminated 18
2.7 Cross section of a completely encased continuous fiber with small gaps at the inter strand adhesion points illustration (Left) and viewed from a sample (Right) [3]. 19
2.8 Schematic of a dual head extruder with separate nozzles and feeders for each material type [4]. 20
2.9 Demonstration of how the fiber volume fraction can greatly affect the tensile strength of the 3D printed object for a nylon-carbon continuous fiber composite [4]. 22

3.1 Sketch of a typical 3D printing process of a fiber reinforced polymer composite. The fiber filled polymer filament is extruded through a nozzle and then laid down as successive layers to form a composite. 26
3.2 Parts are printed at four different positions on the printing platform. . . 28

3.3 Stress-strain curves of ABS and CF-ABS samples from the Prusa 3D printer. 30
3.4 Stress-strain curves of CF-ABS samples of varying positions from the Prusa 3D printer. 31
3.5 Stress-strain curves of CF-ABS samples from the Flashforge 3D printer based on the position on the print bed (Figure 3.2). 31
3.6 Comparisons of stress-strain curves of CF-ABS samples from different 3D printers. Samples were printed at the I position. 32
3.7 Comparisons of stress-strain curves of CF-ABS samples from different 3D printers. Samples were printed at the position IV. 33
3.8 Stress-strain behaviors of oriented CF-ABS samples from bending test. Samples are printed from the Flashforge 3D printer. 34
3.9 Comparison of stress-strain responses of CF-ABS composites from oriented infill samples and the default "rectilinear" samples (position I and Position II). Samples are printed from the Flashforge 3D printer. 35
3.10 Stress-strain responses of compression molded CF-ABS composite samples. 36
3.11 Comparison in stress-strain responses between compression molded sample (slow-cooled) and 3D printed sample from each printer (position I). . . . 37
3.12 Perimeter of a 3D printed object with internal infill strands creating the bulk of the sample [5]. 38
3.13 The orientation of the perimeter may not always align with the infill fiber and thus affect the products mechanical properties. 39
3.14 Difference in perimeter cross sectional area percentage between a tensile (left) and bending (right) test specimen. 41
3.15 Recorded experimental data for carbon fiber reinforced tensile samples. . 43
3.16 Modulus of elasticity calculated for each tensile test sample recorded showing no trend and high variance in values. 43
3.17 Stress/strain results for polymer only samples of batch 1 tested using the tensile testing method. 45
3.18 Stress/strain results for polymer only samples of batch 2 tested using the tensile testing method. 45
3.19 Stress/strain results for polymer only samples of batch 3 tested using the tensile testing method. 46
3.20 Stress/strain results for polymer only samples of batch 1 tested using the bending testing method. 47
3.21 Stress/strain results for polymer only samples of batch 2 tested using the bending testing method. 47
3.22 Stress/strain results for polymer only samples of batch 3 tested using the bending testing method. 48
3.23 Variation of axial modulus of CF-ABS composite as a function of filament orientation angle. 50

4.1 Sketch of a typical 3D printing process of a fiber reinforced polymer composite. The fiber filled polymer is extruded through a nozzle and then laid down as successive layers to form a composite. 53

4.2 Linear infill patterns of 3D printed parts with respect to orientation angle. From left to right: 0°, 30°, 60°, 90°. 55
4.3 Dynamic testing of carbon-fiber composite plates: (Top) Schematic diagram of the experimental modal testing; (Middle) LABVIEW block diagram used for generating the time and frequency spectrums; (Bottom) Sample setup in the dynamic test. 57
4.4 Analysis systems used in ANSYS Workbench to produce the FE model for multi-layered composites. 58
4.5 The stress strain curves of carbon-fiber ABS composites with various infill angles. 60
4.6 Plots of the first (left) and second (right) mode shapes of a homogeneous aluminum plate. 62
4.7 Frequency spectrum showing amplitudes for different frequencies of a homogeneous aluminum plate. 62
4.8 The spectrum of the first mode frequencies of 3D printed carbon-fiber plate with various infill angles. The rectangular plates were fixed on the left-right sides. 63
4.9 Recorded natural frequencies for fixed left/right side (Left) and top/bottom side fixed (Right) oriented rectangular samples of carbon-fiber ABS: mode 1. 64
4.10 Recorded natural frequencies for fixed left/right side (Left) and top/bottom side (Right) oriented rectangular samples of pure ABS. 64
4.11 (Left) Coarse structured mesh pattern consisting of 300 elements. Refined structured mesh pattern consisting of 1200 elements (Right). 66
4.12 Dynamic modal results from FEM from the coarse mesh (Left) and refined mesh (Right) under the same fixed top/bottom loading conditions. . . . 67
4.13 Mode shapes of carbon-fiber reinforced ABS with respect to the orientation of the lamina plies for case with fixed left and right edges. 69
4.14 Mode shapes of carbon-fiber reinforced ABS with respect to the orientation of the lamina plies for case with fixed top and bottom edges. 70
4.15 Modal frequency of sample for the fixed left and right side case with respect to infill orientation angle. 72
4.16 Modal frequency of sample for the fixed top and bottom sides with respect to infill orientation angle. 72
4.17 Modal response of the square sample with respect to infill orientation for both cases when mirrored. 73

5.1 Keyence HVX microscope used for observing the reinforcing fibers inside the polymer matrix at the cut and sanded ends. 76
5.2 Cross section of the 90-degree sample showing the fibers length across the extruded filament (magnified ×250). 77
5.3 Further magnified image of the 90-degree samples cross section (magnified ×1000). 78
5.4 Magnified image of the 0-degree samples cross section showing only small reflective dots of carbon fiber (magnified ×500). 79

5.5 The further magnified cross section shows how the reflective carbon strands are dispersed can greatly vary in size (magnified ×1000). 80
5.6 ImageJ altered microscopic image with the bright colored fibers selected due to their reflection of the microscopes light. 81
5.7 Image processed microscope image used to calculate the average size of fibers in the reinforced filament. 82
5.8 ABS filament into bulk material form after being chopped into 1-2mm pellets. 83
5.9 Roll of continuous carbon fiber from Markforge used to create discontinuous fibers with set aspect ratios. 84
5.10 Set of 3D printed gears used to dhear the carbon fiber wire to a specified length to determine aspect ratio. 84
5.11 Filament extruder and Arduino controlled auto-roller for creation of 3D printer filament with specified aspect ratio. 85
5.12 PulseXE FDM printer used for sample production coupled with a roll of reinforced filament produced using the filament extruder machine. 87
5.13 Layer-by-layer infill orientation specification in Simplify 3D used to create the oriented fiber reinforced test samples. 89
5.14 Stress/strain response of control samples with no fiber reinforcement. . . 93
5.15 Young's modulus of each control sample without fiber reinforcement of the re-extruded pellet filament. 93
5.16 Mechanical response of 2.5% by volume reinforced samples in various orientations. 94
5.17 Young's modulus of the 2.5% samples based on orientation of reinforcing fibers. 95
5.18 Stress strain responses of the further reinforced 5% samples with the same 1mm length reinforcing fibers. 96
5.19 Young's modulus of the 5% samples showing the drastic difference between the 0 degree and 90 degree samples. 97
5.20 Stress/strain responses of the 7.5% fiber samples and the increase in its brittle mechanical response. 98
5.21 The 7.5% fiber reinforcement sample Young's modulus showing how drastic the change into a brittle response the samples exhibited.n 98
5.22 Stress/strain response of the samples containing the highest reinforcing fiber content volume ratio of 10%. 99
5.23 Young's modulus response of the 10% fiber content samples exhibiting the highest magnitude compared to the other sample sets. 100
5.24 Summary of the average Young's modulus for each fiber percentage and infill. 100
5.25 Normalized Young's modulus for each fiber content ratio compared to the 90 degree sample for each orientation. 101
5.26 Varied stress/strain responses of the 2.5% low volume fraction reinforcing fiber samples with the longer 1.5mm fibers. 102
5.27 Young's modulus response of the 2.5% samples exhibiting varied results in the transverse 90 degree orientation. 103

5.28 Stress/strain response of the 5% samples with two sample anomalies of the first 0 degree sample and the first 45 degree sample. 104
5.29 Young's modulus responses of the 5% samples further showing the 0 degree anomaly affecting the average value with a considerable drop. 105
5.30 The 7.5% sample stress/strain response show more distinct separations between fiber orientation and sample response. 106
5.31 The Young's modulus for the 7.5% samples showed a more balanced distribution of values and seemed to be free of the anomalies seen in the 2.5% and 5% samples. 106
5.32 Mechanical response of the 1.5mm samples which behave more chaotically with the misaligned fiber orientations compared to the 1mm samples. . . 107
5.33 Normalized modulus response of samples with 1.5mm reinforcing fibers. . 108
5.34 Theoretical longitudinal Young's modulus response for varying infill percentages and fiber length. 110
5.35 Theoretical transverse modulus for varying fiber content despite varying fiber lengths. 111
5.36 Comparison of the 1mm fiber length samples vs the Halpin-Tsai theoretical values. 112
5.37 Comparison between the theoretical and measured values of the 1.5mm samples and the Halpin-Tsai calculations. 112
5.38 The transverse responses of the samples showed no correlation to fiber content as expected with the Halpin-Tsai calculations and was dominated by artifacts of 3D printing instead of fiber content/length. 113

6.1 Eiger.io slicer with materials specified on the right side of the user interface. The materials specified are the OnyxTM as the polymer matrix and carbon as the reinforcing fiber. 117
6.2 The polymer infill is specified (Left). The Fiber content is then specified using the reinforcement tab (Right). 118
6.3 Internal view component of Eiger.io slicing software were the fiber orientations are specified by the user. This image depicts a cross section of the 0 degree angle fibers shown in blue with the polymer reinforcement shown in white. 119
6.4 Mechanical responses of the Onyx only control samples with no continuous fiber reinforcement from the MarkForge printer. 122
6.5 The calculated Young's modulus of the control samples based on sample data set using Equation 6.2 & 6.3. 123
6.6 The max stress of the samples using the same data set numbering as the Young's modulus data. 123
6.7 First set of data for the continuously reinforced samples and their calculated responses. 124
6.8 Stress/Strain response from the second set of samples tested from the Markforge printer. 125
6.9 Third and final set of data from the continuously reinforced samples tested. 125

6.10 Focused results comparing the 0, 45, and 90 degree samples from each batch for CLCT calculations. 127
6.11 Change in Young's modulus based on fiber orientation for continuous fiber bending samples. 128
6.12 Comparison of average max stress based on reinforcing fiber orientation. 129
6.13 Comparison of the continuous and discontinuous fibers (2.5% and 5% 1mm samples) normalized Young's modulus. 130
6.14 Sketch of an un-oriented lamina with its reinforcing fibers drawn to be aligned with the dotted lines 131
6.15 Orientation of infill fibers with respect to θ with the longitudinal and transverse directions in the 1 and 2 directions respectively. 133
6.16 Longitudinal modulus prediction using the Tsai-Wu criterion for a single layer continuous fiber reinforced composite lamina. 135
6.17 Lower transverse modulus of an oriented lamina ply for the continuous fiber reinforced lamina ply which mirrors the longitudinal modulus. . . . 136
6.18 Shear modulus calculated using the Tsai-Wu criterion for the oreinted single play lamina based on reinforcing fiber angle. 137
6.19 Change in effect of Poisson's ratio with respect to orientation angle resulting in the shear force being distributed more along the axial direction of the fibers. 137
6.20 Geometry representation of sample with nominal print dimensions using a surface element in the ANSYS geometry modeler. 140
6.21 Worksheet of each specified individual laminate and its respective material, thickness, and reinforcing fiber orientation 141
6.22 The two types of mesh are used to conduct a grid independence study to ensure the mesh is not affecting the simulation results. 142
6.23 Displacement in the Z direction for the coarse mesh with a 10 N force applied at the center (top) and the same force applied at the center for the fine mesh (bottom). 143
6.24 Comparison of ANSYS simulation results and physical test samples using the same averaging methods for calculation stress and strain based on force and displacement. 144

A.1 CAD representation of the extruder nozzle (Left) and heat block (Right) of the extruder assembly. 150
A.2 CAD representation of the heat break (left) and heat sink (Right) of the extruder assembly. 150
A.3 CAD assembly of an E3D extruder assembly 151
A.4 CAD assembly of modified E3D extruder assembly with a continuous fiber injector for coaxial extrusion used for planning needle placement before machining existing assembly 152
A.5 Machined extruder assembly with angled injection needle for continuous fiber extrusion for coaxially extruded composites 153
A.6 Coaxially extruded continuous carbon fiber samples from modified extruder with white ABS polymer filament. 154

Chapter 1 INTRODUCTION

1.1 Background information

To understand the complexities associated with the anisotropic behaviors of 3D printed fiber composites, a cumulative background knowledge on additive manufacturing and composites is required. Not all 3D printers or 3D printing programs operate the same and composites themselves greatly vary in design and technique. To ensure an understanding of the concepts covered in the later sections of this document, three major concepts were investigated and described in the sub-chapters below

1.1.1 Additive manufacturing

Additive manufacturing has been revolutionizing the manufacturing sector that allows the production of engineering parts without the need of a large facility. More typical methods of production use costly molds, include large machines, or require an expansive collection of tools. Additive manufacturing instead branches away from a sophisticated production line with multiple workers present and uses a simpler system of a single-user and a single-machine. A variety of different additive manufacturing techniques exist each with its set of advantages and limitations. All additive manufacturing techniques are similar in one aspect, they combine individual layers of material by stacking them one atop each other to create the final geometry. The method of layer production and layer adhesion are the main differences between additive manufacturing methods with a subset of the various methods referred to as three-dimensional printing (3D printing). The 3D printing subset is a revolutionary manufacturing method that allows the production of engineering structures almost directly from modeling software on a computer [6–13]. This paper will focus on the fused deposition modeling (FDM) method of 3D printing as it is one of the most com-

monly used methods and tends to be the simplest. The 3D printing process begins with designing a three-dimensional model of a product with a computer aided design (CAD) software. The complete 3D model is subsequently imported into a 3D printer and digitally sliced into a set of thin "layers" by a slicing software. To fabricate the three-dimensional product, the solid polymer filament, typically in the form of wires, is heated up above its melting temperature and extruded through the printer nozzle onto a build platform to form a horizontal, two-dimensional layer. Repeating this process, multiple 2D layers are built on top of the others to create the final 3D product as seen in 1.1

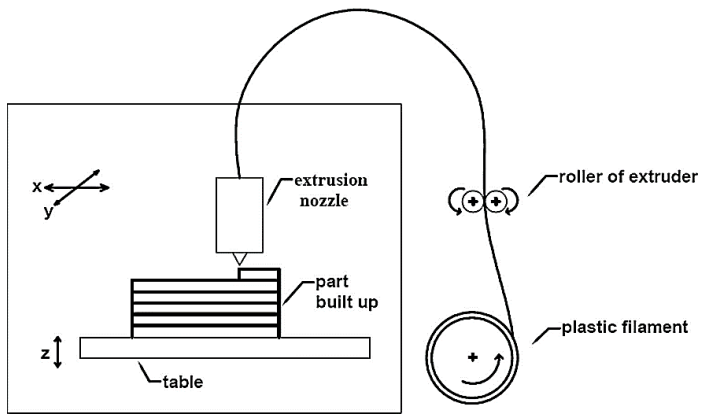

Figure 1.1: Schematic of how the bulk filament material is extruded in several layers to construct the desired part.

These layers typically consist of continuous strands placed along another in a specified pattern. The distance between the strands of material that make the layers is directly associated with the infill density and part quality. The quality of a print can be edited via user input to produce smaller layers at the cost of more production time. The smaller layers assist the printer to better capture the geometries of the desired part [14] as demonstrated in Figure 1.2. The patterns in the material also vary based on user input such that it can be optimized for strength or production speed. The movement of the filament strands is controlled by a combination of controllers typically a motor driven belt or screw mechanism moving either the extrusion head and/or the entire build plate.

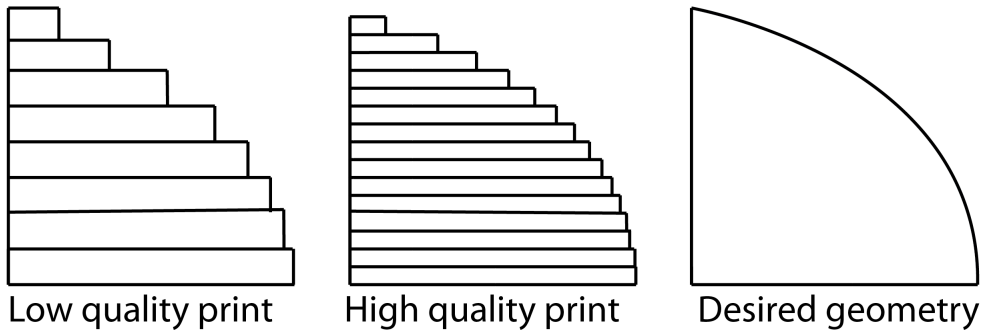

Figure 1.2: The effect of the layer height and quality of a print to capture the geometry desired known as the stair stepping effect.

There are typically two main types of movement configurations for FDM 3D-printers, the Cartesian and Delta configurations as seen in Figure 1.3 [15]. The Cartesian configuration consists vertical and planar movements, typically the vertical movement is in-dependent of the planar movements. An example is the cartesian movement in Figure 1.3 with planar movements controlling the bed while the vertical movement is controlling the extrusion head. The opposite can also be found with planar movements controlling the extrusion head and vertical movements controlling the bed depending on the manufacturer. For the Delta configuration all controller movement is placing the extrusion head while the bed stays stationary.

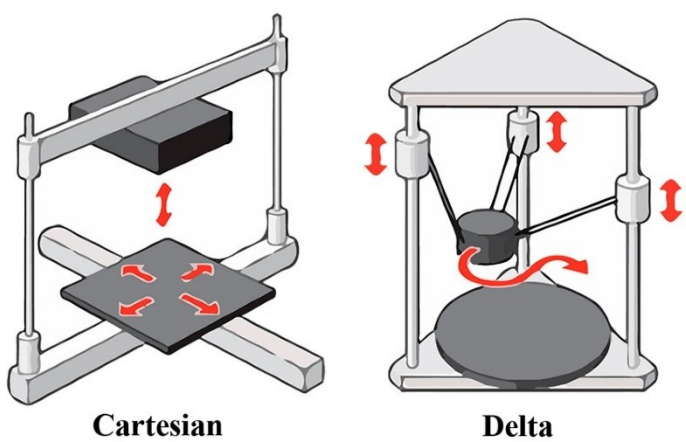

Figure 1.3: Visual representation of how both cartesian and delta configurations operate to deposit filament strands. (With permission from Creative Commons)

The movement of the motors can vary for each machine, yet most machines use the same numerical control language G-Code. The G-code is generated using what is known as a slicing software. The slicing software turns a three-dimensional object into several "layers" that make up the desired structure by "slicing" it. Each layer then is converted into several linear movements that the 3D printer can follow known as the G-code, an example of a G-code snippet can be seen in Figure 1.4. The G-code then commands the movement of the motors to precisely deposit the filament material and forms the final product.

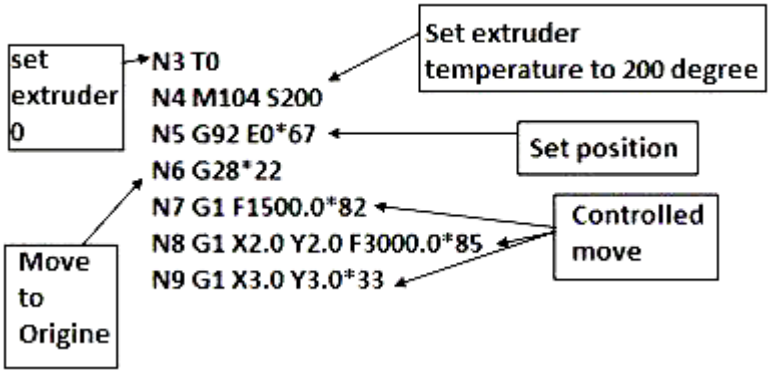

Figure 1.4: Example of how the G Code numerical instructions relate to the movements/actions of the 3D printer. (With permission from Creative Commons)

The process begins with the part being modelled in a CAD program by updating an engineering drawing, or by being directly created into the CAD program using the creators' vision for a design. Once the 3D model is created, it is then exported to a file type compatible with a slicing software (I.E. STL or OBJ). The slicing software breaks down the CAD file by "slicing" it into multiple digital horizontal layers. Each layer is then turned into a series of linear movements for the 3D printer to follow [16]. The linear movements themselves would depend on several user inputs (i.e., infill type, and density) so the focus will mainly be on the generation of the movements for the 3D printer. The movement instructions are collectively called the G-code which is used for many manufacturing purposes [17]. The G-code is the instructions read

by the 3D printer to command the various servos moving the extruding head as well as commanding the extruder to place material on the printing surface.

1.1.2 Additive manufacturing of composite materials

Composites have been successfully used in aerospace and space industries and are gaining momentum in the automotive industry. With a yield strength of more than ten times that of steel or aluminum, and a density of only about one-fifth that of steel and one-half that of aluminum, composites have become the top choice for producing lightweight vehicles [6]. The common manufacturing methods for composites include autoclave molding, compression molding or thermoforming, filament winding, resin transfer molding, pultrusion, etc. [7]. Among those methods, autoclave molding is the oldest molding process for making large composite structures. This method essentially has no restrictions on sizes and shapes of the products; however, it is a labor-intensive process due to the involvement of hand lay-up. In contrast, compression molding or thermoforming is the simplest forming process for composites. In this process, heat and pressure are used to transform a flat composite sheet into a desired three-dimensional shape. These methods produce composite products with desirable mechanical properties, yet hand layering techniques are labor intensive and molding techniques often require expensive molds or specialized post processing autoclaves. As such there have been movements to produce these mechanically favorable composites using the direct and low-cost method of 3D printing. The introduction of reinforcing fibers can sometimes prove difficult to implement in additive manufacturing methods, especially the loose substrate and resin pool methods. The different densities in the material can cause an uneven distribution in liquid matrix materials, and the scattered powder methods often are not precise in fiber concentrations/placement. There do exist some continuous fiber FDM based 3D printing technologies currently available on the market such as Markforged and Anisoprint; however, the samples produced are highly anisotropic and careful consideration for fiber orientation needs to

be considered. This is a well-known artifact when using 3D printing and disclaimers are used on these companies' websites stating that careful consideration needs to be taken in fiber placement and orientation. New additive manufacturing methods such as selective composite formation which uses a metallic fiber impregnated photopolymer resin as seen in the work of Cunico and De Carvalho [18]. These types of methods are heavily limited by the need for the resin matrix to UV curable and need to be produced in a way that the reinforcing fibers don't impede the distribution of the UV curing laser. These newer methods might look promising; however, they are mostly concepts that have yet to be fully investigated and are not as widely accepted manufacturing methods like FDM.

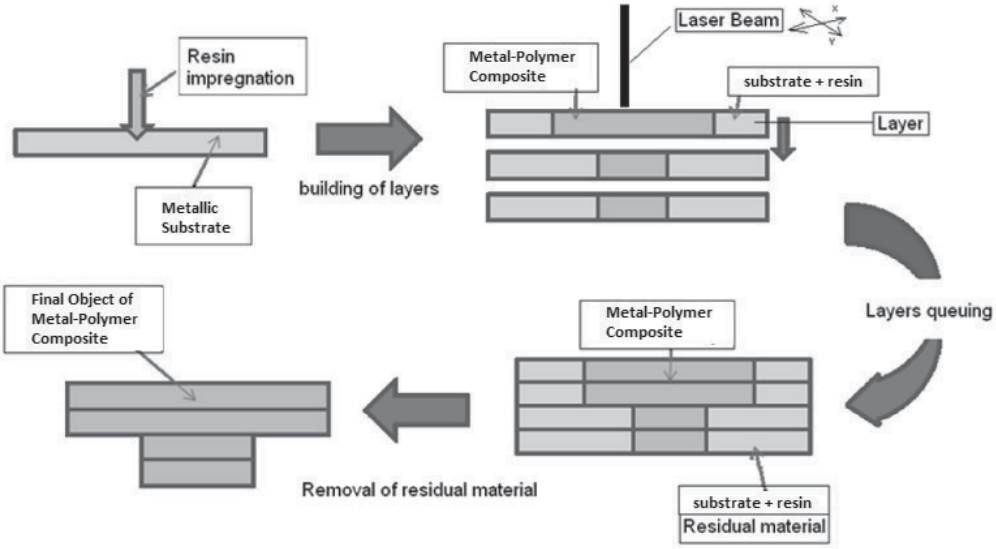

Figure 1.5: Illustration depicting the selective composite formation manufacturing method using the resin impregnated metallic substrate (With permission from Springer Nature)

Methods deriving from the traditional FDM process have also been developed utilizing both continuous strands and short fibers. One of the more basic methods is to use a 3D printed filament impregnated with short reinforcing fibers that can be used with most ordinary 3D printing machines. The reinforced fiber filament is inserted into the extruder and functions similarly to a pure polymer filament. The

only modifications needed would be to alter the printing parameters (mainly the extruder and print bed temperature) to accommodate the new filament and replace the typical soft brass nozzles with a more durable material. The reinforcing fibers tend to be abrasive and can file away at the soft nozzle material; to accommodate this the brass nozzle's thermal conductance is sacrificed and replaced with either a hardened steel alloy or the nozzle tip is replaced with a durable ceramic material. To incorporate continuous fibers more considerable hardware and software changes need to be implemented. One of the least intrusive methods for implementing these continuous fibers are those similar to the method depicted in Figure 1.6.

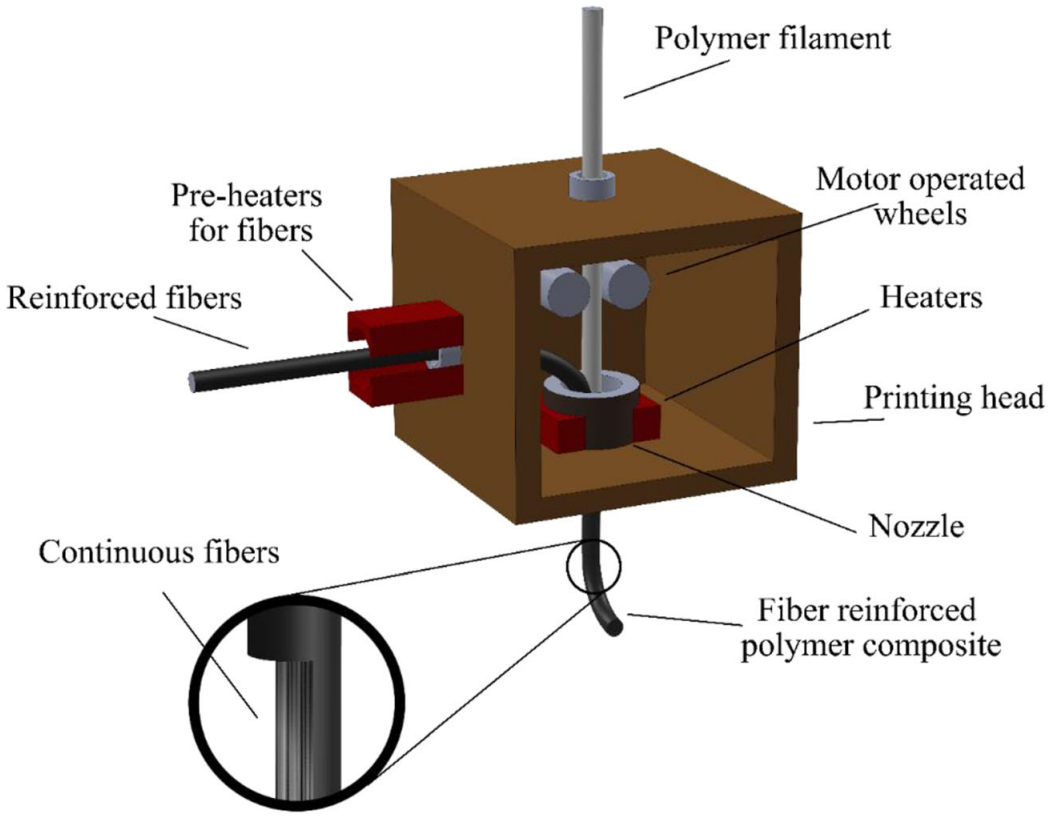

Figure 1.6: Modified 3D printer extruder assembly to incorporate a continuous reinforcing fiber strand from a bulk roll.

1.2 Current limitations and setbacks

As covered in a previous sub-chapter, traditionally manufactured composites often undergo an enclave post-process that involves an environmentally closed system. This results in a uniform pressure and temperature across the composite as its being manufactured resulting in the individual layers being bonded together with minimal gaps. In 3D printing the product is exposed to ambient temperature and pressure as its being manufactured and the products geometric precision is defined by the machine's movements. Shifts in pressure and temperature can cause manufacturing defects within a part, and the precision of the dimensions between the strands of deposited filament can be limited by the machine's hardware. Microstructural analysis revealed that the fiber reinforced filaments and printed samples contained a higher quantity of large voids when compared to the pure polymer filaments and printed samples (Figure 1.7). The black dots show the voids in the final products microstructure and how the introduction of reinforcing fibers with different thermal properties can cause manufacturing defects. This only compounds the defects and difficulties associated with determining the anisotropic mechanical properties of pure polymer 3D printing.

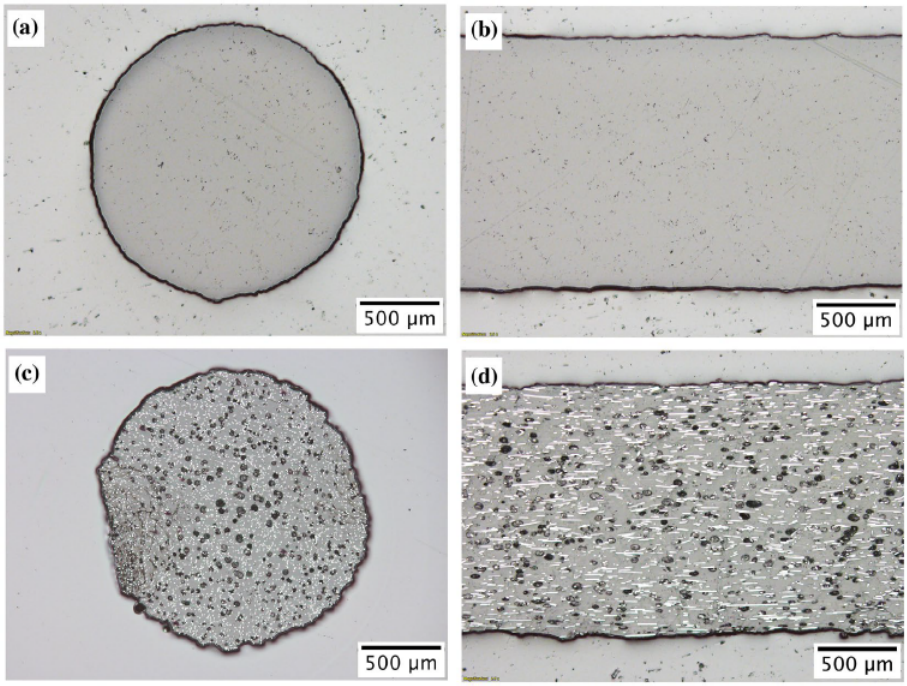

Figure 1.7: Comparison of filament microstructures for a pure polymer filament [transverse (a) & longitudinal (b)] and for a fiber reinforced filament [transverse (c) & longitudinal (d)] [19].

This then leads to the main question with composites in additive manufacturing and specifically 3D printing: if the manufacturing conditions for more conventional methods such as hand-layering techniques differ in processing steps, thus it is fair to assume that the mechanical properties of the end products will vary greatly. Studies tend to show that not only do the products have different mechanical values, but the 3D printed products tend to exhibit more anisotropic behaviors that are difficult to predict. Currently there is not an industry-wide-accepted method for predicting the anisotropic behaviors of 3d printed products in general, and the inclusion of unidirectional reinforcing fibers only tends to complicate the matters. In this aspect, simulation methods to better understand the utilization of short and continuous fiber-reinforced filaments would greatly aid in pushing 3D printing forward to more useful applications in industry. Despite this very limited work is found in the literature on this topic and current manufacturing implementations follow a more "guess and

check" method that utilize "rules of thumb" to attempt to optimize fiber placement.

1.3 Motivation

Currently there is no universally accepted method to predict the mechanical behavior of a 3D printed object before manufacturing it. The variety of 3D printing infill methods and materials allows for the final products have a diversity of favorable mechanical properties. The issue with this variety is that the nature of the manufacturing method causes the final product to have highly anisotropic mechanical properties that are difficult to solve for. Each method of infill introduces its own unique microstructures and each method of introducing reinforcing fibers tends to further complicate the necessary calculations. Current design optimizations tend to follow a "guess and check" method where the prototypes are optimized by observing its failure methods. While these methods are becoming more efficient through the use of machine learning algorithms and user experience, these methods require multiple samples to be produced before the final design is reached and is time expensive. Instead, the current goal of the research conducted is to apply a well-accepted and time-proven method to an emerging field of manufacturing. The method in question is the Classical Laminate Composite Theory (CLCT) and previous research has shown that this method can already be applied to pure-polymer composites. Now the added complexities of both short and long reinforcing fibers are being addressed, as well as the designing and testing of a theoretically universal method for introducing continuous fibers.

Copyright© Jordan Garcia, 2023.

Chapter 2 LITERATURE REVIEW

The term 3D printing covers a variety of manufacturing methods such as: Fused Deposition Modeling (FDM), Stereolithography (SLA), Digital Light Processing (DLP), Selective Laser Sintering/Melting (SLS/SLM), and Laminated Object Manufacturing (LOM). The FDM process consists of a spool of filament material being fed into a heated extrusion nozzle. This process of using a heated extruder could use virtually any thermoplastic filament material [20]. The filament material is melted and deposited on a print bed in layers to form the product. These layers typically consist of continuous strands placed along another in a specified pattern. The distance between the strands of material that make the layers is directly associated with the infill density and part quality. The quality of a print can be edited via user input to produce smaller layers at the cost of more production time. The smaller layers assist the printer to better capture the geometries of the desired part [21]. Yet now with the introduction of reinforcing fibers, the smaller layers could interfere with the adhesion between the fiber and matrix Figure 2.1. The patterns in the material also vary based on user input such that it can be optimized for strength or production speed. The movement of the filament strands is controlled by a combination of controllers typically a motor driven belt or screw mechanism moving either the extrusion head and/or the entire build plate. With the inclusion of a continuous strand of fiber, the direction of material deposition will also align the fiber along the extruded polymer. The most common method of 3D printing is the Fused Deposition Modeling, and thus the FDM method is used for testing and sample production in the later chapters.

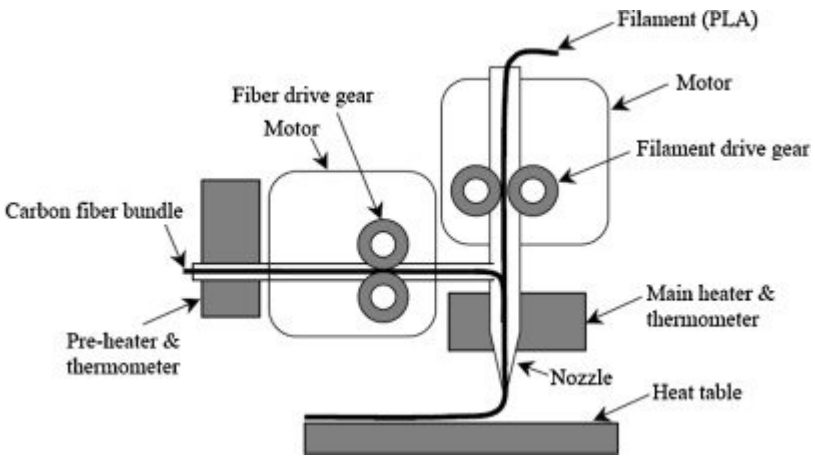

Figure 2.1: Schematic depicting the co-extrsuion process with the fiber being extruded along with the polymer matrix [22].

2.1 State of composite printing

Composite materials have been in use in a variety of different industry applications for several decades, with one of the most recent advancements being the fabrication of composites using additive manufacturing methods. Due to the recent innovation of the composite additive manufacturing processes' there is a lack of review for additive manufacturing of continuous fiber composites [3D composite 1-0].

Multiple additive manufacturing methods exist for creating continuous fiber reinforced composites such as stereo-lithography (SLA) , Direct Energy Deposition (DED), and Finite deposition modeling (FDM). Stereolithography (SLA) is the use of focused laser beams on the surface of a vat of liquid photopolymer to produce 3 dimensional solid objects [23]. The photopolymer gets solidified by the laser and creates a single layer similar to the FDM method. The solid layer is then lowered into the liquid and the next layer is solidified atop the previous layer and adheres to it as seen in Figure 2.2. The laser is used to irradiate and cure the polymer and is controlled by a dynamic system of mirrors. These mirrors control the direction of the beam and "write" the cross section of the model on the polymer surface [24]. Similarly to the FDM method, stair stepping effects are noticeable if the surface is not

perpendicular to the laser beam and the layer thickness is higher. The SLA method however, requires another step of post-processing for the removal of excess material to make it safe to handle. This includes rinsing with water as well as rinsing with ethyl alcohol before removing supports.

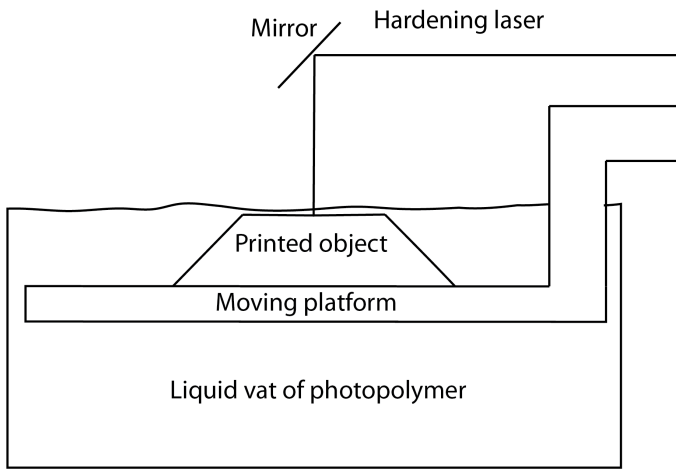

Figure 2.2: Example of 3D printing using the stereo-lithography method.

Direct energy deposition is an additive manufacturing method that uses a constant flow of material and melts/fuses the material vie concentrated thermal energy to create a layer as seen in Figure 2.3 [1]. This method is theoretically capable of printing entire composite structures; however, they are mostly used to repair or add additional material to an already existing object [25].

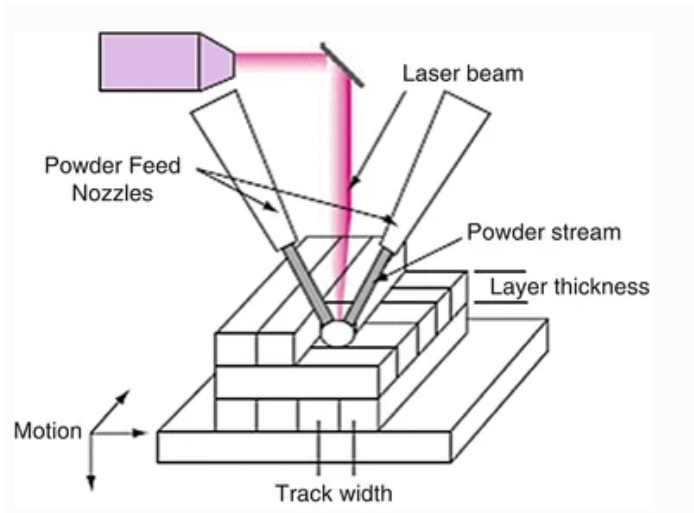

Figure 2.3: Example of 3D printing using the direct energy deposition method for a powder based material (With permission from Springer Nature https://www.springer.com/journal/170/ [1].)

The most common method for 3D printing is the Finite Deposition Modeling method due to its manufacturing convenience and simplicity [26, 27]. The basis of FDM is the extrusion of the bulk filament or fiber roll through an extruding nozzle onto the print bed, yet how exactly the reinforcing fiber is introduced can vary. While the material of the reinforcing fibers can vary, the length of the fibers used also vary greatly. For this study the types of fiber reinforcement were separated into two sections, the discontinuous fibers and continuous fibers. Continuous fiber composites tend to have the most preferable mechanical properties; however, they are often synonymous with high cost due to the expensive equipment and material cost used for manufacturing these composites [1]. Discontinuous or short-fiber composites are traditionally less expensive and are normally less difficult to manufacture while still retaining some of the benefits of reinforcing fibers [2]. The FDM method is the dominant method for 3D printing composites [28]. This is partially due to the price of FDM 3D printing has also drastically reduced from $20,000+ to less than $1,000 [29]. While there is a financial incentive for the use of FDM, there are still limitations to this method. FDM printers fail to achieve the dimensional accuracy of

other 3D printing methods with an average accuracy of around 0.5mm; however other manufacturers claim higher accuracy levels (Markforge claims accuracy of .16mm [26].

2.1.1 Discontinuous fiber FDM

Most composite 3D printing is done using discontinuous fibers due to the relative ease of use and reduced cost when compared to the continuous fiber systems. Discontinuous fiber reinforcement FDM consists of extruding a bulk filament that is reinforced with short reinforcing fibers or powder. Several traditional FDM printers can become discontinuous fiber printers by extruding a polymer filament with chopped fibers mixed throughout to create discontinuous fiber composites [Ani2-23&24]. The process is very similar to polymer-only FDM extruding with a few modifications needed to minimize wear/damage to its components (Figure 2.4). The part most affected by the switch to composite materials is the extruder nozzle and thus manufacturers often recommend upgrading the hardware [Nozzle wear].

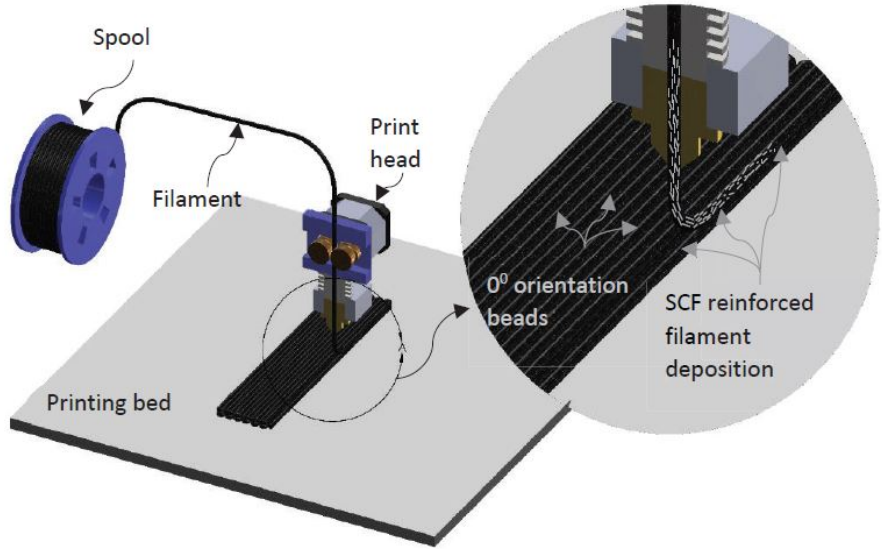

Figure 2.4: Spool of short fiber reinforced polymer extruded through a heated print head (With permission from Springer Nature https://www.springer.com/journal/170/ [2].)

Due to the spool containing the fibers, the FDM method is especially capable of producing parts with varying fiber content; however, the influence of the fiber content

on the final parts mechanical properties have not yet been extensively studied [30]. Manufacturers wind the spool of bulk material and can input varying quantities of carbon content which is normally specified in the material property sheets although they can often be vague on the percentages. Thus the user would simply purchase the desired pre-manufactured filament with the desired reinforcing fiber and content, then simply use this bulk filament spool with a slightly modified desktop FDM 3D printer. One limitation is the fiber content would not be adjustable as a new roll would need to be manufactured in order to modify any quantities. These rolls would also still need the flexibility to wind/unwind from the spool, thus high reinforcement of a brittle fiber may be problematic [31]. There is also the issue of 3D printing is already notorious for producing anisotropic final products and the introduction of short fibers only further complicates the system. And thus the main issue with FDM or 3D printing in general is the process creates final parts that tend to have anisotropic properties that differ from the materials used to fabricate them [32]. There are various attributing factors for these anisotropic mechanical behaviors varying from inter-layer bonding, microstructure, fiber reinforcement method, extrusion temperature, material limitations etc. As the printer deposits material the extruded material, the layers can have poor inter-layer adhesion or porosity in the micro-structure and negatively affect the overall mechanical behavior (Figure 2.5) [26, 33].

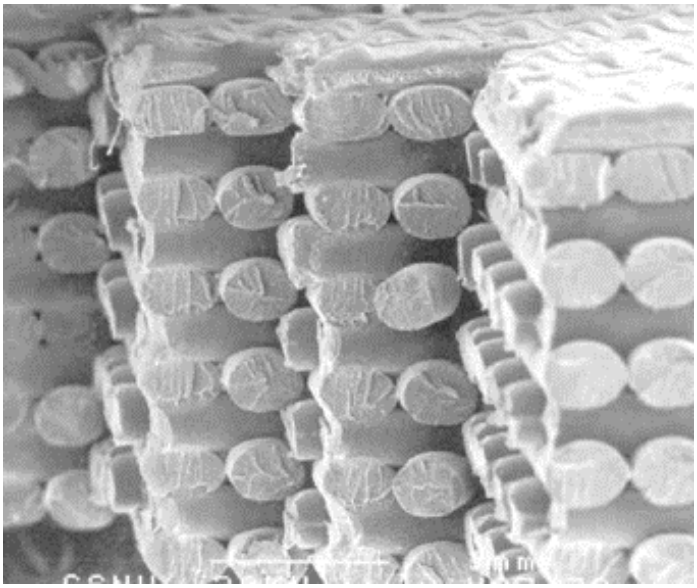

Figure 2.5: Scanning Electron Microscope (SEM) image of the micro-structure of the extruded fiber filaments.

Aside form the layers not adhering to each other there is also the issue of the fibers not perfectly adhering to the polymer matrix they are extruded within. This raises the issue that not only can the final product have issues with inter-layer adhesion and inter-strand adhesion, but now for fiber reinforced FDM the fiber-matrix interface adhesion needs to be considered as well. This takes the focus of temperature control and print speed down from the macro-scale into the micro-scale where the fiber-matrix adhesion is observed. Printing materials are often limited due to requiring both the polymer matrix and reinforcing fiber having similar melting temperatures and viscosity's [31]. To address these issues, reinforcing fiber and matrix materials are often pared for material compatibility. Certain fibers tend to adhere better to certain matrix materials and further compliment the mechanical properties [34]. Several print settings are adjusted to maximize adhering and minimize gaps in the fiber/matrix interface 2.6 [2]. Some printers such as the MarkForge does not allow the user to modify the extruding temperature to avoid poor adhesion [26]. Continuous fiber printers are typically set to have higher extruder temperatures to assist in better interlamellar bonding and less void space due to lower viscosity's [35].

Interlamenar bonding has also seen improvement by reducing the speed of extrusion and movement; however, this tends to significantly increase production time and thus cost. Then there is the ever present factor of the atmospheric temperature and build space humidity that can affect the viscosity and material solidification [35].

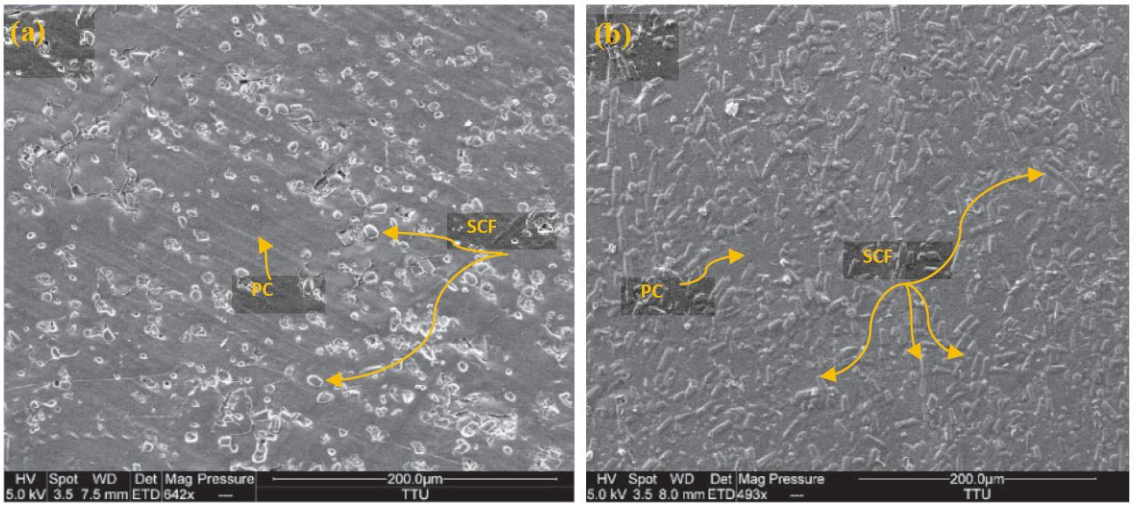

Figure 2.6: Field Emission Scanning Electron Microscopy (FESEM) performed to observe the fiber-matrix interface showing with proper preparation the interface gaps can be reduced or even eliminated [2].

2.1.2 Continuous fiber FDM

Continuous fiber composites traditionally have the best mechanical properties but can difficult or costly to manufacture, especially when attempting to use additive manufacturing methods. Traditionally, continuous fiber composites used specialized equipment such as vacuum enclaves or labor-heavy hand layering techniques. As previously mentioned the use of additive manufacturing methods greatly improve the convenience and reduce the initial cost when compared to traditional methods, but the mechanical properties tend to suffer depending on the printing style used.

It was previously mentioned in the discontinuous fiber subsection that fiber and matrix materials are picked to assist in interface adhesion, this is especially true for continuous fiber composites. When selecting matrix and fiber materials for contin-

uous composites the fiber and matrix material are selected to minimize weight and maximize energy absorption [30]. With better fiber-matrix adhesion the energy can be more easily distributed from the encompassing matrix to the typically stronger but brittle reinforcing fiber. As seen in Figure 2.7, even with a properly selected pair of materials there is still the present issues of voids in the micro-structure simply as an artifact of 3D printing [36]. Certain methods have been proposed to reduce the gaps in printing such as using square or triangular nozzle to help by curtailing void space [35].

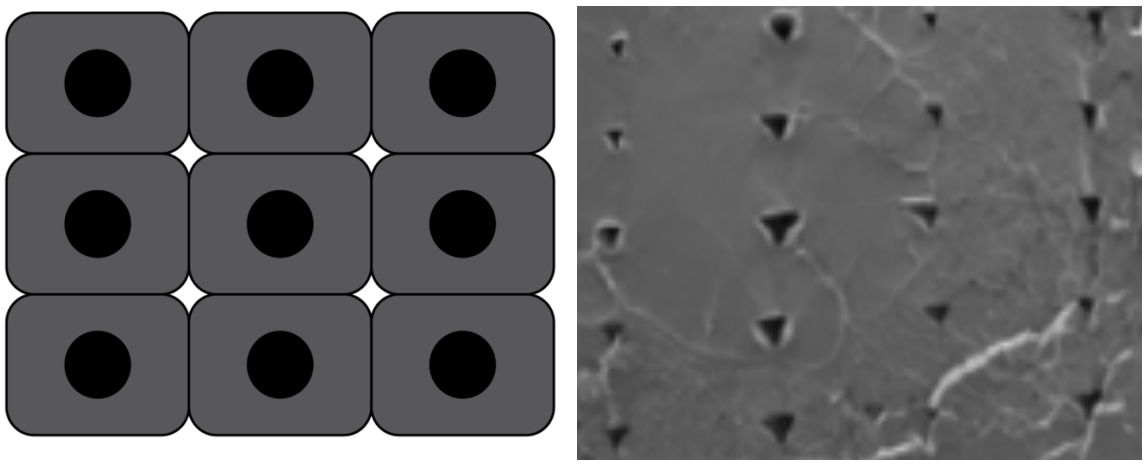

Figure 2.7: Cross section of a completely encased continuous fiber with small gaps at the inter strand adhesion points illustration (Left) and viewed from a sample (Right) [3].

The method of printing composites between FDM printers can vary based on the type of filament/material used as well as how the extruded strands are deposited. In 2014 MarkForge released the first commercial printer with an individual extrusion nozzle for the reinforcing fiber and polymer matrix material. There also exist systems that extrude both the fiber and filament through the same nozzle, this is known as coaxial extruding. These systems reduce the number of extrusion nozzles to just one. While these systems do create continuous fiber reinforced composites, they are not capable of reinforcing only select fibers and tend to be more susceptible to homogeneous products from the manufacture [37]. As the fiber and polymer are

inserted into the extruder together, inconsistencies on the bulk material diameters would result in inhomogeneous products due to insufficient impregnation of the fiber in the encasing polymer matrix. To assist in these shortcomings, methods have been proposed such as using laser-based pre-impregnation methods to aid in penetration and diffusion [26]. These types of systems would be similar to the DED method as an initial step for the FDM process.

One method of introducing reinforcing fibers is the dual head 3D printer which has the fiber being introduced into the composite through the nozzle and a saw-like mechanism cuts the long fiber after it is extruded between layers. This method does not produce products with fibers homogeneous through the entire product.

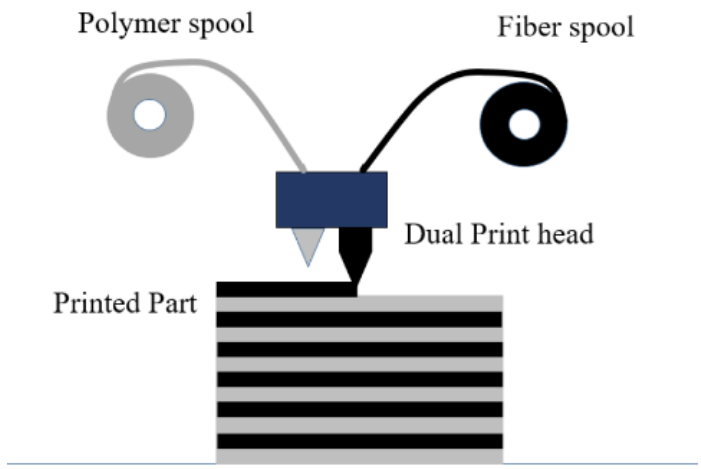

Figure 2.8: Schematic of a dual head extruder with separate nozzles and feeders for each material type [4].

Other FDM printers can create continuous fiber composites by extruding both the encasing polymer matrix and reinforcing fiber through the same nozzle, also known as coaxial extruding. Other printing methods for continuous fiber 3D printing include using a two nozzle system where one extrudes the polymer matrix while the other extrudes the reinforcing fiber [26]. This method does not require all layers to be reinforced with fiber and allows selecting layers with no fiber reinforcement which the other methods do not accommodate. The coaxial style printers tend to be more

susceptible to creating un-homogeneous products due to the fiber not being properly impregnated as a result of the high temperature concentration at the extrusion nozzle [38].

2.1.3 Mechanical testing and models

The methods used for testing 3D printed composites were also investigated in relevant literature. Unfortunately there is a lack of review of continuous fiber composites produced by FDM as this invention is relatively recent. So far mechanical testing has been extensively observed for each parameter in printing slicing software's ranging from infill types, build orientations, temperature, material selection, print resolution [3]; however there is a noticeable bias on the quantity of tensile testing papers versus bending testing samples, as well as a lack of focus on the properties of the size/shape of the reinforcing fiber, with little known about its dynamic properties [3, 4, 26, 30, 35, 36, 39].

This is partially due to the anisotropic nature of 3D printed structures and inconsistent findings [40], and there is a lack of accepted testing standards. Currently 3D printed composites follow testing method standards for traditionally manufactured composites. It has also been shown that FEA analysis can be sufficient to explain the failure methods of 3D printed composites when appropriately used [41].

The fiber volume fraction has been noted to drastically affect the tensile strength of sample (Figure 2.9), yet the fiber thickness and orientations are often not stated or overlooked.

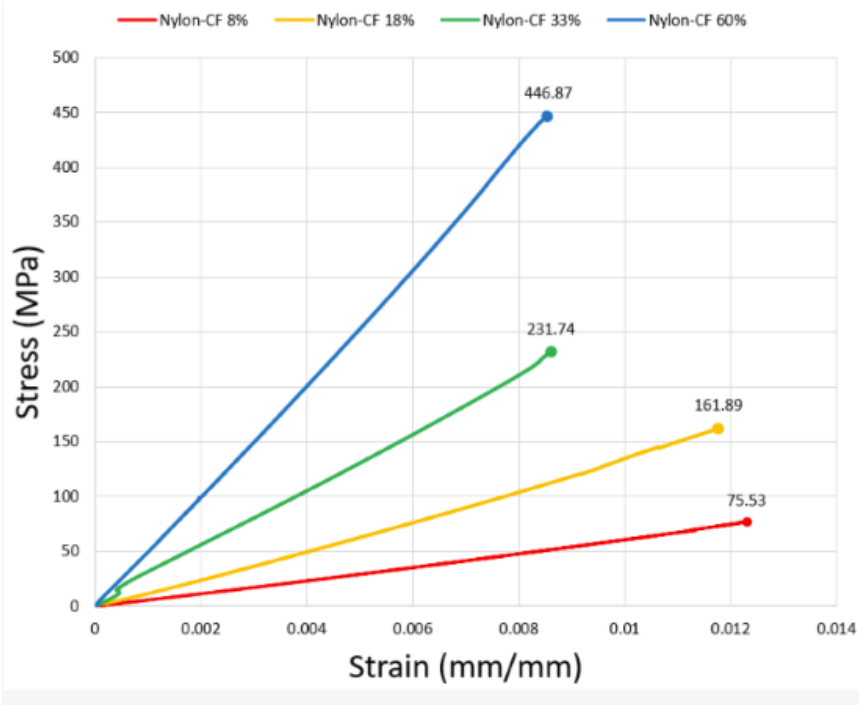

Figure 2.9: Demonstration of how the fiber volume fraction can greatly affect the tensile strength of the 3D printed object for a nylon-carbon continuous fiber composite [4].

Literature does show some interesting relations for 3D printed composites that are not normally found in traditionally manufactured composites. According to the mechanical testing of 3D printed composite samples, the shear modulus of the 3D printed samples is actually negatively affected by the fiber volume content and the transverse properties are dominated by porosity and inter-layer adhesion [30]. This means that in the transverse direction your mechanical response is dominated by your printing parameters, and in the shear direction the reinforcing fiber is actually weakens the overall mechanical response. There is also the discoveries of the affects of the infill on the overall mechanical properties. It was found that increasing the infill percentage could aid in the tensile properties in the longitudinal direction; however, when subjected to an impact load, the solid infill objects have a low resistance due to the air gaps in the structure absorbing the shock [26].

Several methods for predicting the anisotropic behaviors of 3D printed parts have

been proposed and published, each with its own application. Some models are proposed that focus on varying fiber volume fraction and fiber orientations using the Rule Of Mixing (ROM) which assumes either uniform stress, constant strain, or constant stress [[42]. This method has shown promise for low volume fraction composites specifically for predicting its tensile properties [26]. This method however, does not work well with higher fiber volume fractions.

Other methods have been proposed to use approaches used for traditionally manufactured composites. Using yield criteria for traditional composites such as the Tsai-Hill criterion are used to predict the overall stress/strain response in tension. One downside of these types of yield criteria is the difficulty in prediction the bending behavior due to the bi-modular behavior of the yield criterion. These types of solving methods can also be computationally expensive through the need to use a custom equation solver written by the research group that has not yet been optimized for performance [27]. Other traditional methods such as using Laminate Composite Theory (LCT) have been proposed but research has been focused on specific alternating patterns such as alternating 90 degree orientations. The size and volume fraction of fibers need to be more extensively evaluated for a more accurate application for LCT to be applied to 3D printing.

Constitutive models have also been proposed using experimental data to predict a products mechanical response based on its fiber content [3D comp 3]. The tests performed showed that the longitudinal modulus had a linear relation between it and the products fiber content.The transverse modulus had a higher variance and a 2nd order polynomial was used. This constitutive equation also relied on a ROM based approach for lower fiber contents. Other constitutive methods used LCT as their base [39]. Similarly to LCT the layers of the 3D printed object were observed to behave in an orthotropic manner. One setback of these models is not being able to account for the affects of the orientation of the object being built [43]. These models have also focused on tensile type failures and have not been studied for flextural

loading.

As shown, several prediction methods are proposed by different researchers for specific applications, yet there still is not a universally accepted method for predicting the mechanical properties of the 3D printed products. A few strides made in literature are the correlation between 3D printed objects and traditionally manufactured composite laminates. There is also the uniform agreement that analytical or computational models are preferable alternatives to mechanical testing, especially for continuous fiber samples [32]. The following chapters looks into using well known and accepted methods for traditional manufacturing composite design and modifying them to apply to additive manufacturing methods. The literature cited seem to unanimously agree that there are undeniable similarities between these types of processes and there has been extensive discoveries made for tensile based testing. For bending or dynamic testing methods, there is a lack of published literature.

Copyright© Jordan Garcia, 2023.

Chapter 3 ANISOTROPIC BEHAVIOR OF 3D PRINTED SHORT FIBER COMPOSITES – STATIC MECHANICAL PROPERTIES

3.1 Introduction

3D printing allows for inexpensive productions of engineering parts compared to other conventional composite manufacturing methods such as autoclave molding or injection molding which often demands for expensive molds and possibly high labor costs. Although 3D printing methods possess numerous advantages over conventional methods, they can introduce new challenges. During the 3D printing, reinforcing fibers that are randomly distributed in the polymer matrix often become aligned due to the shear flow near the nozzle wall when extruded [44–46]. The re-alignments of reinforcement fibers can cause the anisotropic behavior in microstructures and mechanical properties of the final products. Further, as the material is extruded in strands to form two-dimensional layers, the strands may not be closely packed and thus "spaces" or "voids" are inevitably formed between neighboring strands [47]. The presence of "spaces" and "voids" will certainly result in anisotropic structures and properties of the finished products. Finally, the movements (the printing paths) of the extruder can have significant impacts on the uniformity of the products. 3D printers use the numerical control language G-Code to command the movements (paths) of the extruders to deposit the filament materials to form layers. The directions of the movements (paths) for creating layers are often arbitrarily defined by the codes and vary greatly from printer to printer, and therefore, the properties of 3D printed products may be highly directionality-dependent [16]. More recently 3D printing has been used for fabricating composites as it is an automated manufacturing process with a high design flexibility [8–13]. 3D printing consists of designing a part with a computer aided design (CAD) model and converting it into a stereo lithography (STL) file. This STL file is then created into a set of digital instructions for the

printer to follow. In the printer, the solid polymer filament – the construction material – is heated up into liquid and extruded through a nozzle onto the build platform. The nozzle moves around horizontally and vertically to deposit a new layer on top of the previous one (Figure 3.1). Therefore, the 3D printing method is also referred to the "layered manufacturing" method [48]. The focus of this chapter is to examine the anisotropic mechanical behaviors of fiber reinforced composites by additive manufacturing (3D printing). Carbon fiber reinforced acrylonitrile butadiene styrene (CF-ABS) composites will be fabricated using various open-source printers and at various printing configurations. 3D printed fiber composites are further compared with those made through conventional manufacturing method. The anisotropic behavior of the composites will be modeled by using the classical laminate composite theory.

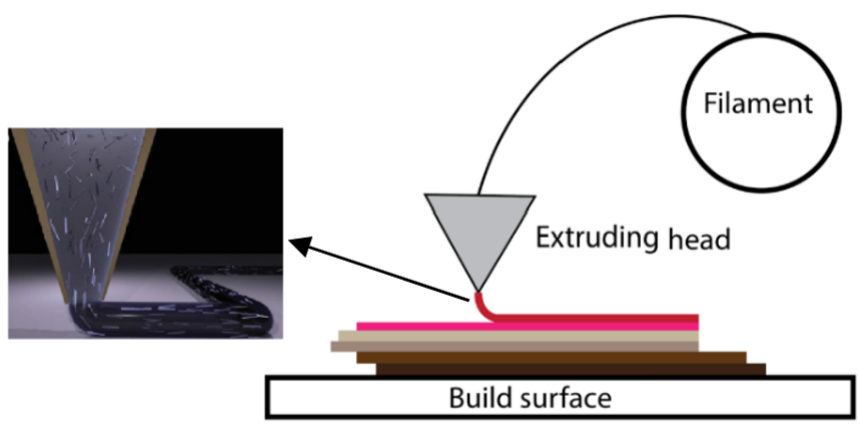

Figure 3.1: Sketch of a typical 3D printing process of a fiber reinforced polymer composite. The fiber filled polymer filament is extruded through a nozzle and then laid down as successive layers to form a composite.

3.2 Materials and methods

For the experiments, the materials used consisted of acrylonitrile butadiene styrene (ABS) resin and short carbon fiber reinforced acrylonitrile butadiene styrene (CF-

ABS) composite. The ABS and CF-ABS filaments, in the form of wires, were purchased form 3DXTECH in 1 kg spools.

3.2.1 3D Printing of CF-ABS composites

Rectangular bending specimens were produced using three open-source 3D printers, each with a unique slicer software: (1) the Flash Forge Dreamer 3D printer with Flashprint slicer software, (2) the Tevo Tornado 3D printer with Cura slicer software, and (3) the Prusa i3 Mk3 3D printer with Slic3r slicer software. The models for these samples were created and exported into .STL files using a CAD software called SolidWorks by Dassault Systems. The solid bending specimen model was designed with the nominal dimensions of 75 (L) x 15 (W) x 3 (t) mm in SolidWorks and then converted into a .STL file. The STL file was imported into each printer and the slicing software would "slice" the 3D solid model into a series of horizontal layers and then deconstruct each layer into a series of instructions for the printer to follow (through the G-code) [49,50]. The samples were printed in batches with four samples being produced at once placed in different positions as seen in Figure 3.2. Each printer's slicing software was then set to print all four solid samples, each with a different position and angle with respect to the build plate. The pattern of the infill would remain as the default "Rectilinear" pattern for a 100% infill density to create solid parts. The default "Rectilinear" setting used by each printer consisted of linear patterns with an alternating 90°angle for subsequent layers. The temperature of the extruded filament was set to 245°C and the printing bed was set to 115°C, as specified by the filament manufacturer to ensure adequate melting of the filament.

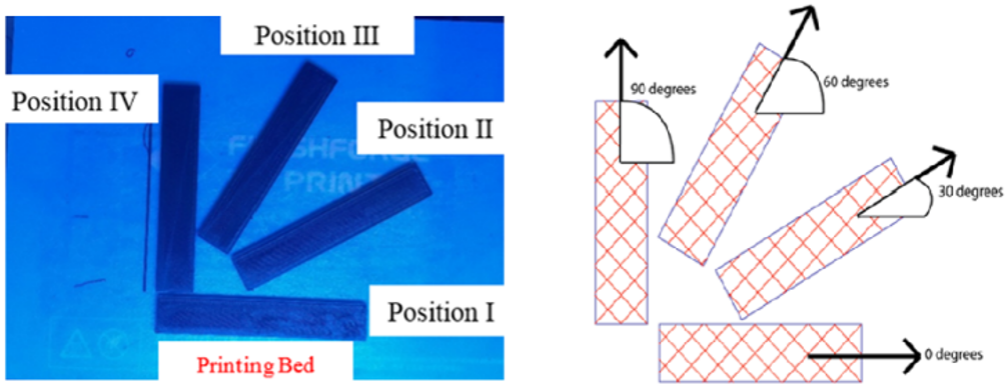

Figure 3.2: Parts are printed at four different positions on the printing platform.

3.2.2 Compression molding of CF-ABS composites

Conventional manufacturing methods for composites often involve in the uses of pressurized, heated molds while 3D printing produces composites in a mold-less, pressure-less, open environment through the "layered" fabricating technique. Thus, it is reasonable to hypothesize that 3D printing method would produce products with different microstructure and mechanical properties from those manufactured by conventional means. To explore these differences, compression molded CF-ABS samples with the same nominal dimensions was prepared and then compared to the 3D printed samples. For consistency, the filaments used for 3D printing were cut into pellets (approximately 1mm in length) and subsequently used for compression molding. The chopped CF-ABS pellets were filled inside a square-shaped aluminum mold, 10 (L) x 10 (W) x 3(t) mm, and then placed between two heated plates in a hydraulic pneumatic press. The plates were heated to 245°C, the same temperature used in 3D printing, and then compressed ejecting any excess material. The heated plates would continue to heat the compressed mold for 2 min. and then allow it to cool. The cooling process would vary at two different rates: (1) fast-cooled and (2) slow-cooled. At a fast-cooled rate the mold would immediately be removed from the hydraulic pneumatic press and allowed to cool naturally in a room temperature environment.

For the slow-cooled case the mold would remain in the hydraulic pneumatic press while the power of the press was turned off. The mold would remain in residual heat until cooled to room temperature. To obtain the same dimension rectangular bending samples, the square-shaped CF-ABS plates were subsequently cut using a laser-cutter machine. The same CAD model that was used to create the 3D printed samples was imported into the laser-works software. This software would turn the 2-dimensional outline of the CAD model into a path for the laser to follow and precisely cut out the samples. This process would guarantee that the compression molded samples and the 3D printed samples were identical in size.

3.2.3 Mechanical testing

Both 3D printed and compression molded samples were tested using in bending on a PASCO Material Tester equipped with PASCO Capstone software. The samples were loaded between two-point supports and the force was applied at the middle using a wedge-like applicator until failure. Prior to testing the testing apparatus was calibrated using samples and data provided by PASCO. During testing load and deflection data were recorded using their respective sensors. The data was then processed and used for subsequent analysis.

3.3 Results and discussion

Acrylonitrile–butadiene–styrene (ABS) is one of the most widely used industrial thermoplastic and the most common material used in 3D printing. Figure 3.3 depicts a typical stress-strain response of an ABS sample obtained through 3D printing (the Tevo printer). It is seen that the ABS resin displays a typical elastic-plastic behavior: an initial elastic deformation followed by a large-strain plastic deformation. However, with the insertion of short carbon fibers ($\approx 15\%$), the resultant CF-ABS composite become predominately elastic (Figure 3.3). The Young's modulus of the CF-ABS composite was estimated as 6416 MPa, which is almost five times of the modulus

of ABS pure resin ($\approx 1410MPa$). The CF-ABS has a failure limit 0.03%, opposed to a failure limit over 15% for the ABS pure resin.

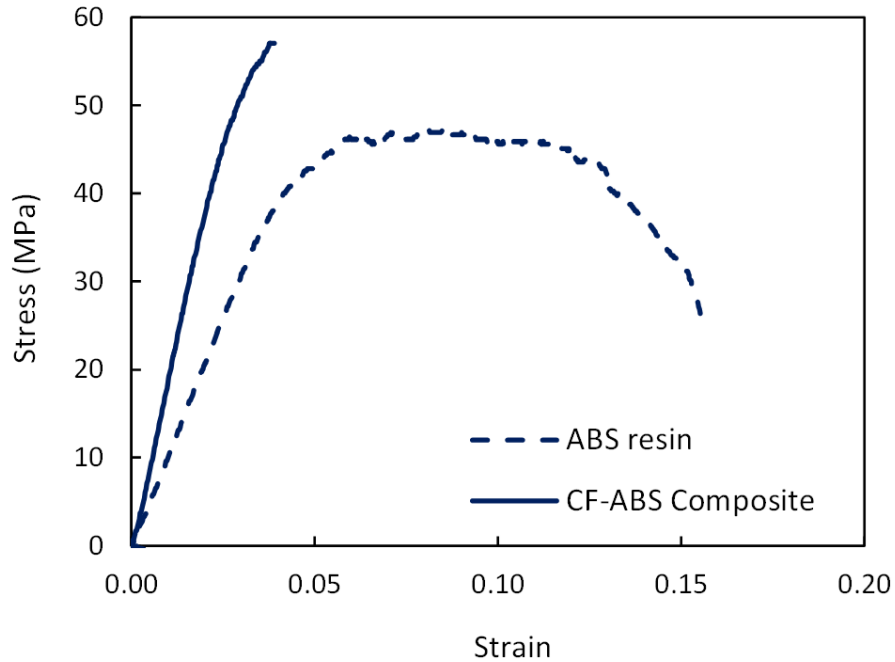

Figure 3.3: Stress-strain curves of ABS and CF-ABS samples from the Prusa 3D printer.

Ideally the choice of a manufacturing method should not alter the mechanical properties of a finished product; however, this is not the case with 3D printing. As a mold-less, pressure-less manufacturing method, 3D printing produces parts by depositing successive layers in an open environment. As a result, the 3D printed parts often contain "voids" and have poor adhesions between strands/layers, which lead to anisotropic structure and mechanical properties. The formations of "voids" or poor adhesions/connections of strands/layers further depend on the directions of printing. Figure 3.4 & Figure 3.5 show the resulting stress-strain curves of CF-ABS composites from the various printers. It is seen that samples from positions I and IV have greater failure strain than samples from positions II and III. This "split" in the results can be attributed to the use of the default "Rectilinear" infill pattern. As illustrated in Figure 3.2, the "Rectilinear" infill path follows a grid-like pattern oriented along the

printing surface which results in the positions I and IV having similar infill paths and the positions II and III having different infill paths. Due to such differences in infill patterns, the printed parts, although made using the same material and the same printer, exhibit different mechanical behaviors.

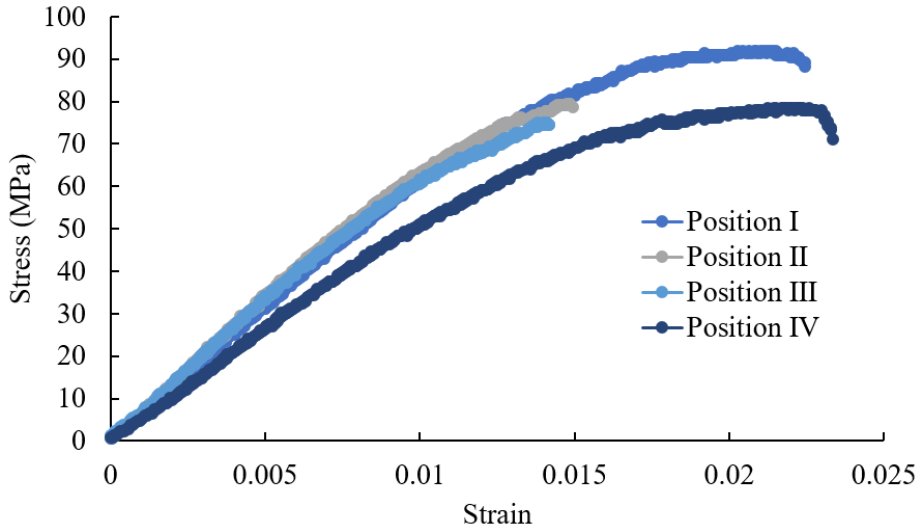

Figure 3.4: Stress-strain curves of CF-ABS samples of varying positions from the Prusa 3D printer.

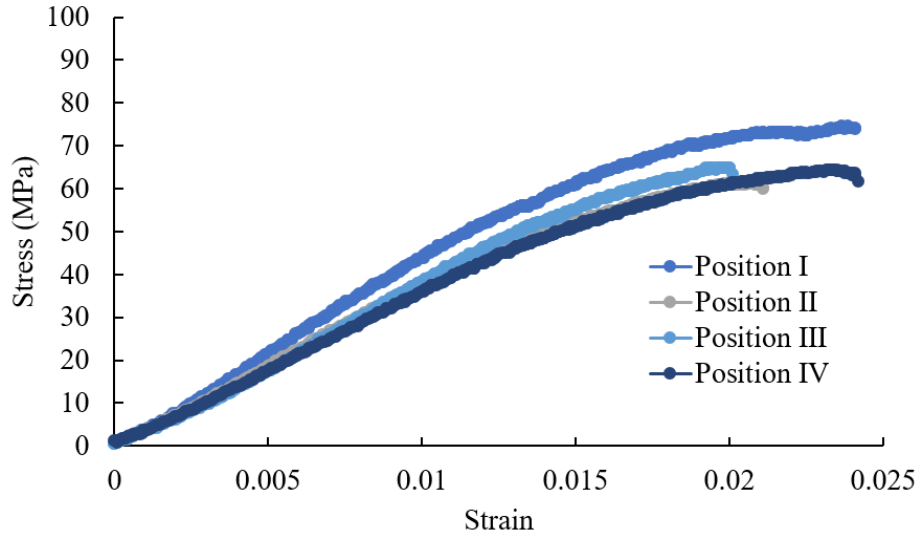

Figure 3.5: Stress-strain curves of CF-ABS samples from the Flashforge 3D printer based on the position on the print bed (Figure 3.2).

Figures 3.5&3.4 show that not only is there a difference in the stress-strain curves resulting from how the sample is oriented on the print bed, but the stress-strain curves also vary by printer used. Although the same printing conditions are used for G-code generation for each printer, there lies a significant difference on the performance of the printed samples among the machines. A quick comparison of sample positions between printers shows how different the stress-strain curves can vary: the greatest variation being how the Prusa has a significantly higher maximum strength and Young's modulus than the other two 3D printers. This is partially attributed to the fact that the Prusa printer has tighter tolerances with the amount of material extruded, allowing for better adhesion's between strands/layers. The Flashforge printer is ranked in the second in performance, partially due to the fact that this printer is equipped with an enclosure and thus has a better temperature control.

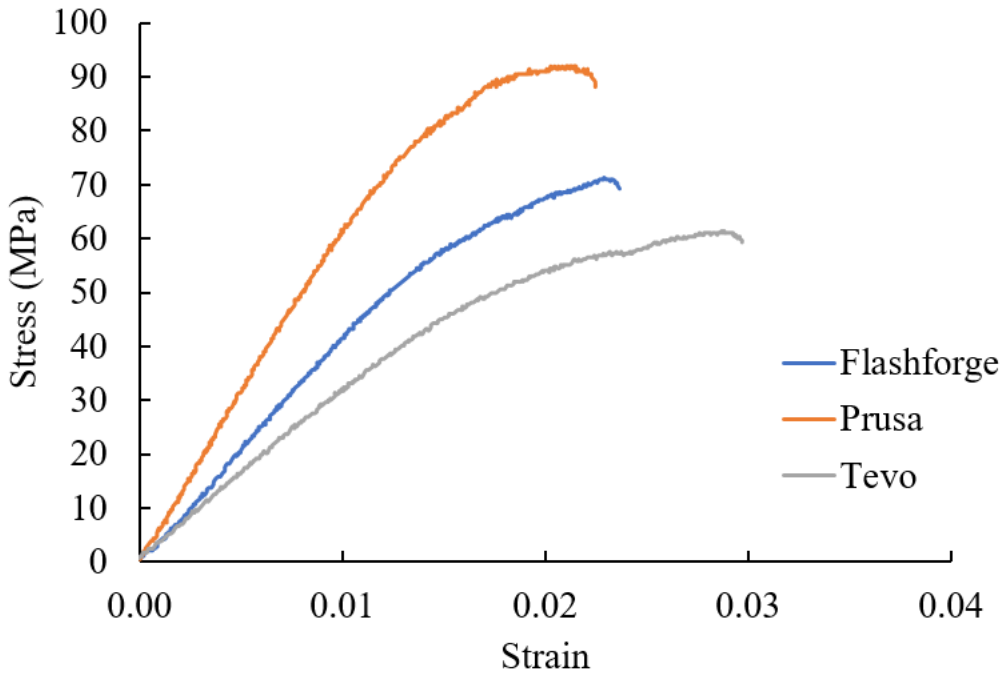

Figure 3.6: Comparisons of stress-strain curves of CF-ABS samples from different 3D printers. Samples were printed at the I position.

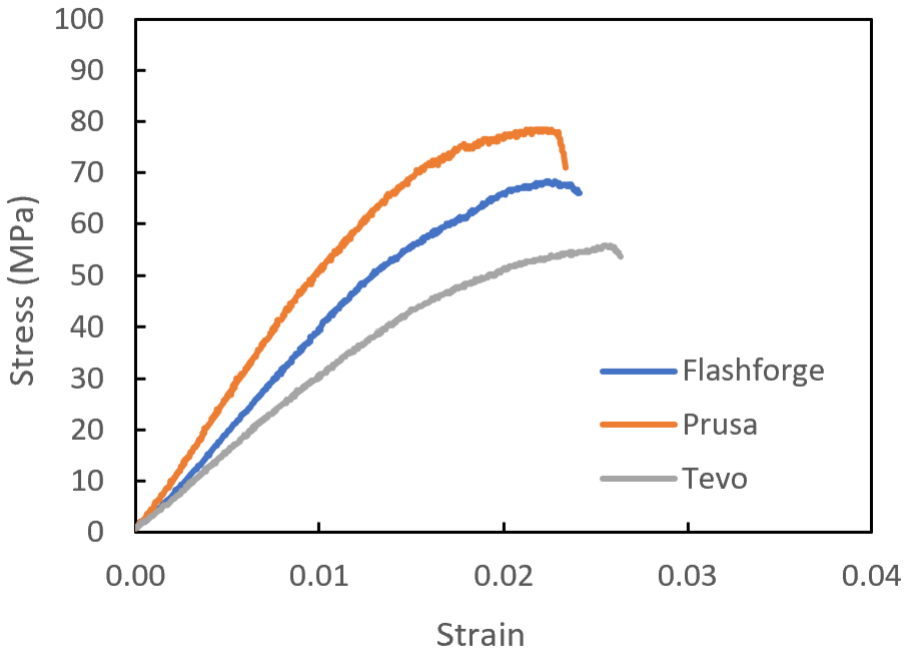

Figure 3.7: Comparisons of stress-strain curves of CF-ABS samples from different 3D printers. Samples were printed at the position IV.

3.3.1 Stress-strain curves of CF-ABS composites from different printers

In 3D printing, a solid is first drawn in the form of a CAD model and saved as a STL file. The model is then sent to a 3D printer where it is digitally "sliced" by the slicer software into many horizontal layers. On each layer, the slicer generates the digital instructions (paths) for the 3D printer nozzle to deposit the filaments. Most 3D printer slicing software are equipped with the default printing method, the "Rectilinear" printing path, which may not yield the best quality of parts. To examine the effect of the orientation of filaments (and fibers), the slicing codes used for the present three printers were modified to allow the extruders to print the "linear" paths. These would cause all the strands of infill material to be oriented along the printing bed at a user-inputted angle and thus aligning the reinforcing fibers. New samples were produced using the same print settings as before, except an oriented linear infill was utilized instead. The samples were printed in batches of six samples each with

a different infill orientation with respect to the build surface. The infill orientations would vary from being aligned to the length of the rectangular specimens (0-degree) and increase in misalignment by 15-degree until perpendicular with the sample. The samples are then tested in bending and the resultant stress-strain curves are shown in Figure 3.8. It is seen that the stress-strain responses of the samples would decrease with increasing misalignment of the fibers with respect to the loading conditions.

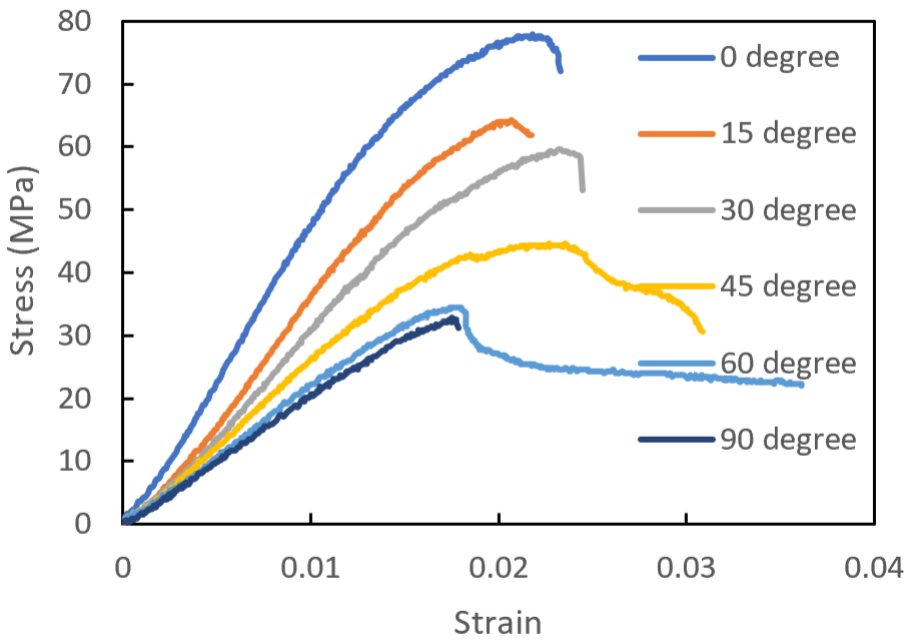

Figure 3.8: Stress-strain behaviors of oriented CF-ABS samples from bending test. Samples are printed from the Flashforge 3D printer.

Figure 3.9 is a comparison of the CF-ABS parts produced by 3D printing with default printing path (Rectilinear) and with modified printing paths (Linear). It is seen that the parts obtained at the optimal printing (0-degree) and the worse printing (90-degree) would serve as the upper and lower bonds and that the parts printed by using the default method would fall in between these bonds. This indicates that the 3D printed parts can theoretically be "tailored" in order to achieve the "best" performance.

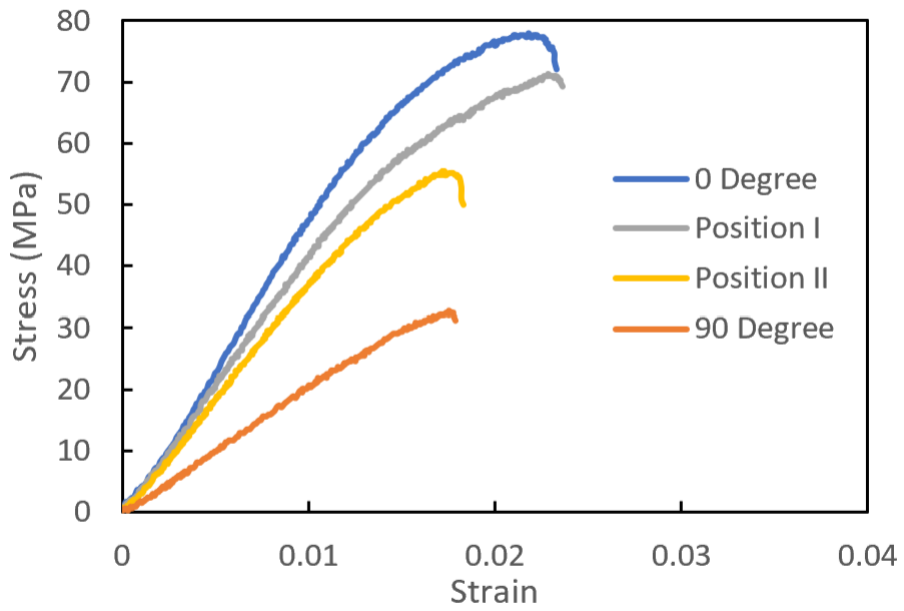

Figure 3.9: Comparison of stress-strain responses of CF-ABS composites from oriented infill samples and the default "rectilinear" samples (position I and Position II). Samples are printed from the Flashforge 3D printer.

3.3.2 Stress-strain curves of CF-ABS composites from compression molding

For comparison, the CF-ABS bending samples were fabricated by the conventional manufacturing method, i.e., the compression molding, using identical processing parameters and then tested using the same procedure as used for the 3D printed samples. To minimize any disparities, all samples were tested in the same time and in a random order. As depicted in Figure 3.10, all compression molded samples exhibit identical stress-strain responses. There is negligible variation in stress-strain curves between slow-cooled and fast-cooled samples, so the effect of cooling rate on mechanical properties is deemed to be at the minimum. Quantitative properties of the compression molded samples were estimated from the stress-strain curves.

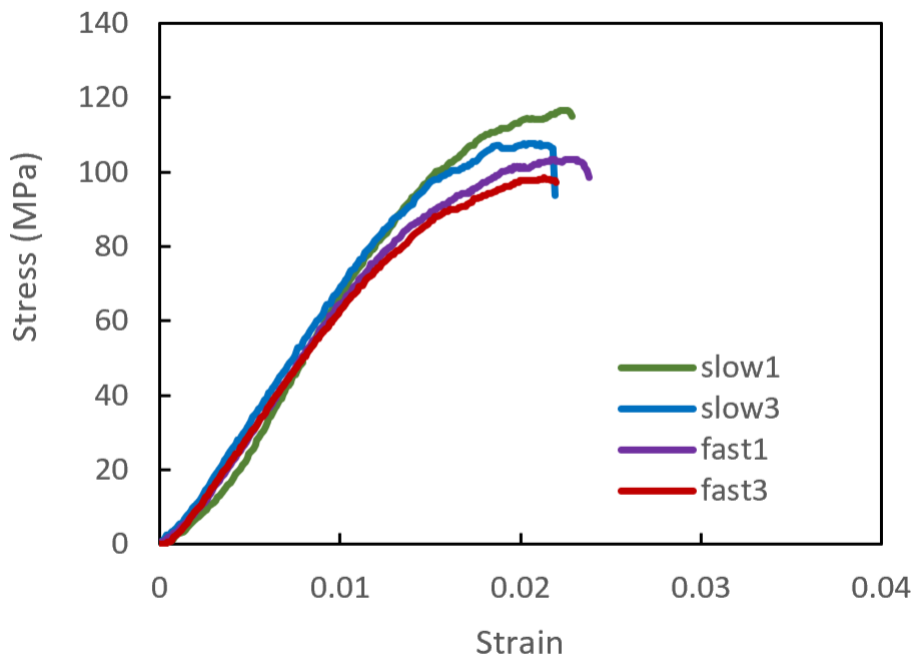

Figure 3.10: Stress-strain responses of compression molded CF-ABS composite samples.

Figure 3.11 shows the comparison of stress-strain curves between compression molded samples and 3D printed samples. For 3D printed samples, results obtained at position I were used since they represent the strongest sample from each 3D printer (Figures 3.4 & 3.5 & 3.6 & 3.7. It is seen that even the best quality samples from 3D printing fail to match those from compression molding. For example, the compression molded CF-ABS composite has a maximum strength of 116 MPa, as opposed to the averaged maximum strength of 74 MPa of the three 3D printed samples. These results support the hypothesis that the methods of manufacturing can significantly affect the properties of the finish products and that 3D printing method generally produce parts with inferior microstructure and mechanical properties to those from conventional manufacturing.

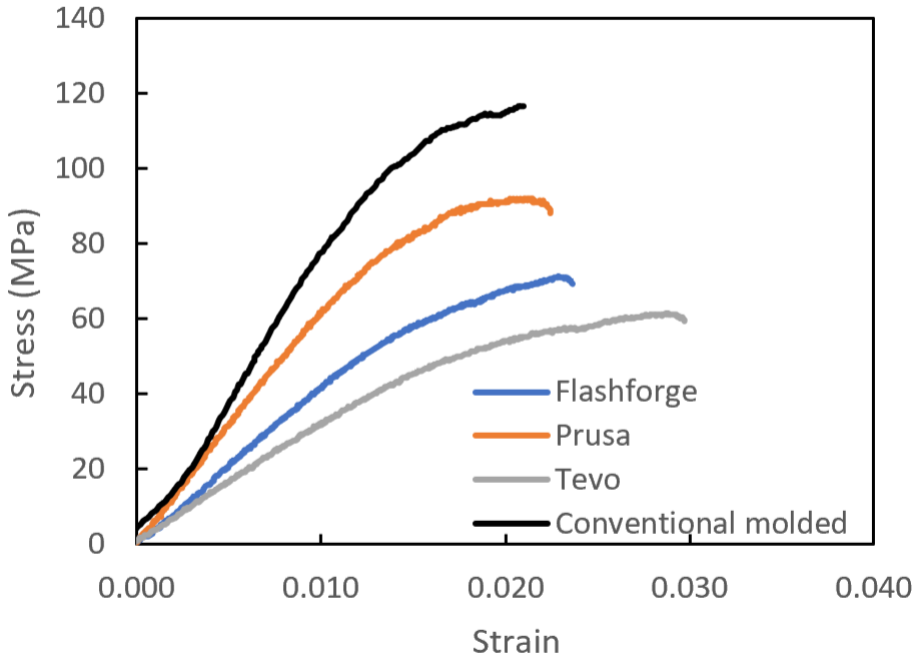

Figure 3.11: Comparison in stress-strain responses between compression molded sample (slow-cooled) and 3D printed sample from each printer (position I).

3.4 Perimeter/contour effect

When 3D printing an object one or more outlines are typically placed before the infill is distributed, this is often called the perimeter or contour of the geometry [51]. This perimeter is a single continuous strand that encompasses the geometry of the final product by first printing it outside walls. Afterwards the infill of the product is placed for the layer. While the number of perimeter walls can be modified, a minimum of at least a single perimeter is used for each layer as it can significantly improve a products mechanical properties [51–53]. Not only can it assist in distributing applied loads, its a major component of surface finish and the aesthetics of the final part [Steuben 2015]. While the layer perimeters can provide beneficial mechanical properties, when attempting to predict a products mechanical properties it simply becomes another parameter to consider. For the sake of narrowing the focus of this paper, the printer set defaults of 2 perimeters are set as the standard for current and future samples.

While adding perimeter layers does provide a more similar test piece to an industry produced product, it introduces some complications in testing methods, especially for tensile testing. The width of the extruded infill is often specified by the user and typically within ±5% the nozzle diameter for best results, while the perimeter is often in the order of 1-2 millimeters [54]. This means that the strand deposited to form the perimeter is considerably larger than the strands deposited to form the infill. This means that is the product has a relatively thin cross section, a significant portion of the cross section will be the perimeter and not the infill (Figure 3.12). For large sample testing the perimeter occupies a low percentage of the cross section, yet this percentage increases as the cross section narrows and number of infill strands deceases. Meaning mechanical testing methods with thin cross sections would be more susceptible to the mechanical effects of the perimeter versus a sample with a significantly larger cross section.

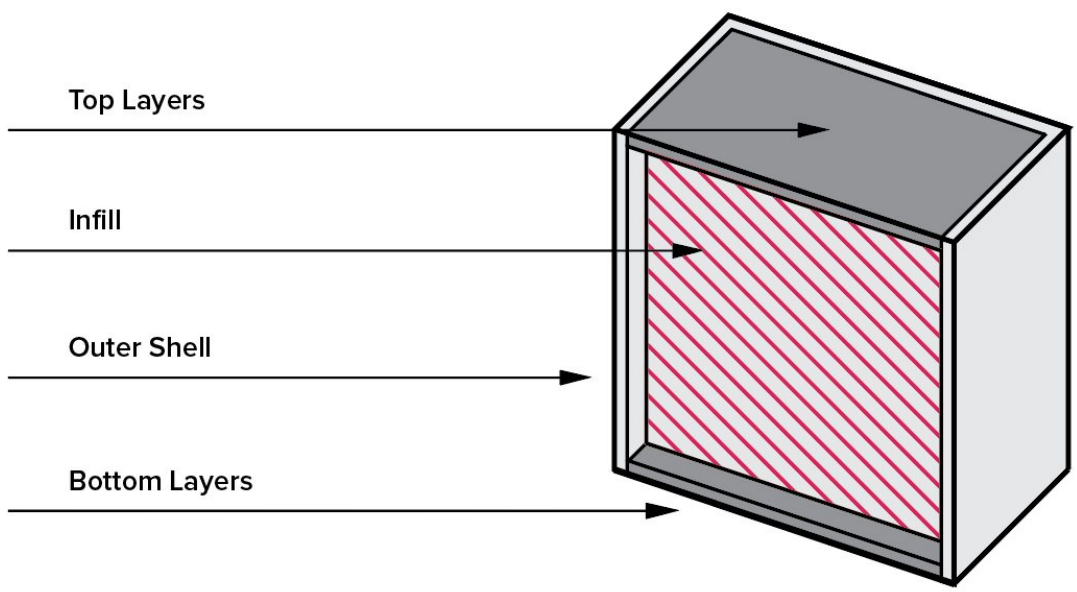

Figure 3.12: Perimeter of a 3D printed object with internal infill strands creating the bulk of the sample [5].

3.4.1 Sample testing effects

As previously mentioned the perimeter of a 3D printed object is necessary for creating products with preferable surface finishes and can affect the overall mechanical response [?, ?, ?, 53]. The severity of the effects of the perimeter/contour is then investigated using both bending and tensile testing method samples. According to Laminate Composite Theory, the mechanical properties of the composite lamina's are directionally dependant. Meaning the mechanical response of the lamina will change based on the direction the reinforcing fibers are facing. Therefore, unless the infill fibers are not facing in a direction parallel to the perimeter, the infill is going to have a different mechanical response than the perimeter surrounding it (Figure 3.13).

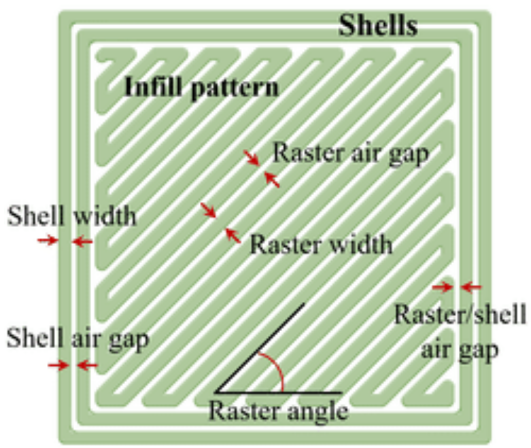

Figure 3.13: The orientation of the perimeter may not always align with the infill fiber and thus affect the products mechanical properties.

Figure 3.14 shows how the cross sectional area of a tensile testing sample can have a significant portion be taken by the perimeter versus the infill strands. LTC uses the content of the fiber compared to the content of polymer matrix to calculate the modulus of the longitudinal direction 3.1. This system of equations does have the assumption of a single uniform fiber; however, the manufacturer does not specify the length/homogeneity of the fibers. Thus these equations are used as a preliminary observation. These equations do however capture the orientation dependence

of composites. If the fiber is rotated then the fiber would no longer be aligned with the direction of loading and the modulus would change accordingly. The longitudinal modulus is written as

$$E_1 = E_f V_f + E_m V_m \tag{3.1}$$

where E_f, E_m are the modulus of elasticity of the fiber and polymer matrix respectively, and V_f, V_m are the volume fractions for the fiber and polymer matrix respectively. The volume fraction is the ratio of the volume of the material versus the final products total volume. According to the manufacturer, the fiber volume fraction of the filament is 15% and modulus for the reinforcing fiber has a tensile modulus of $\approx$ 34.5GPa. Combining these together we get that the theoretical longitudinal modulus is $\approx$ 6.840 GPa. For a sample with all fibers oriented along the length of the part, the modulus would theoretically be 6.840 GPa. We find that for a sample oriented in the transverse direction the modulus of elasticity is found using Equation 3.2 where E_T is the transverse modulus.

$$\frac{1}{E_T} = \frac{V_f}{E_f} + \frac{V_m}{E_m} \tag{3.2}$$

Using the manufacturer specified values, the transverse modulus would then be approximately 1.93 GPa. We then use a combination of our longitudinal and transverse moduli to find our approximate modulus for our entire structure. Figure 3.14 shows how the perimeter consumes a percentage of the cross sectional area and is aligned parallel with the longitudinal direction, while the infill direction can be aligned in the transverse direction. Therefore we can approximate our modulus of our final product by using the same equations as before except for longitudinal and transverse in place of fiber and polymer matrix (Equation 3.3).

$$E = E_0 V_0 + E_{90} V_{90} \tag{3.3}$$

Where E is the final products modulus, E_0 is the transverse modulus and $E_9 0$ is the transverse modulus.

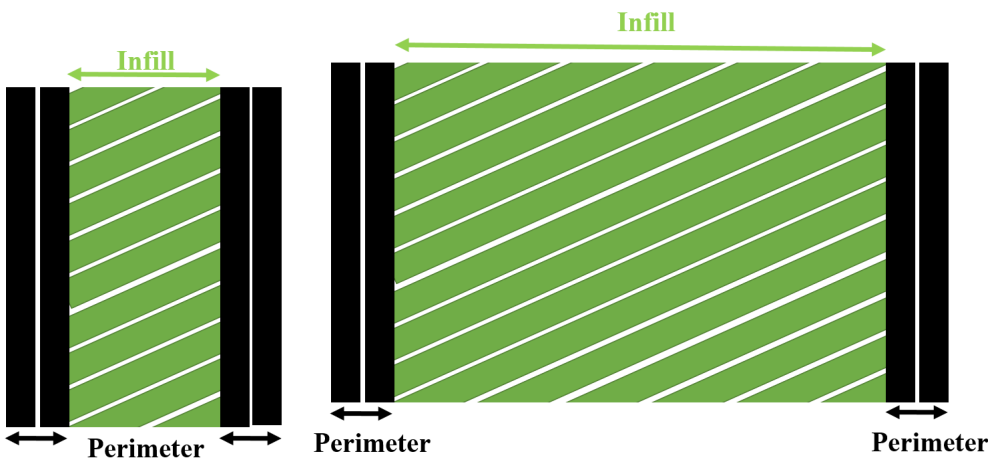

Figure 3.14: Difference in perimeter cross sectional area percentage between a tensile (left) and bending (right) test specimen.

To compare the theory to experimental testing, the same dimensions of the bending specimens are used with the consideration of two 0.5mm thick perimeter walls. By assuming a uniform cross section, we can use the cross sectional area fractions to approximate the volume fraction of the fiber/matrix. With the sample having a width of 15mm and 1mm of perimeter for each side, the infill dictates 87% of the fiber orientation, while the perimeter dictates the remaining 13%. Plugging these values into Equation 3.3 we get our total final modulus to be approximated as 6.84 GPa when both infill and perimeter are oriented in the direction of loading. For the perimeter being oriented but the infill being orthogonal in the transverse direction, the modulus decreases to 2.57 GPa. For a tensile sample the total width would be closer to 3mm where as the perimeter would still consume 1mm of the cross section on each side of your sample. Thus the infill would only control 33% of the cross sectional area and your transverse infill modulus would give a final product with a modulus of 5.22 GPa. While this is a higher value than the bending samples and would be the smarter design choice for this specific geometry, the tensile test samples simply fail to capture the effects of the infill orientation changes due the perimeter strands taking a significant portion of the cross sectional area.

To test this hypothesis, dog-bone shaped tensile samples were produced and tested

following the same notation as the bending samples. The dog-bone center sections were a 3mm $\times$ 6.5mm cross section and were 82mm long. The samples were clamped on both ends and pulled until failure occurred. The stress was calculated using Equation 3.4 and the strain was calculated using Equation 3.5.

$$\sigma = \frac{F}{A} \tag{3.4}$$

$$\epsilon = \frac{\delta L}{L} \tag{3.5}$$

Where σ is the stress, ϵ is the strain, F is the force recorded by the load cell, A is the cross sectional area, δL is the change in length and L is the initial length. The results of the tests are plotted below in Figure 3.15 and showed not noticeable correlation. As Figure 3.16 shows, the modulus has not direct correlation for the angles tested and there seemed to be a high variation is results. The 90 degree samples seemed to vary especially so which can be caused by the fiber becoming less oriented. With the unoriented fiber, the perimeter layers would be doing the majority of the work but the values simply appear to be too unstable.

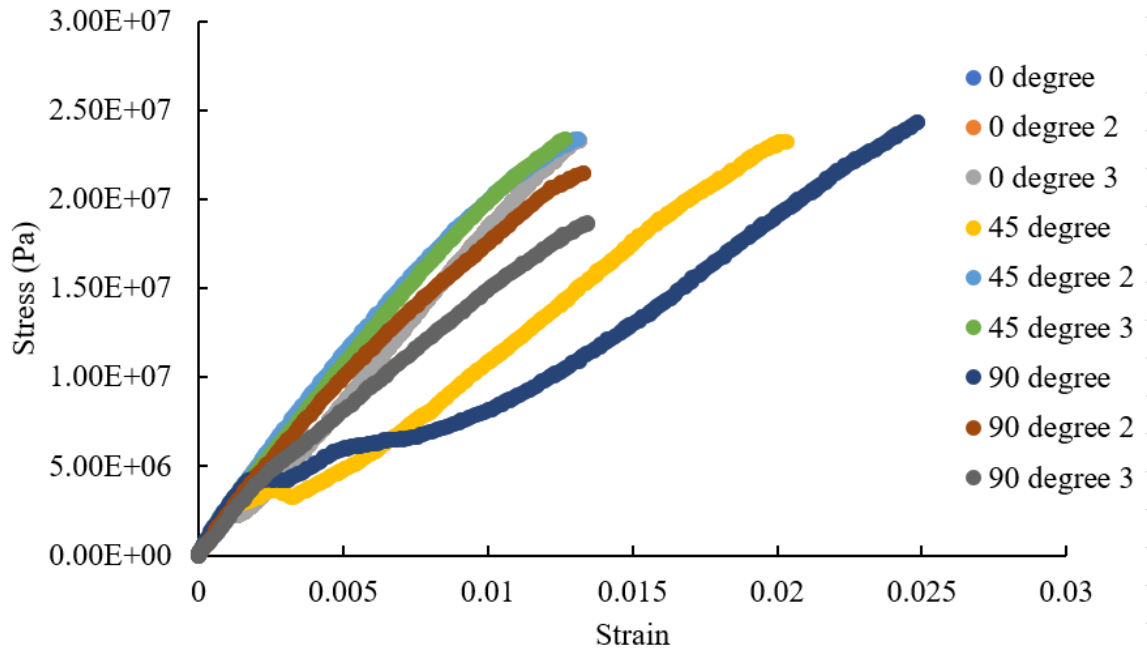

Figure 3.15: Recorded experimental data for carbon fiber reinforced tensile samples.

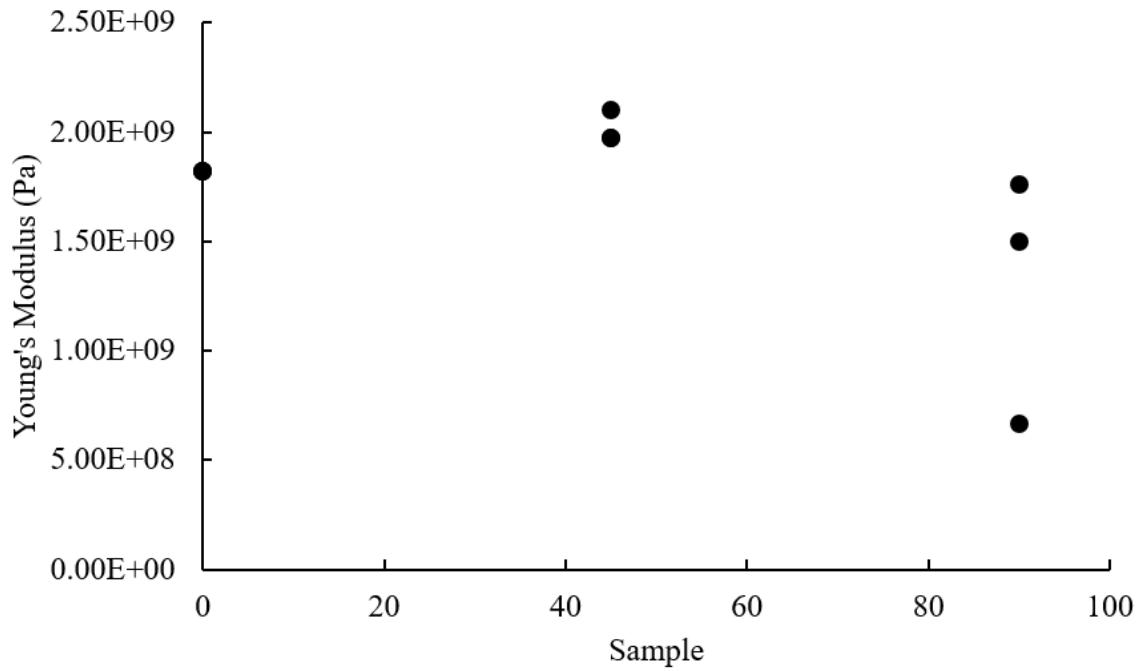

Figure 3.16: Modulus of elasticity calculated for each tensile test sample recorded showing no trend and high variance in values.

Comparing the theoretical results with the data collected from the experimental tests, it was found that the bending test predictions were 25-28% above the experimental values consistently. The tensile samples on the other hand had completely different values ranging from a 70-85% difference to the predicted values. This is mainly attributed to the nature of the perimeter layers dominating the total mechanical response. It should be noted that although the values were vastly different from the predicted results, the experimental result averages only varied by a maximum of 10%. This means that the orientation of the infill strand had very little effect on the total mechanical response, which the model predicted for the tensile responses. The magnitude changes and variance are likely due to the small areas and samples needed for tensile testing. The slightest imperfection due to the artifacts of 3D printing would be emphasized as the voids would be proportionately larger.

3.4.2 Recorded differences in sample types

It has also seen in previous studies that the use of tensile testing specimens also tend to give significantly brittle responses compared to their bending counterparts. This is shown using data from a 3D printed polymer-only study conducted previously [55]. Both sample sets used the same 3D printer, filament, and testing apparatus to study the affects of the direction of extrusion. From this study it was found that the tensile testing samples had brittle responses and rarely captured any ductile behavior. Figures figs. 3.17 to 3.19 show data from multiple sets of 3D printed tensile samples. These samples were printed in batches containing multiple orientations with each sample in a batch printed simultaneously. The cross section of the samples were printed with the nominal dimensions of 2mm width, 3mm thickness, and 40mm length. The data showed that the samples with aligned fibers to the direction of tensile loading (0°) had the most preferable mechanical properties and showed the most ductility.

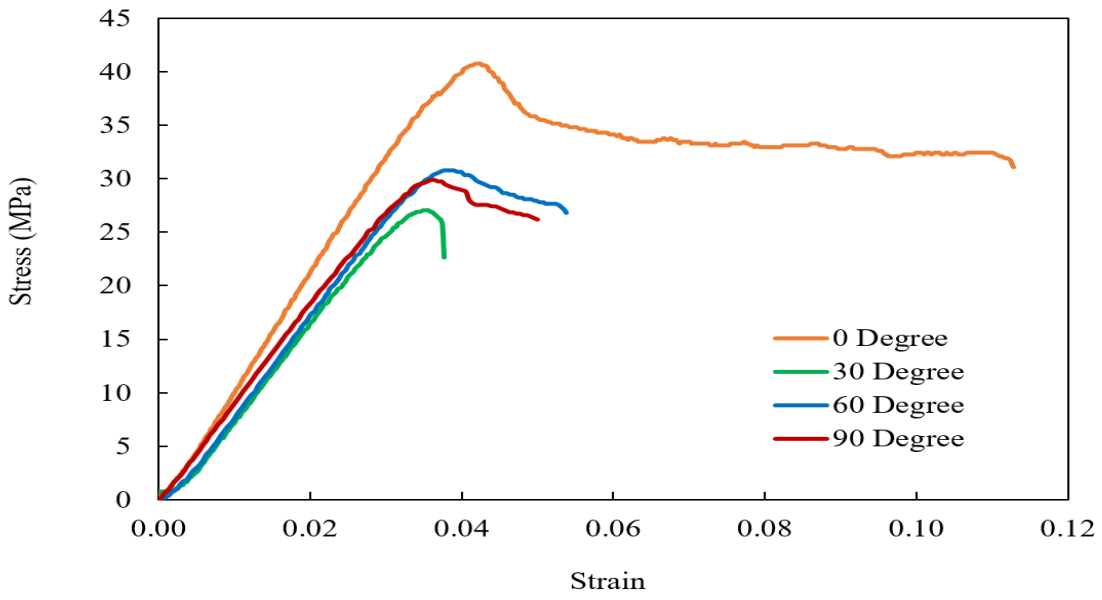

Figure 3.17: Stress/strain results for polymer only samples of batch 1 tested using the tensile testing method.

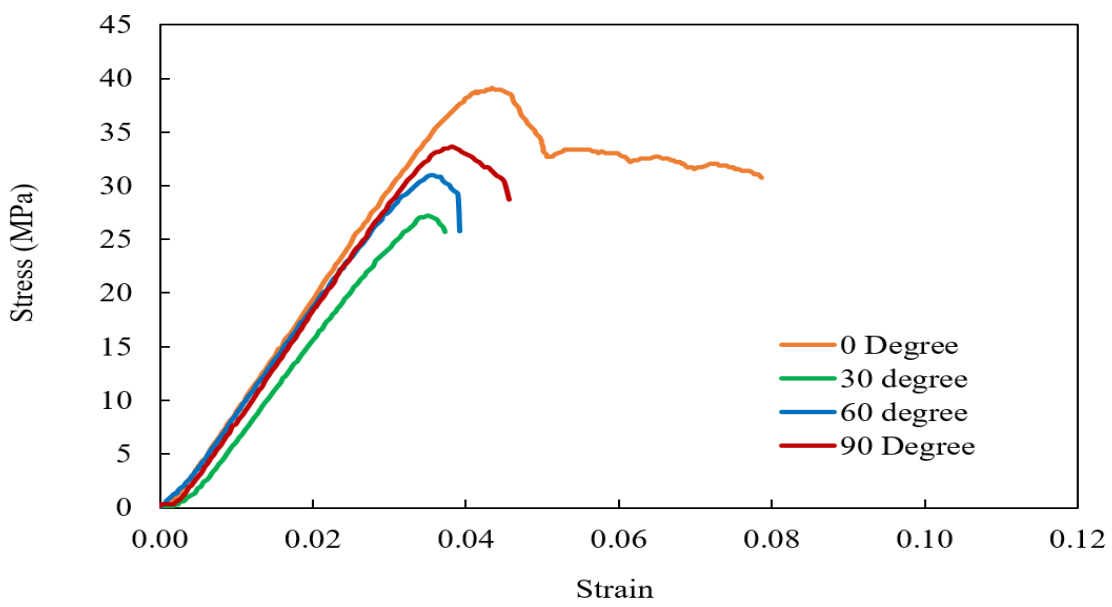

Figure 3.18: Stress/strain results for polymer only samples of batch 2 tested using the tensile testing method.

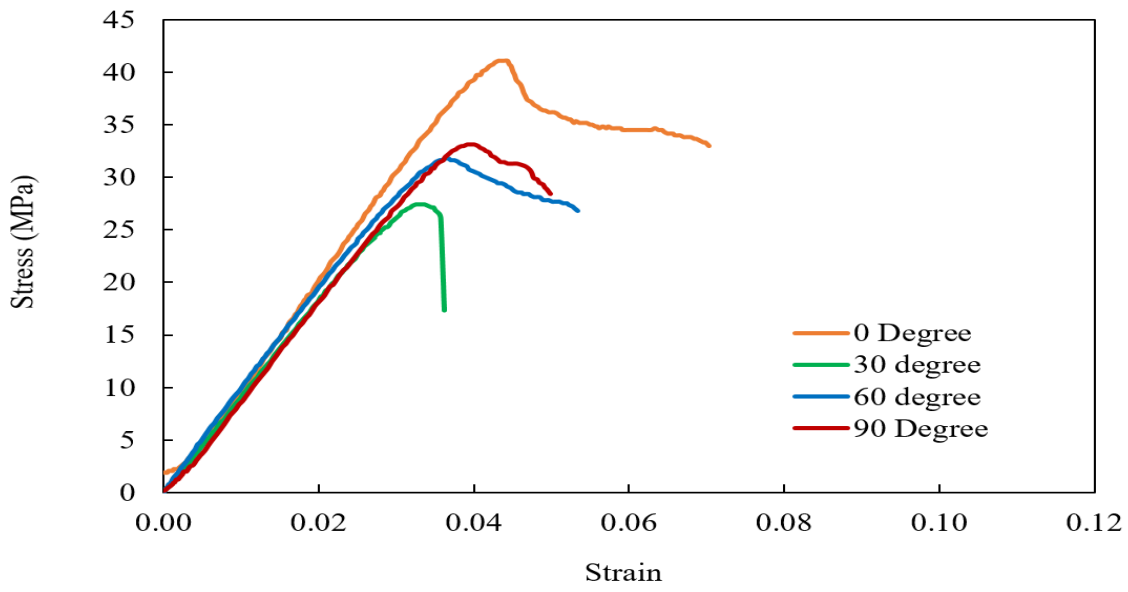

Figure 3.19: Stress/strain results for polymer only samples of batch 3 tested using the tensile testing method.

The bending samples shown in Figures figs. 3.20 to 3.22 were produced with nominal dimensions of 15mm width, 3mm thickness and 75mm length. It was shown for these samples that the plasticity of the samples is more accurately captured than the tensile samples. Even the 0 degree samples from the tensile testing samples did not capture as much of the plastic deformation present in the bending tests. This is attributed to the bending samples being able to gradually fail when being subjected to an increasing load while the tensile samples would abruptly fail. This is also attributed to the increasing importance of the perimeter effect previously mentioned. Considering the addition of brittle reinforcing fibers for 3D printed composites, the bending style of testing would be more applicable to capture a more total response when compared to tensile testing samples. As such bending tests are used for further investigation of the mechanical properties for 3D printed composites.

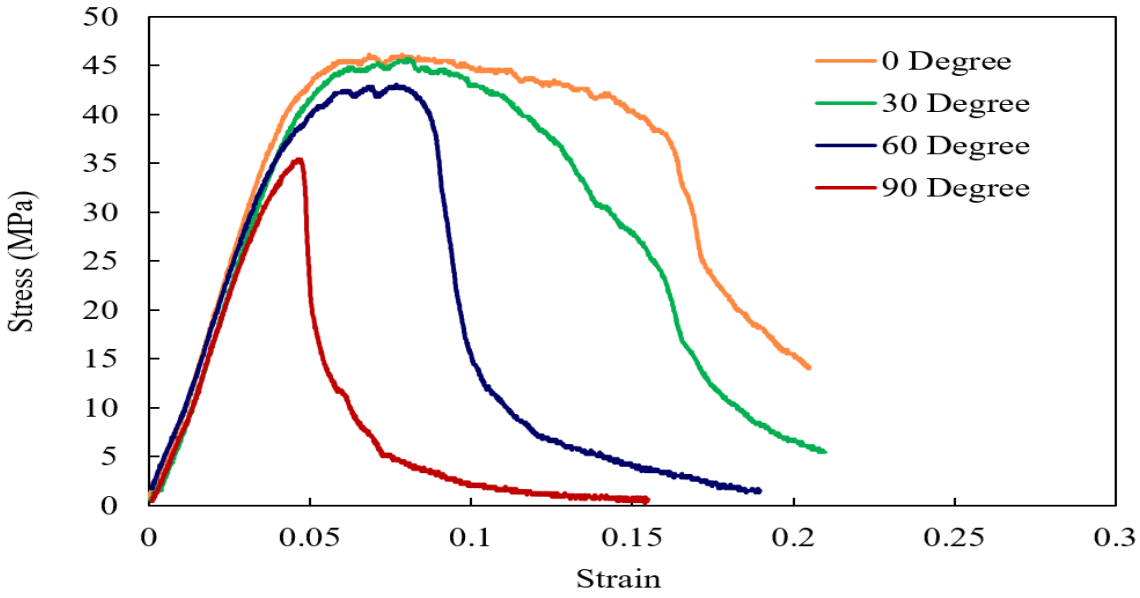

Figure 3.20: Stress/strain results for polymer only samples of batch 1 tested using the bending testing method.

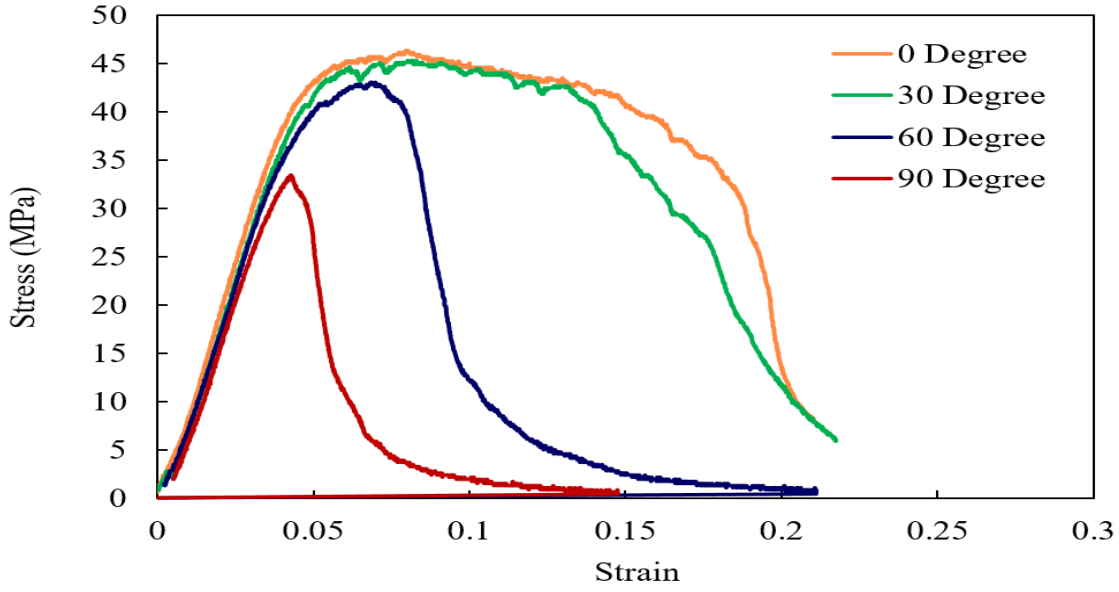

Figure 3.21: Stress/strain results for polymer only samples of batch 2 tested using the bending testing method.

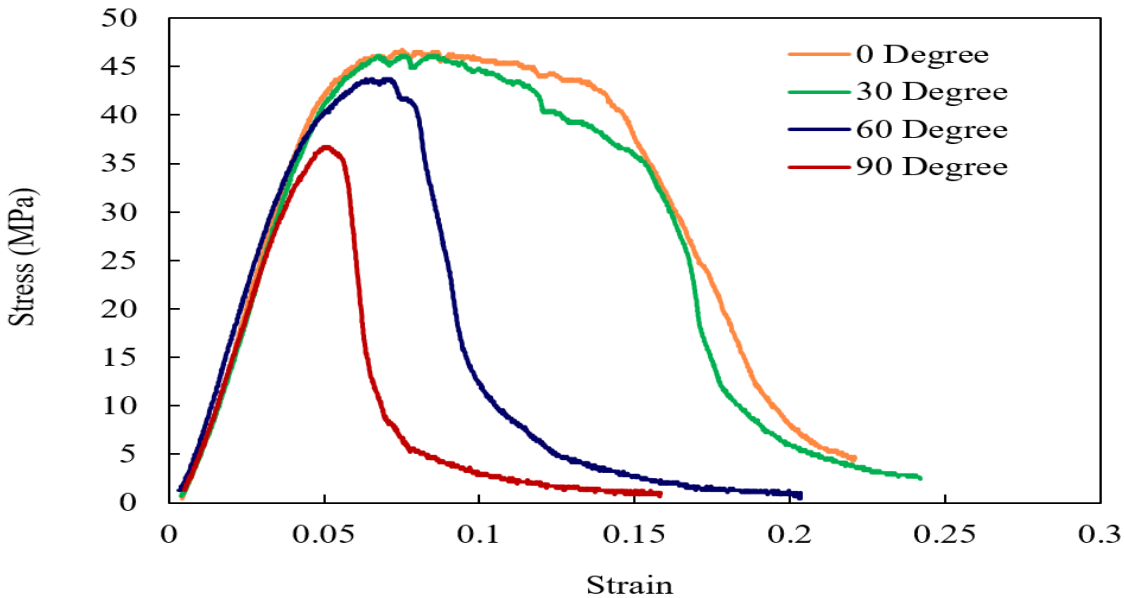

Figure 3.22: Stress/strain results for polymer only samples of batch 3 tested using the bending testing method.

3.5 Theoretical analysis of mechanical properties of 3D printed fiber composites

The orientation dependent mechanical properties of a 3D printed composite may be analyzed by using the theory for laminate composite [**?**]. As 3D printers produce parts by creating layers of linear strands of melted plastic, laminate composites are created by stacking up multiple individual laminas (or layers) at different orientations [**?**]. The strain-stress relation of an arbitrarily oriented layer in a composite may be described through the compliance matrix S (Equation 3.6).

$$\begin{Bmatrix} \epsilon_{xx} \\ \epsilon_{yy} \\ \gamma_{xy} \end{Bmatrix} = \begin{bmatrix} S_{xx} & S_{xy} & S_{xs} \\ S_{yx} & S_{yy} & S_{ys} \\ S_{sx} & S_{sy} & S_{ss} \end{bmatrix} \begin{Bmatrix} \sigma_{xx} \\ \sigma_{yy} \\ \tau_{xy} \end{Bmatrix} \tag{3.6}$$

where $S_{xx}, S_{yy}, S_{ss}, S_{xs}(S_{sx})$ and $S_{ys}(S_{sy})$ are the compliance components, defined by the following set of equations 3.7.

$$
\begin{aligned}
S_{xx} &= m^4 S_{11} + n^4 S_{22} + 2m^2 n^2 S_{12} + m^2 n^2 S_{66} \\
S_{yy} &= n^4 S_{11} + m^4 S_{22} + 2m^2 n^2 S_{12} + m^2 n^2 S_{66} \\
S_{xy} &= m^2 n^2 S_{11} + m^2 n^2 S_{22} + (m^4 + n^4) S_{12} - m^2 n^2 S_{66} \\
S_{xs} &= 2m^3 n S_{11} - 2mn^3 S_{22} + 2(mn^3 - m^3 n) S_{12} + (mn^3 - m^3 n) S_{66} \\
S_{ys} &= 2mn^3 S_{11} - 2m^3 n S_{22} + 2(m^3 n - mn^3) S_{12} + (m^3 n - mn^3) S_{66} \\
S_{ss} &= 4m^2 n^2 S_{11} + 4m^2 n^2 S_{22} - 8m^2 n^2 S_{12} + (m^2 - n^2) S_{66}
\end{aligned}
\tag{3.7}
$$

Where $m = cos\theta$, $n = sin\theta$, and θ is the orientation angle of the filament.

Constants S_{11}, S_{22}, S_{12}, and S_{66} can be directly computed from the fundamental material properties, E_{11}, E_{22}, G_{12} and ν_{12} [47].

$$
S_{11} = \frac{1}{E_{11}}, S_{22} = \frac{1}{E_{22}}, S_{12} = S_{21} = \frac{-\nu_{12}}{E_{11}}, S_{66} = \frac{1}{G_{12}} \tag{3.8}
$$

In Equation 3.8 the longitudinal modulus (E_{11}) would correspond to the modulus of elasticity of the 0-degree oriented sample and the transverse modulus (E_{22}) would correspond to the 90-degree orientation sample. The shear modulus (G_{12}) is hard to measure experimentally, but can be determined through the relationship of the fundamental material properties measured in tension (Equation 3.9)

$$
G_{12} = \frac{1}{\frac{4}{E_{45}} - \frac{1}{E_1 1} - \frac{1}{E_{22}} + \frac{2\nu_{12}}{E_{11}}} \tag{3.9}
$$

where the E_{45} would correspond to the modulus of elasticity of the 45-degree oriented sample. From Figure 3.8 and Equation 3.9, material constants of typical CF-ABS are obtained: E_{11}=5058 MPa, E_{22}=1883 MPa, G_{12}=1236 MPa. The major Poisson's ratio was obtained from literature [44], ν_{12}=0.34. Rearranging Equation 3.6, the axial modulus of an arbitrarily oriented CF-ABS composite may be computed

$$
E_{xx} = \frac{1}{S_{xx}} \tag{3.10}
$$

Figure 3.23 shows that the axial modulus (E_x) of a 3D printed composite highly depends upon the filament orientation (θ). Experimental results obtained from Figure 6 are also plotted against the theoretical predictions and consistent trend is observed. The composite printed at unidirectional, with 0-degree orientation would have the optimal performance while the composite printed at unidirectional, with 90-degree orientation would have the worst performance. Composites printed with any other angle ($0° < \theta < 90°$) or at any other ply arrangement (e.g., angle-ply laminate) would have the modulus fall in between these two limits.

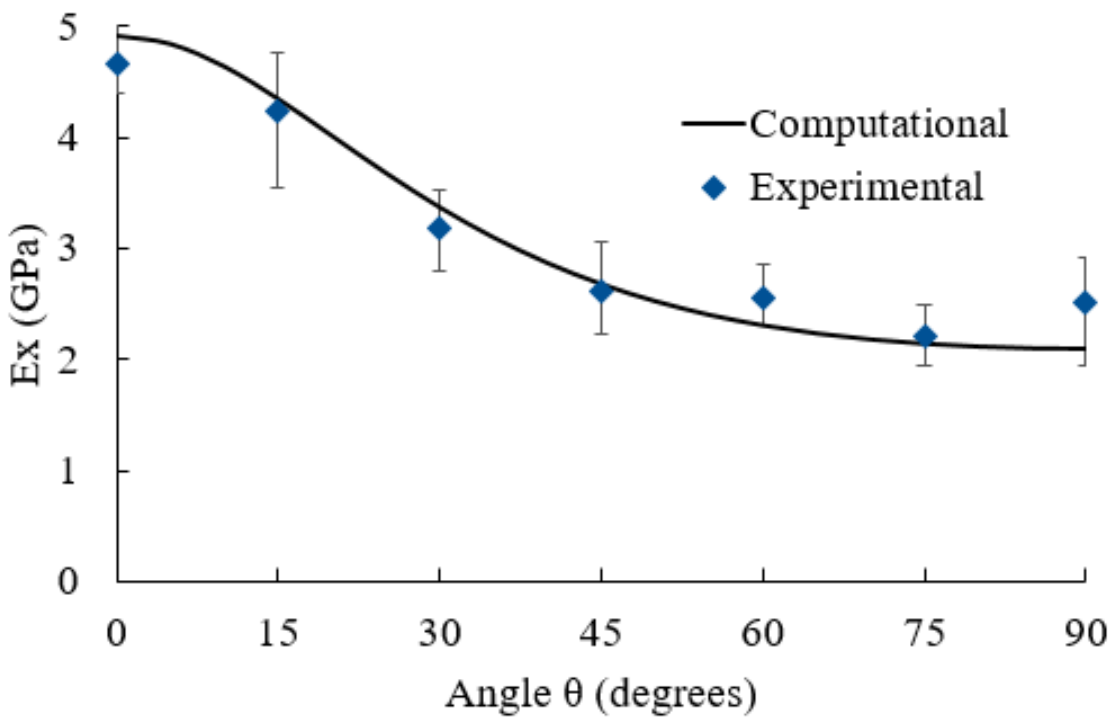

Figure 3.23: Variation of axial modulus of CF-ABS composite as a function of filament orientation angle.

The default "Rectilinear" infill pattern used by most 3D printers consists of linear patterns with an alternating 90°angle and thus is essentially an [±45] angle-ply composite. The modulus of a composite at such arrangement is known to be polymer matrix-dominated since it depends primarily on its in-plane shear modulus of the individual layer [47]. To maximize the strength of reinforcement fibers, alternative

laminate configurations are needed. These findings indicate that the 3D printing process needs to be properly "designed" or "tailored" by using the laminate composite theory. By designing the right printing directions of each strand and the proper configurations of each layer, the optimal microstructure and thus the optimal mechanical properties of the composite can be achieved.

3.6 Conclusion

While 3D printing may seem to be an attractive option for producing short fiber composites quickly and inexpensively, it can introduce microstructure complexities not found in traditionally manufactured parts. In this study, CF-ABS composites have been fabricated through 3D printing and compression molding. The 3D printed sample results show that using the default slicing software settings the mechanical properties can change not only due to which 3D printer is used but how the sample is oriented along the printing bed. The results also show that even the best samples obtained by 3D printing methods fail to meet the mechanical properties of samples produced by conventional compression molding technique. With modifications to the slicing software parameters the material infill can be changed to a linear infill and orient the reinforcing fibers within the part. Just as predicted using the laminate composite theory, the mechanical properties of 3D printed composites highly depend upon the orientation angle of individual strand and the arrangement of individual layer. This implies that the printing codes (printing directions) used in 3D printers can be properly "designed" and "tailored" by following the laminate composite theory so that the optimal microstructure and mechanical properties may be achieved.

Copyright© Jordan Garcia, 2023.

Chapter 4 ANISOTROPIC BEHAVIOR OF 3D PRINTED SHORT FIBER COMPOSITES – DYNAMIC MECHANICAL PROPERTIES

3D printing (or additive manufacturing) allows for rapid production of engineering parts when compared to other more traditional composite manufacturing methods such as compression/injection molding or hand layups for that require expensive molds and possibly high labor costs [6–12]. The 3D printing process consists of a spool of filament material being fed into a heated extrusion nozzle. This process of using a heated extruder could use a wide range of thermoplastic filament materials. The filament material is melted and deposited on a print bed in layers to form the product as seen in Figure 4.1. These layers typically consist of continuous strands placed along another in a specified pattern. The distance between the strands of material that make the layers is directly associated with the infill density and part quality. The quality of a print can be edited via user input to produce smaller layers at the cost of more production time. The smaller layers assist the printer to better capture the geometries of the desired part. The patterns in the material also vary based on user input such that it can be optimized for strength or production speed. The movement of the filament strands is controlled by a combination of controllers typically a motor driven belt or screw mechanism moving either the extrusion head and/or the entire build plate. 3D printing process has been increasingly used for fabricating fiber composites as it is an automated fabrication process with high design flexibility. However, the reinforcing fibers used in 3D printing can become highly oriented due to the shearing forces between the fibers and nozzle wall when extruded [14, 15, 56]. These build orientations can have significant impacts on the properties of 3D printed parts. Recent investigations [57, 58] have revealed that the build orientation can greatly affected the final properties and ultimately the performance of parts. It was reported that the composites built in different orientations exhibit significant

anisotropic behavior [59,60], in addition to affecting the printing quality and printing time [61, 62]. So far, all studies on the anisotropic behaviors of 3D printed fiber reinforced composites have been focused on the static aspect. There has been no report on the anisotropic mechanical behaviors from the dynamic point of view. The current paper will investigate the dynamic properties of 3D printed fiber composites through experimental testing and computational modeling. Carbon-fiber reinforced acrylonitrile butadiene styrene (CF-ABS) composites will be fabricated at various printing configurations. The composites will be tested under dynamic loading and the resultant mode frequencies and modal shapes will be examined as a function of printing orientations.

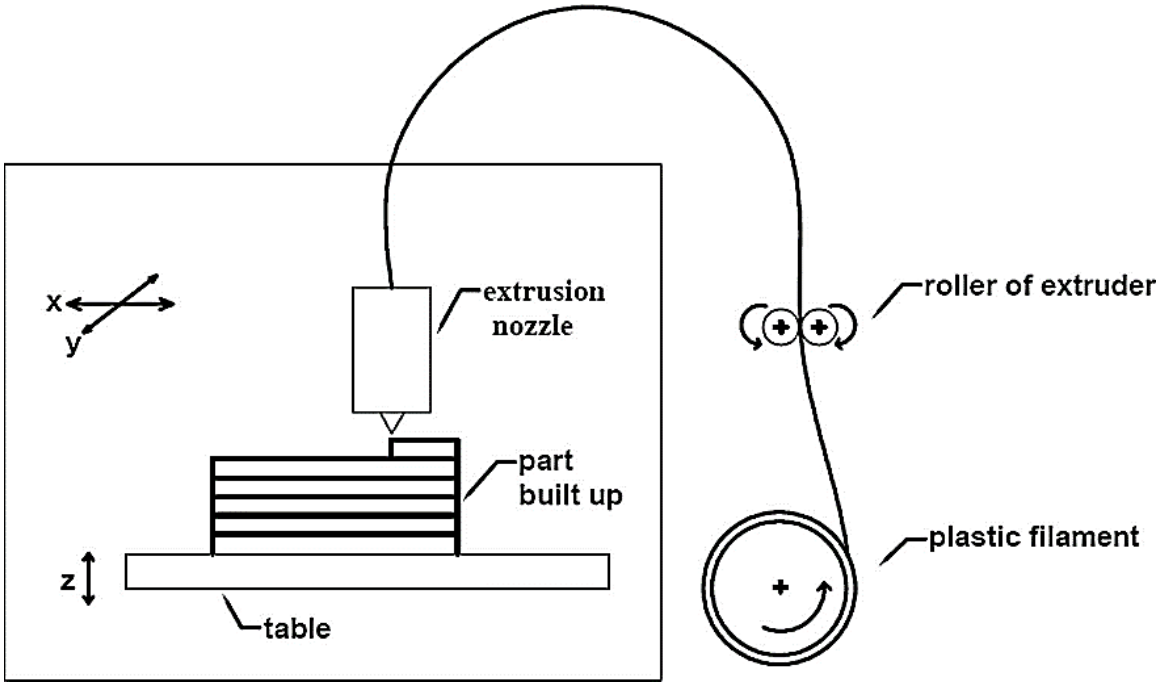

Figure 4.1: Sketch of a typical 3D printing process of a fiber reinforced polymer composite. The fiber filled polymer is extruded through a nozzle and then laid down as successive layers to form a composite. [?]

4.1 Materials and procedures

4.1.1 Materials and samples

For the experiments, the material used consisted of acryloni-trile butadiene styrene (ABS) reinforced with short, aligned carbon-fibers (CF) in the form of wires. The filament was purchased from 3DXTECH in 1 Kg spools, with a manufacturer specified nominal fiber content of 10%. For the experiments, the material used consisted of acryloni-trile butadiene styrene (ABS) reinforced with short, aligned carbon-fibers (CF) in the form of wires. The filament was purchased from 3DXTECH in 1 Kg spools, with a nominal fiber content of 10%. Rectangular plate specimens were produced using the Flash Forge Dreamer 3D printer equipped with a slicer software Flashprint. The models for these samples were created and exported into .STL files using the CAD software SolidWorks by Dassault Systems. The rectangular plate specimens would be designed with the nominal dimen-sions of 15 mm x 75 mm x 3 mm (thickness) in SolidWorks and then the .STL file would be imported by the slicing software for printing. The slicing software would then "slice" the 3D model into a series of horizontal layers and then decon-struct each layer into a series of instructions for the printer to follow (through the G-code) [21, 22]. The plate samples were printed in batches in different positions and orientations (0°, 15°, 30°, 45°, 60°, 75°, 90°), as seen in Figure 4.2. The pattern of the infill would remain as the default "Rectilinear" pattern for a 100 percent infill density to create solid parts. Left to the Rectilinear setting, the infill consisted of linear patterns with an alternating 90-degree angle for subsequent layers. The temperature of the extruded filament was set to 245 degrees Celsius, and the printing bed was set to 115 degrees Celsius as specified by the filament manufacturer to ensure adequate melting of the filament.

4.1.2 Experimental procedures

To investigate the vibrational characteristics of the 3D printed composites, modal analysis experiments were conducted. The systems engineering software LabVIEW

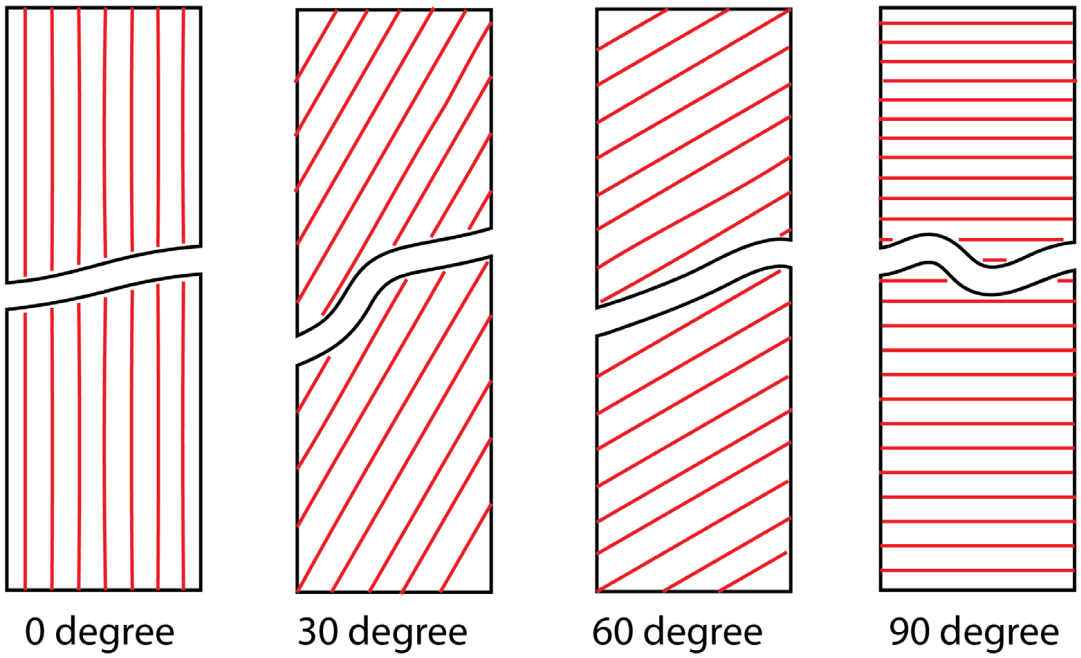

Figure 4.2: Linear infill patterns of 3D printed parts with respect to orientation angle. From left to right: 0°, 30°, 60°, 90°.

was used in conjunction with accelerometer equipment to collect the real time vibrational data (Figure 4.3). The focus of the data gathered would be the observation of the sample's natural frequencies and any relations to orientation angle or method of manufac-turing. Figure 4.3 also shows how the samples were placed in a holding system that secures the sample to ensure the edges are fixed. Using beeswax, the accelerometer was adhered to the center of 3D printed sample. Controlled impacts were administered to the samples and the vibrational responses were then recorded and exported for post processing. The data from these experiments would provide repeating peaks at the same frequencies despite the location of the impact/accelerometer. Similar to a tuning fork used as a resonator, the resonant frequencies from these impacts would provide the modal frequencies of the structure [63]. Both the time and frequency spectrums of the vibrational responses were recorded, from which the resonant frequencies of the samples were identified. The samples used for gathering vibrational data varied in multiple aspects: geometry, orientation, and material.

For geometry, the samples were printed in a rectangular shape (15 mm $\times$ 75 mm $\times$ 3 mm (thickness)). The samples would also vary in how the infill of the samples were oriented with respect to the boundary conditions (0°, 15°, 30°, 45°, 60°, 75°, 90°). Testing would then vary on which sides of the sample were clamped to create a fixed boundary condition while the other sides are either free to move or fully flexed. Finally for the material selection, both pure ABS filaments and carbon-fiber reinforced ABS filaments were used to produce composite samples.

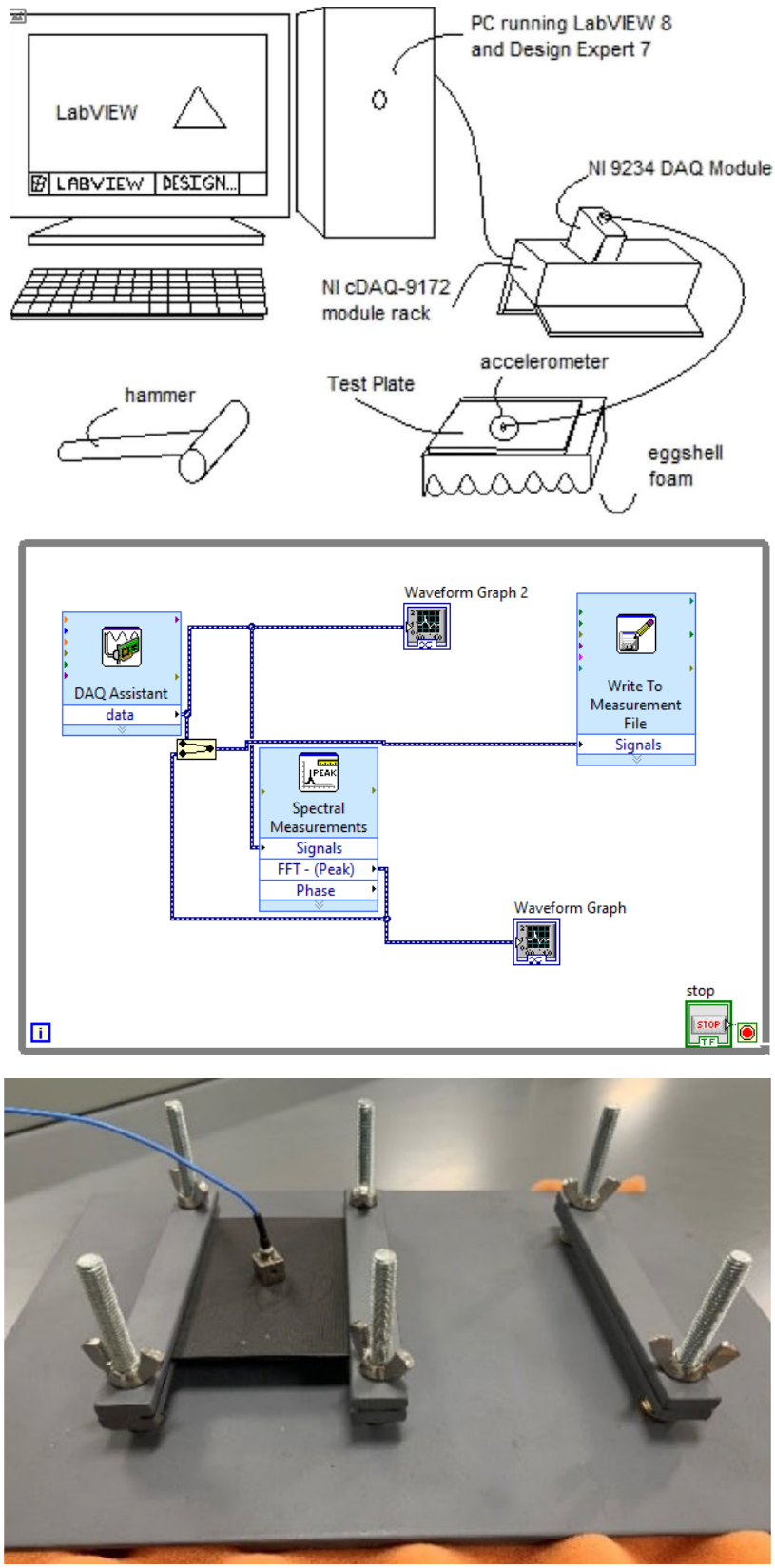

Figure 4.3: Dynamic testing of carbon-fiber composite plates: (Top) Schematic diagram of the experimental modal testing; (Middle) LABVIEW block diagram used for generating the time and frequency spectrums; (Bottom) Sample setup in the dynamic test.

4.2 Computational procedures

To comprehensively investigate the vibrational characteristics, particularly the modal shapes of the 3D printed samples, the computational modal analysis was further conducted. ANSYS Workbench was used for the modal analysis simulations of 3D printed objects. The geometry of the objects was created using the Design Modeler system and imported into the Ansys Composite Prep (ACP) preprocessor. In the Engineering Data component, the material constants would be inputted for the orthotropic lamina plies along with the material density. Each orthotropic ply will be used to represent a single layer in the 3D printed sample. The geometry would be imported and meshed in the model component and imported to a Modal analysis system. The loading conditions are inputted in the Setup component and desired outputs (modal frequencies) are specified in the Solution component to be exported for comparison. Finally, the results from the analysis can be viewed in the results component. A visual interface of the modeling process can be seen in Figure 4.4 where blue connections signify an importing of information from a separate system.

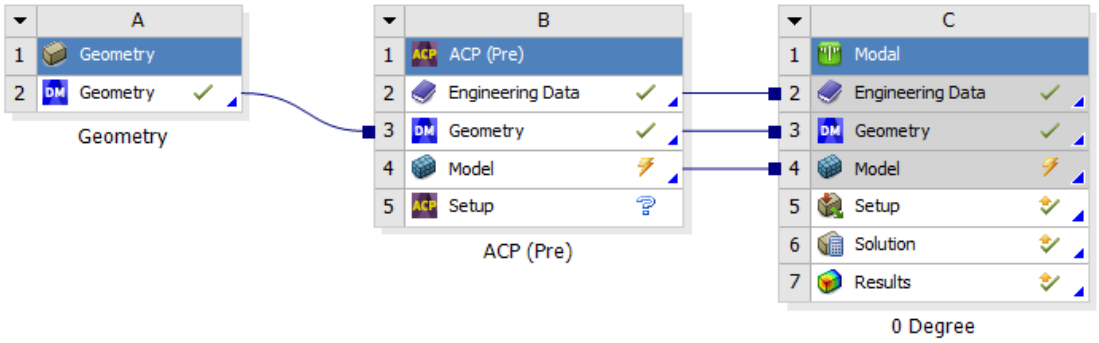

Figure 4.4: Analysis systems used in ANSYS Workbench to produce the FE model for multi-layered composites.

The finite element models use the orthotropic lamina ply properties to model the laminate composites and require the user to input the material constants specific to the material being used. The following constants were needed for both the pure

ABS plastic material as well the carbon-fiber reinforced variant: E_{11},E_{22}, ν_{22}, and G_{12}. These material constants would need to be determined through experimental testing from simple unidirectional specimens. Batches consisting of three samples with different printing directions (0°, 45°, 90°) were prepared using the pure ABS and carbon-fiber reinforced materials. The stress-strain responses of the carbon-fiber ABS composites are shown in Figure 4.5.

Using the stress-strain information gathered, the fundamental material properties can be determined through the following. The longitudinal modulus (E_{11}) would correspond to the modulus of elasticity of the 0 degree oriented sample, and the transverse modulus (E_{22}) would correspond to the 90 degree orientation sample. The shear modulus was determined using the relation of the fundamental material properties depicted by Equation 6.1. Where E_{11}^{45} is the modulus of elasticity of 45-degree composite sample, which can be obtained from the stress-strain curve in Figure 4.5. Table 1 tabulates the fundamental properties of both pure ABS and carbon-fiber reinforced ABS composite.

$$G_{12} = \frac{1}{\frac{4}{E_{11}^{45}} - \frac{1}{E_{11}} - \frac{1}{E_{22}} + \frac{2\nu_{12}}{E_1 1}} \tag{4.1}$$

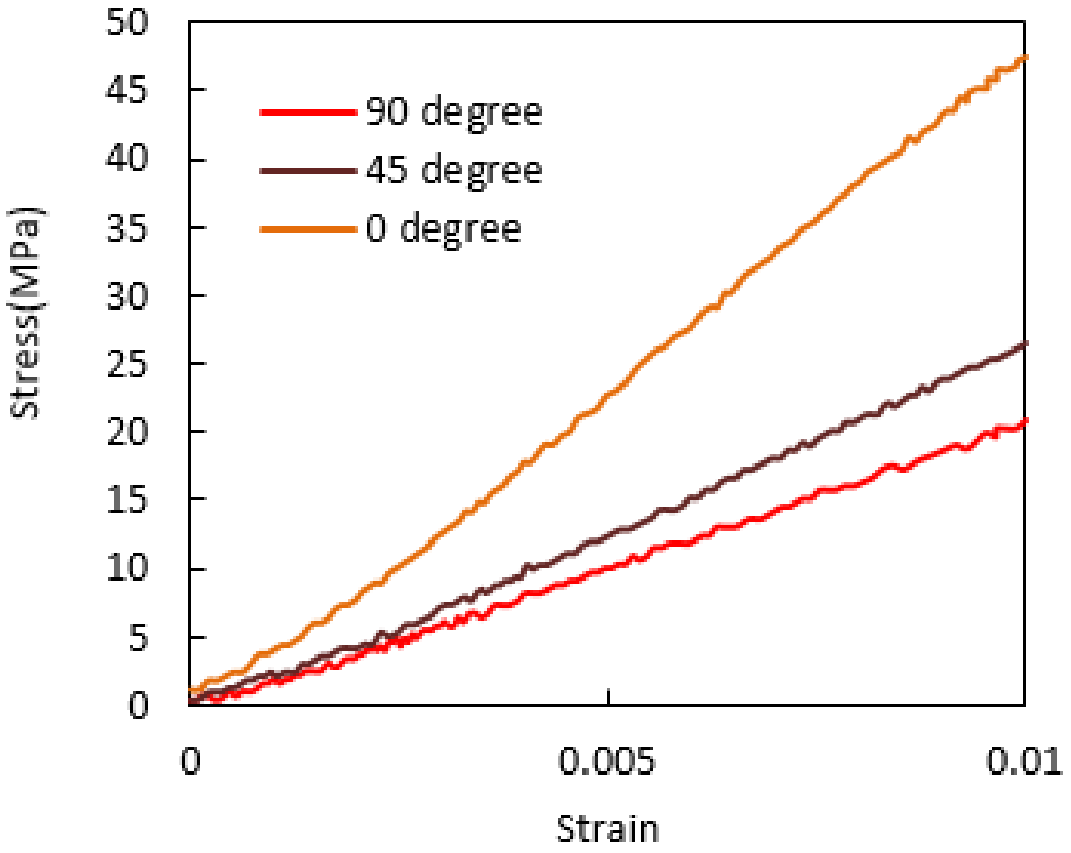

Figure 4.5: The stress strain curves of carbon-fiber ABS composites with various infill angles.

Material	Longitudinal modulus	Transverse modulus	Shear modulus	Major Poisson's ratio
Pure ABS	1256	1074	484	0.3
Carbon-fiber ABS	4919	2096	1069	0.34

Table 4.1: Summary of fundamental material properties of ABS resin and carbon-fiber ABS composite in MPa.

4.3 Results and Discussion

4.3.1 Validation of experimental method

To validate the experimental procedures, a homogeneous aluminum plate, 6" (length) × 6" (width) × 0.125" (thickness), was first examined. For a plate made of homogeneous material, the modal frequencies $f(n_x, n_y)$ and shapes $z(x, y)$ at the free-free condition are given by [24]:

$$f(n_x, n_y) = \frac{\pi}{2}\sqrt{\frac{Eh_p^2}{12\rho}}\left[\left(\frac{n_x}{L_x}\right)^2 + \left(\frac{n_y}{L_y}\right)^2\right] \tag{4.2}$$

$$z(x, y) = A\sin\left(\frac{n_x \pi x}{L_x}\right)\sin\left(\frac{n_y \pi y}{L_y}\right) \tag{4.3}$$

With the following nomenclature:

E - Young's modulus

h_p - plate thickness

ρ - mass density/unit volume

n_x - x mode index (number of half sine waves along x-axis)

n_y - y mode index (number of half sine waves along y-axis)

L_x - plate width in x direction

L_y - plate width in y direction

Using Equation 4.2, the first and second modal frequencies of the homogeneous aluminum plate are computed as: $f(1, 1) = 680$ Hz and $f(2, 1) = 1369$ Hz. Using Equation 4.3, the corresponding mode shapes are plotted as shown in Figure 4.6, which show the mode indices (n_x,n_y) are (1,1) and (2, 1) for the first and second modes, respectively.

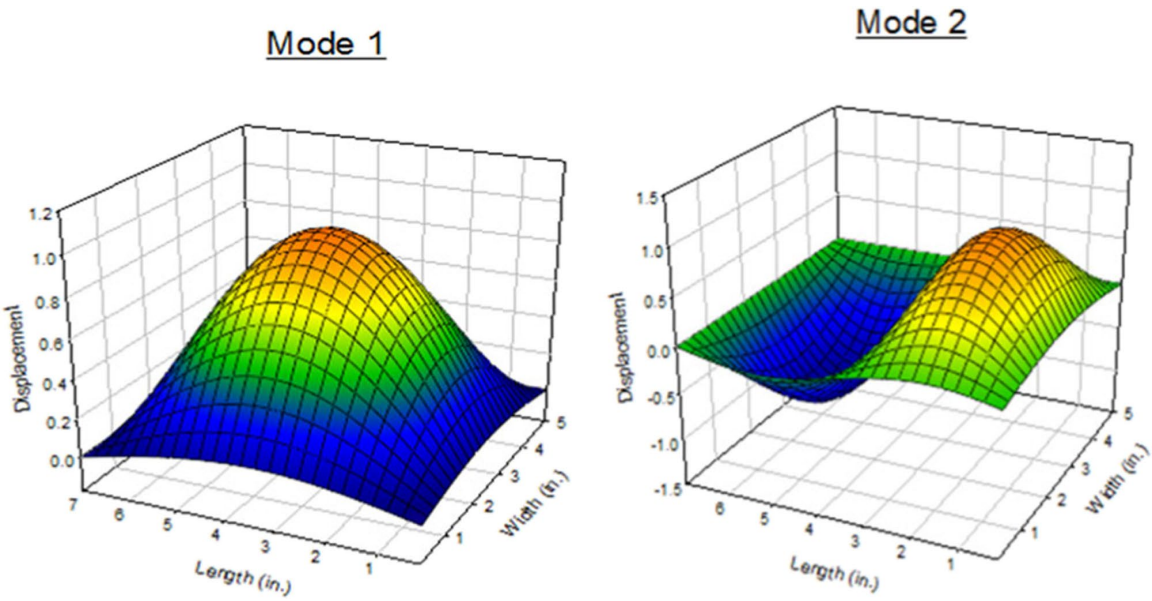

Figure 4.6: Plots of the first (left) and second (right) mode shapes of a homogeneous aluminum plate.

Figure 4.7 shows the frequency spectrum of the aluminum plate from the modal testing, using the procedures described in Experimental Procedure section. The measured first and second modal frequencies are 546 Hz and 1100 Hz, respectively. The measured values are slightly smaller than the theoretical predictions. However, the differences between the measurements and predictions are within 3% when adjusted for the uncertainties.

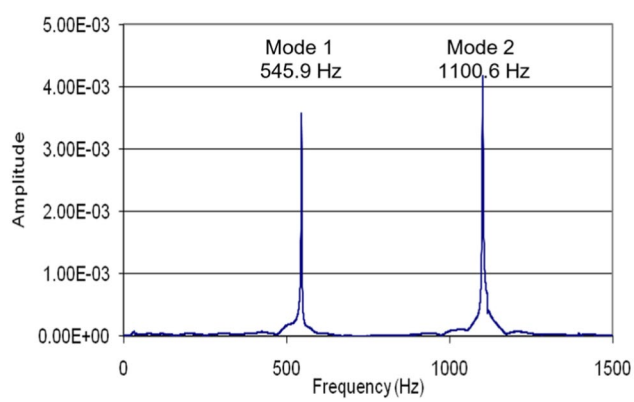

Figure 4.7: Frequency spectrum showing amplitudes for different frequencies of a homogeneous aluminum plate.

4.3.2 Experimental modal responses of composite plates

Composite plates with multiple infill orientations are tested at the dynamic conditions and their modal frequencies are recorded. Two types of boundary conditions are examined: (1) left-right fixed and (2) top-bottom fixed. Figure 4.8 shows a typical frequency spectrum of a fiber reinforced composite with left-right sides fixed. The results show how the orientation of the infill can influence the frequencies at which vibrations harmonize. The change in harmonic frequencies can then be used to assess the samples mechanical properties in a nondestructive way. For the sake of simplicity, only the first modal frequency is reported and used for comparison with the computational results.

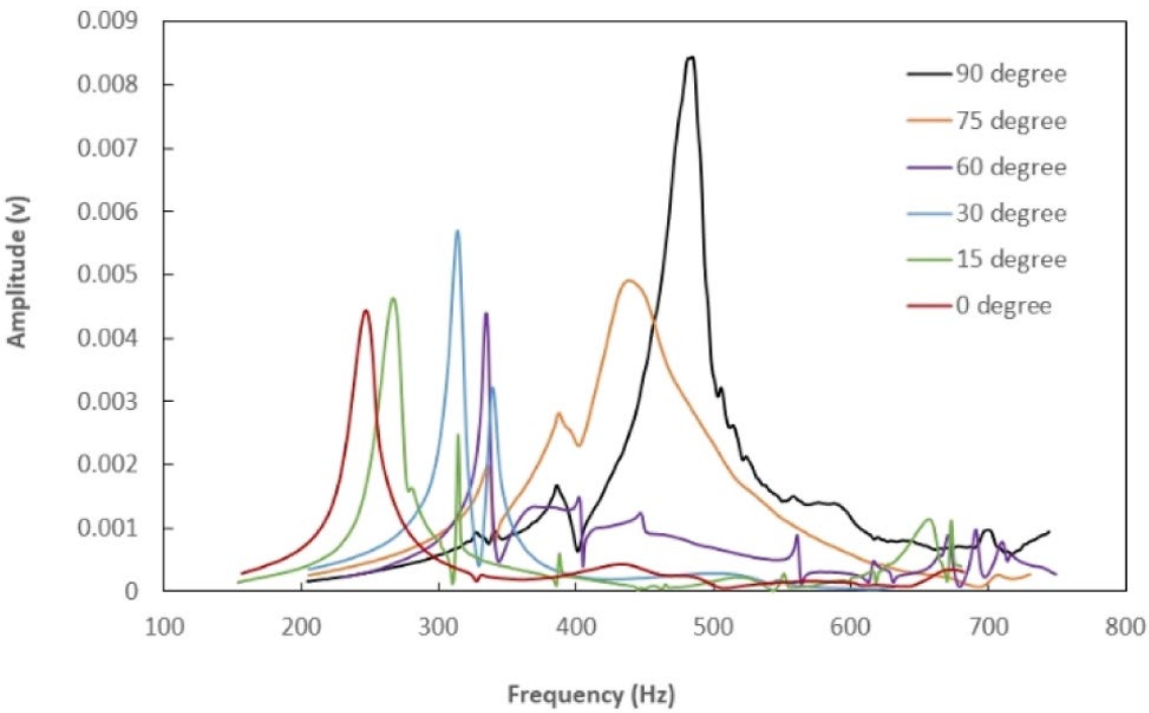

Figure 4.8: The spectrum of the first mode frequencies of 3D printed carbon-fiber plate with various infill angles. The rectangular plates were fixed on the left-right sides.

Figure 4.9 show the changes in the first mode frequency of the rectangular composite plates as a function of infill orientation. Depending on the boundary conditions

(left-right fixed or top-bottom fixed), the first model frequency either increases or decreases. When the plates are fixed at left and right edges, the first mode frequency increases from 249 Hz to 481 Hz, a change up to 78%. When the plates are fixed at top and bottom edges, the first mode frequency decreases from 341 Hz to 157 Hz, a change up to 117%. These results have clearly shown how much of an impact the infill orientation can have on its modal responses when reinforcing fibers are introduced. For comparison, the plates made of pure ABS (without reinforcement fibers) were also tested at the same conditions (Figure 4.10). Results have shown that the infill orientation has little effect on the mode frequencies of the plates (without reinforcing fibers). This can be attributed to the homogeneity of the non-reinforced samples.

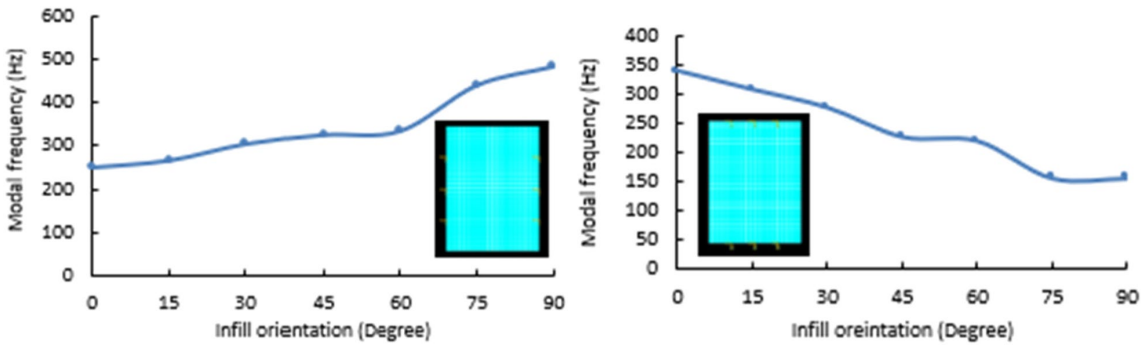

Figure 4.9: Recorded natural frequencies for fixed left/right side (Left) and top/bottom side fixed (Right) oriented rectangular samples of carbon-fiber ABS: mode 1.

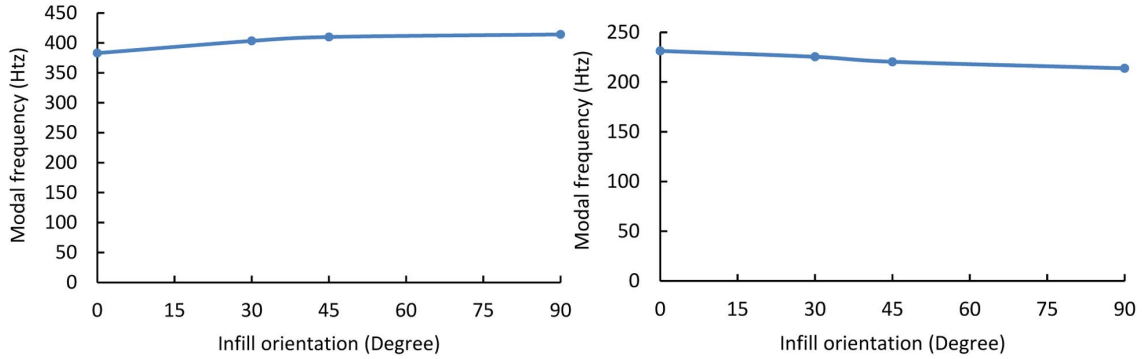

Figure 4.10: Recorded natural frequencies for fixed left/right side (Left) and top/bottom side (Right) oriented rectangular samples of pure ABS.

4.3.3 Computational modal responses of composite plates validation of FEM method

To ensure that the FEM gives results based on the inputted parameters (material properties, loading conditions) and not based on the meshing of the model, a grid independence study was first conducted. Due to the rectangular geometry of the testing sample, a geometrically structured mesh was used. A coarse mesh of 300 elements and a finer mesh of 1200 elements were mapped (Figure 4.11) and tested (Figure 4.12) using the material constants for the carbon-fiber reinforced ABS. For this study, a 2 mm thick plate consisting of 10 lamina sheets each with a thickness of 0.2 mm (a typical thickness for a 3D printed layer). Both plates were fixed on the top and bottom edges with the lamina ply's oriented parallel to the top and bottom edges. With the mechanical properties and loading conditions inputted, the FEM is used to calculate the modal frequencies of the plate. The simulated modal frequencies between the two structured meshes had little to no changes. The greatest change in the results can be seen in the sixth modal frequency (1362 Hz vs. 1377 Hz) with a change of approximately one percent, despite the coarse mesh having a fourth of the number of elements as the fine mesh. Thus, for the purpose of this analysis the mesh is considered converged for the 1200- element case. To further verify the FEM process, the results would be compared to experimental testing of 3D printed s with the same material properties under the same adding conditions.

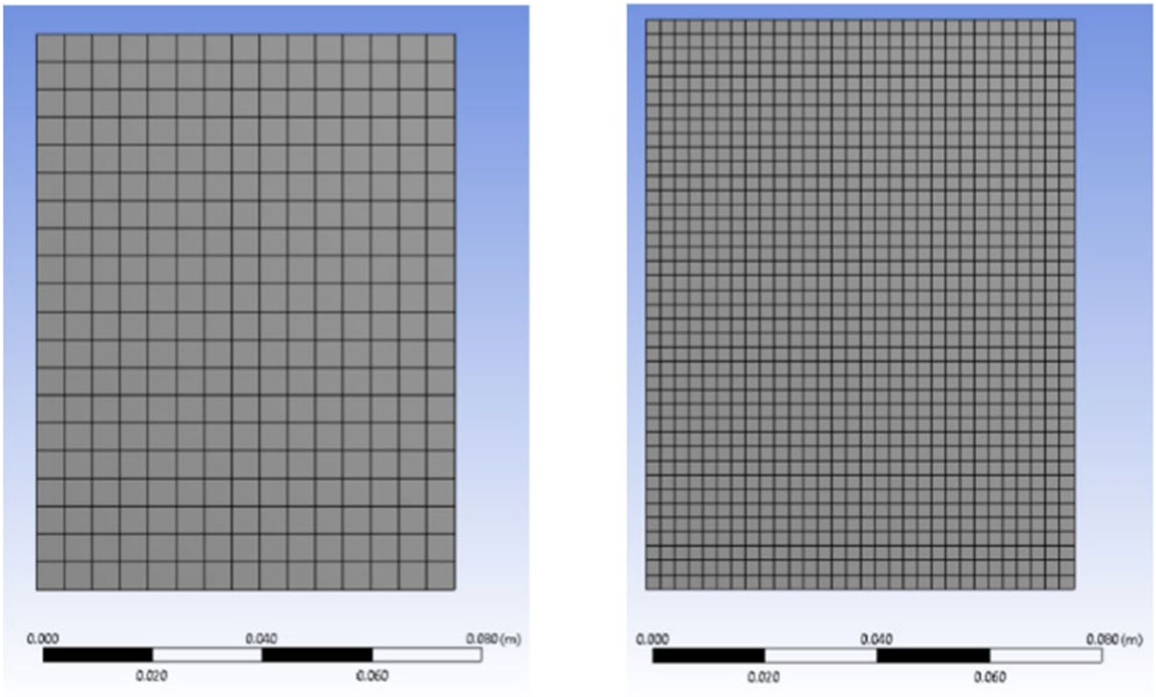

Figure 4.11: (Left) Coarse structured mesh pattern consisting of 300 elements. Refined structured mesh pattern consisting of 1200 elements (Right).

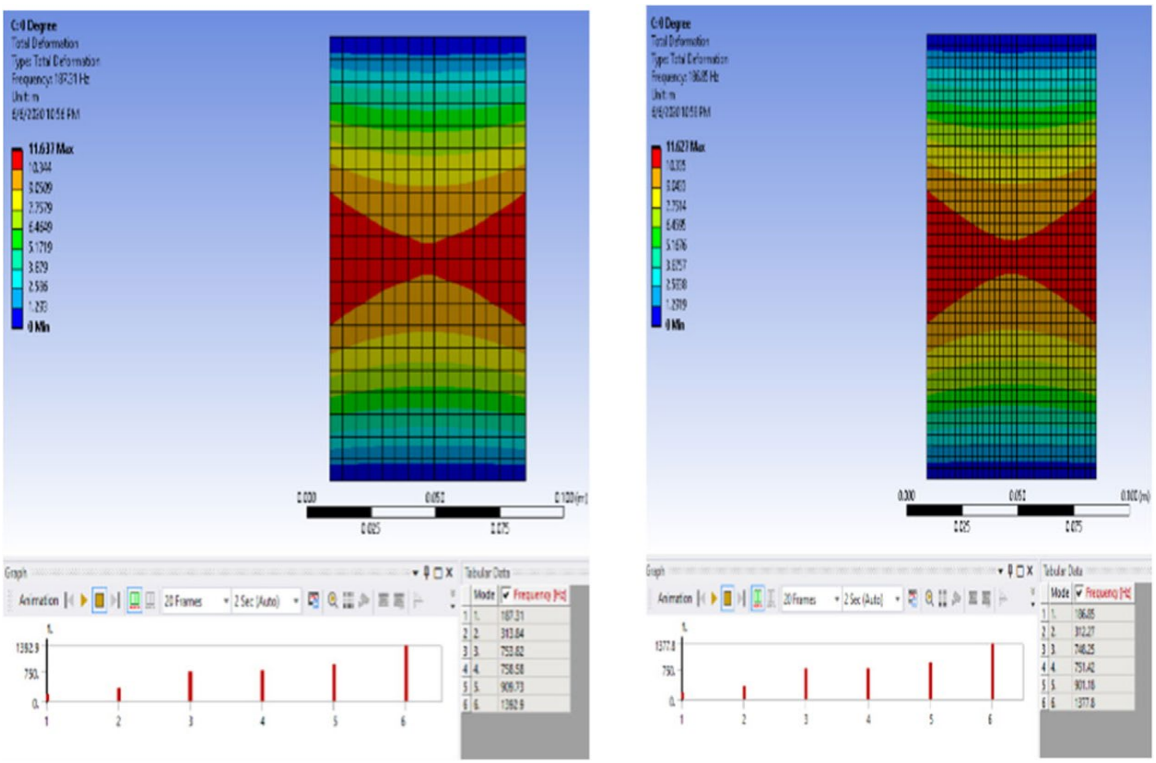

Figure 4.12: Dynamic modal results from FEM from the coarse mesh (Left) and refined mesh (Right) under the same fixed top/bottom loading conditions.

4.3.4 Computational model responses of composite plates

As shown by Equations 4.2 and 4.3, the dynamic characteristics of a plate include the mode frequencies and mode shapes. The mode shapes are particularly valuable from practical design point of view since they show how the plate would vibrate at its resonant frequencies. The vibration of a homogeneous plate is a classical problem and have been extensively studied [24]. However, the vibration of an anisotropic plate can be complicated, and the solutions are not readily available. Because of that, the finite element method is often preferable due to its simplicity. Just as in the verification case a 2 mm thick plate with ten 0.2 mm thick laminas were created using the carbonfiber reinforced ABS properties. To examine how the orientation of these lamina plies would affect the modal responses of the plate, different orientation angles with increasing alignment/ misalignment were analyzed. The test would begin

with the lamina plies oriented parallel to the fixed left and right positions. Figure 4.13 displays the mode shapes of the carbon fiber reinforced ABS composite plates with the fixed left and right edges. The first five modes are extracted at various infill angles (0°, 30°, 60°, 90°). It is observed that infill angles have significantly affected the vibrational shapes of the plates. At lower frequencies, the presence of reinforcing fibers have caused the deformation to be asymmetric. At higher frequencies, the mode shapes are significantly altered. For example, at the 4th mode, the 0-degree plate exhibits a mode index (1,4), while the 90-degree plate a mode index (2,1). At the 5th mode, the 0-degree plate exhibits a mode index (2,1), while the 90-degree plate a mode index (2,2). To further analyze relations between modal frequencies and orientation of lamina plies, a second FEM study was conducted with the same plate but with different boundary conditions. The test would begin with the lamina plies oriented parallel to the fixed top and bottom positions. The lamina plies would then be rotated at an increasing angle of 15 degrees until perpendicular to the fixed top and bottom edges. Figure 4.14 displays the mode shapes of the carbon fiber reinforced ABS composite plates with the fixed top and bottom edges. Again, the first five modes are extracted at various infill angles (0°, 30°, 45°, 60°, 90°). It seems that at this particular boundary condition, the infill angles have even greater influence on the vibrational shapes of the plates. The differences in dynamic characteristics are revealed at much lower modes. For example, at the 2nd mode, although all plates display a mode index (2,1), the patterns of vibration differ considerably between plates at 0-degree/90-degree and plates at other angles. The mode shapes become distinct among all plates at the 3rd mode and beyond. For example, at the 4th mode, the 0-degree plate has a mode index (1,2), the 45-degree plate has a mode index (3, 2), while the 90-degree plate has a mode index (2, 2).

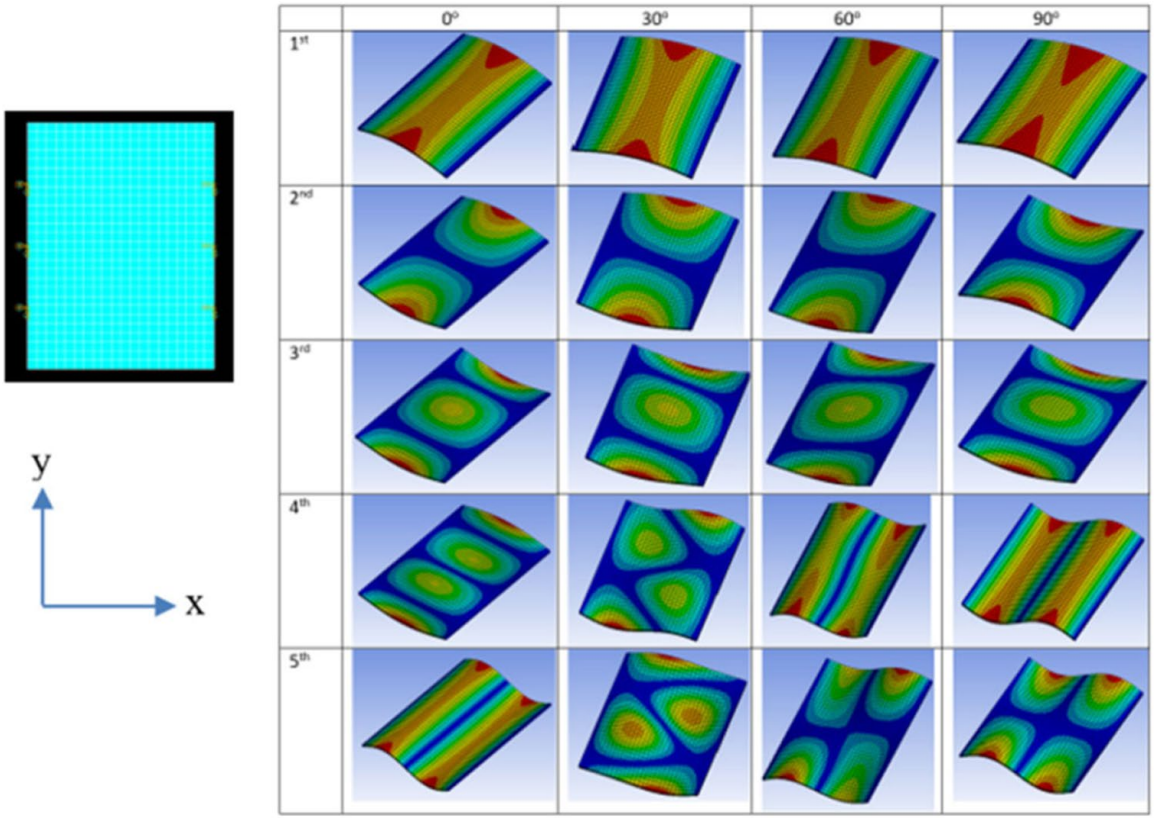

Figure 4.13: Mode shapes of carbon-fiber reinforced ABS with respect to the orientation of the lamina plies for case with fixed left and right edges.

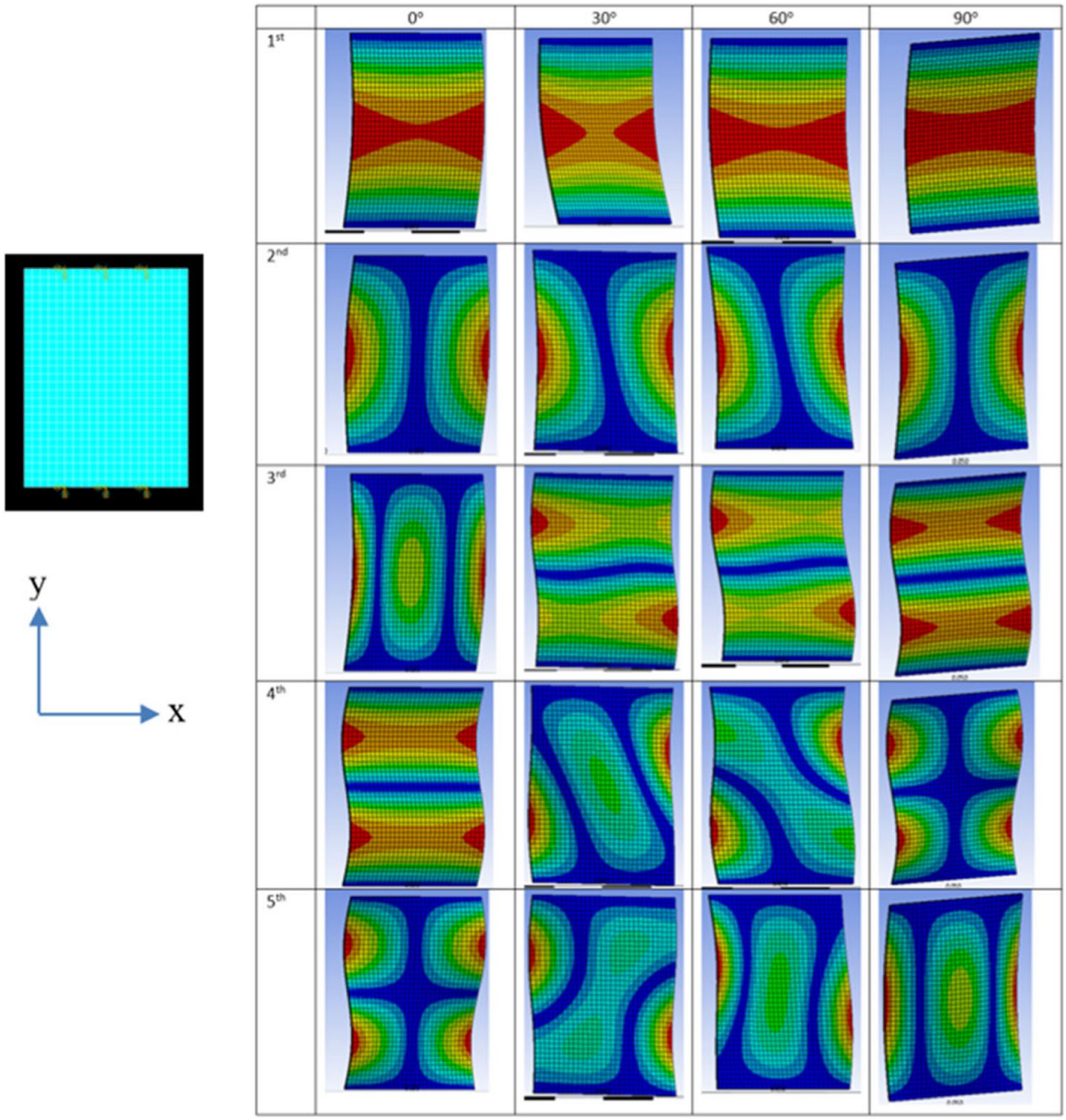

Figure 4.14: Mode shapes of carbon-fiber reinforced ABS with respect to the orientation of the lamina plies for case with fixed top and bottom edges.

4.4 Comparison of experimental data and simulated results

To further verify the FEM results, the simulated modal frequencies are compared to the results found using the LabVIEW experiments. The manufactured test sample ideal dimensions and simulated geometries were identical with the same loading

conditions. Just as with the FEM analysis two loading conditions were used for the experimental analysis, a fixed top and bottom side condition and a fixed left/right side condition. The rectangular samples would thus have a longer span between the two fixing points with the fixed top and bottom sides due to the geometry of the sample; meanwhile, the square samples would have equal distance between fixed points for both conditions.

Consistent with the experimental results, the computational predictions also show an increasing first mode frequency with increasing lamina ply orientation angles 4.15. The magnitude of the frequency varied from the simulated values yet a correlation can be seen. Just as in the FEM simulations, the change in orientation of the 3D printed infill would results in a change in the recorded modal frequencies. The results showed clear trends of continuously increasing or decreasing first modal frequencies depending on loading conditions and infill orientation. For the case with fixed top and bottom sides the highest first modal frequency magnitude occurs when the infill orientation is at the zero degree angle and the lowest with the 90 degree infill 4.16. The comparison shows how the magnitude of the experimental results varied much more considerably for the fixed top and bottom case. It is theorized that with the top and bottom secure, the increase in length between the two fixed points allows the introduction of more defects along the length of the sample. The results are thus more inconsistent as the dynamic response becomes more susceptible to manufacturing defects and artifacts of the 3D printing process. Due to the symmetrical geometry of the square samples, the top/bottom boundary conditions ended up mirroring the left/right loading conditions with overlapping data sets 4.17. The results showed correlation between the orientation of the square sample and its first modal response. The difference between the experimental results and computational model remained nearly constant with the computational model simulating a modal frequency 50Hz less than what was recorded for all orientations. The model showed correlation between the orientation and modal frequency but do to the assumptions needed for the

empirical equations, such as the structure remaining homogeneous throughout the part, error is introduced into the system and the magnitudes vary.

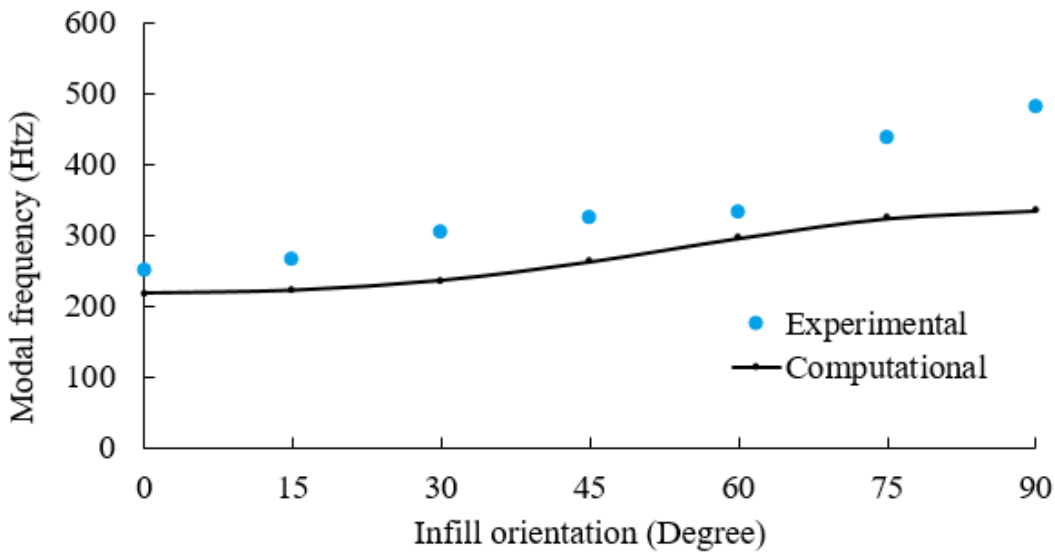

Figure 4.15: Modal frequency of sample for the fixed left and right side case with respect to infill orientation angle.

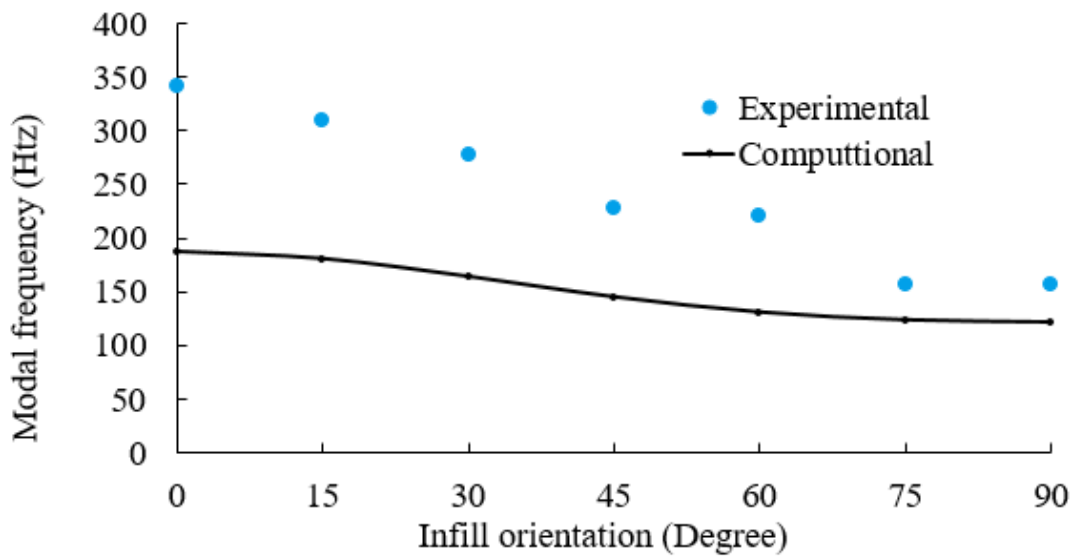

Figure 4.16: Modal frequency of sample for the fixed top and bottom sides with respect to infill orientation angle.

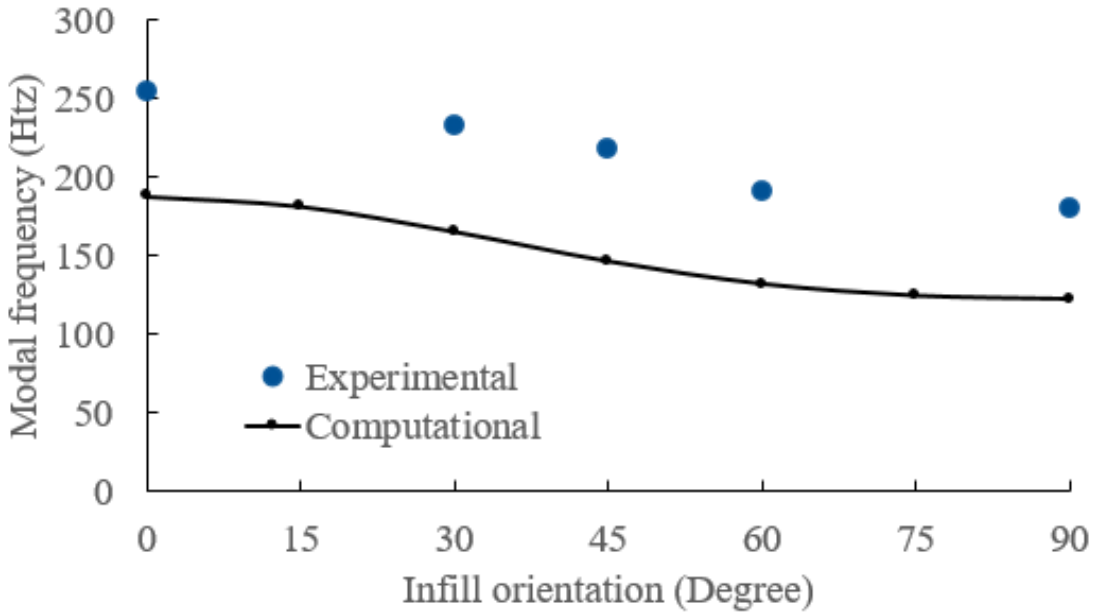

Figure 4.17: Modal response of the square sample with respect to infill orientation for both cases when mirrored.

4.5 Conclusion

The anisotropic dynamic mechanical properties of 3D printed fiber composites have been studied. Rectangular composite plates are 3D printed at various build orientations (0°, 15°, 30°, 45°, 60°, 75°, 90°) and then tested at various boundary conditions. The dynamic characteristics of the plates are further investigated by using finite element method. Results show that the changes in the build orientation have significant influence on the in the mode frequencies of the plates. For the rectangular plates, the mode frequency increases as the increase of the build orientation at the fixed left-right edges and the mode frequency decreases as the increase of the build orientation at the fixed top-bottom edges.The build orientation also has considerable impact on the mode shapes. The building orientation can cause the vibrational shapes to be asymmetric and further changes the mode indices.

Copyright© Jordan Garcia, 2023.

Chapter 5 EFFECT OF FIBER CONTENT AND FIBER ASPECT RATIO ON ANISOTROPIC BEHAVIOR OF 3D PRINTED SHORT FIBER COMPOSITES

5.1 Introduction

Continuous fiber composites tend to have the most preferable mechanical properties; however, they are often synonymous with high cost due to the expensive equipment and material cost used for manufacturing these composites [64]. Discontinuous or short-fiber composites are traditionally less expensive and are normally less difficult to manufacture while still retaining some of the benefits of reinforcing fibers [65]. Similarly to continuous fibers, the volume ratio influences the mechanical properties of the composite [66]. In addition the ratio of the length and diameter of the reinforcing fibers also plays a significant role [67]. This ratio (also known as the aspect ratio) adds another variable to the anisotropic properties of lamina plies where now not only the content of fibers but also the dimensions of the fibers themselves play a role. Short fiber reinforced composites are already used in additive manufacturing techniques; however, the amount of carbon fiber and the length of the discontinuous strands in the filaments are normally not stated or vary greatly [68]. This paper investigates how the dimensional properties of the carbon fiber, (volume fraction and aspect ratio), affect the mechanical properties of 3D printed parts.

5.2 Mass Produced Fiber Filaments

Currently there exist commercial filaments with discontinuous carbon fiber strands suspended in the polymer matrix (typically ABS and nylon) [69]. Traditionally mechanical testing shows how the orientation of the infill behaves similarly to a traditional short-fiber composite, but the internal geometries of the fiber and matrix remained a mystery. The CF-ABS wire roll from 3DXTECH was used to investigate

the ratio of fiber to matrix and the geometric characteristics of the reinforcing fibers. The manufacturer states the filament contains approximately 15 percent of carbon reinforcing fibers; however, the dimensional information on the fibers is either not presented or vague. The website simply states that the fibers are approximately 5-10 micrometers wide and claims the fibers are aligned following the axis of the material [70]. More precise information can be helpful to better determine the mechanical properties of 3D printed composites but are not readily available. For a better understanding of this material, samples were produced and examined visually under a microscope and analyzed using an image processing software.

5.2.1 Microscopic analysis

A batch of samples in both the 0 degree and 90-degree orientations were produced following the same nominal dimensions and slicing patterns as the samples in the sample dimensioning section. These samples were then cut in the center of the sample where the failure would occur in the bending tests [71]. These new ends would then be sanded using varying grit sandpapers starting at a grit of P320 and ending on a P2400 on a ECOMET3 variable speed polisher. The sanded ends were then placed in the Keyence VHX microscope and images of the fibers inside the matrix material were taken (Figure 5.1).

Figure 5.1: Keyence HVX microscope used for observing the reinforcing fibers inside the polymer matrix at the cut and sanded ends.

While the carbon fiber strands and the ABS plastic are both a similar dark color, the light from the microscope reflected on the fibers and gave them a brighter gray color in the images below. Figure 5.2 and 5.3 show the 90 degree orientation where the fibers are aligned along the direction of the cut while Figure 5.4 and 5.5 show the samples with the fibers oriented against the direction of the cut. The 90-degree figures show how the fibers do tend to align with the direction of extrusion and they appear to be uniform through the sample. The images also show how the length of the fibers tends to vary through the samples though the diameter does tend to be mostly uniform. The 0-degree figures tell a similar story with only the ends of the fibers being present in the images. These figures show that there are only dots representing the cut ends of the fiber and no long fiber sections are present. This further confirms that the reinforcing fibers are in fact aligned with the printing direction.

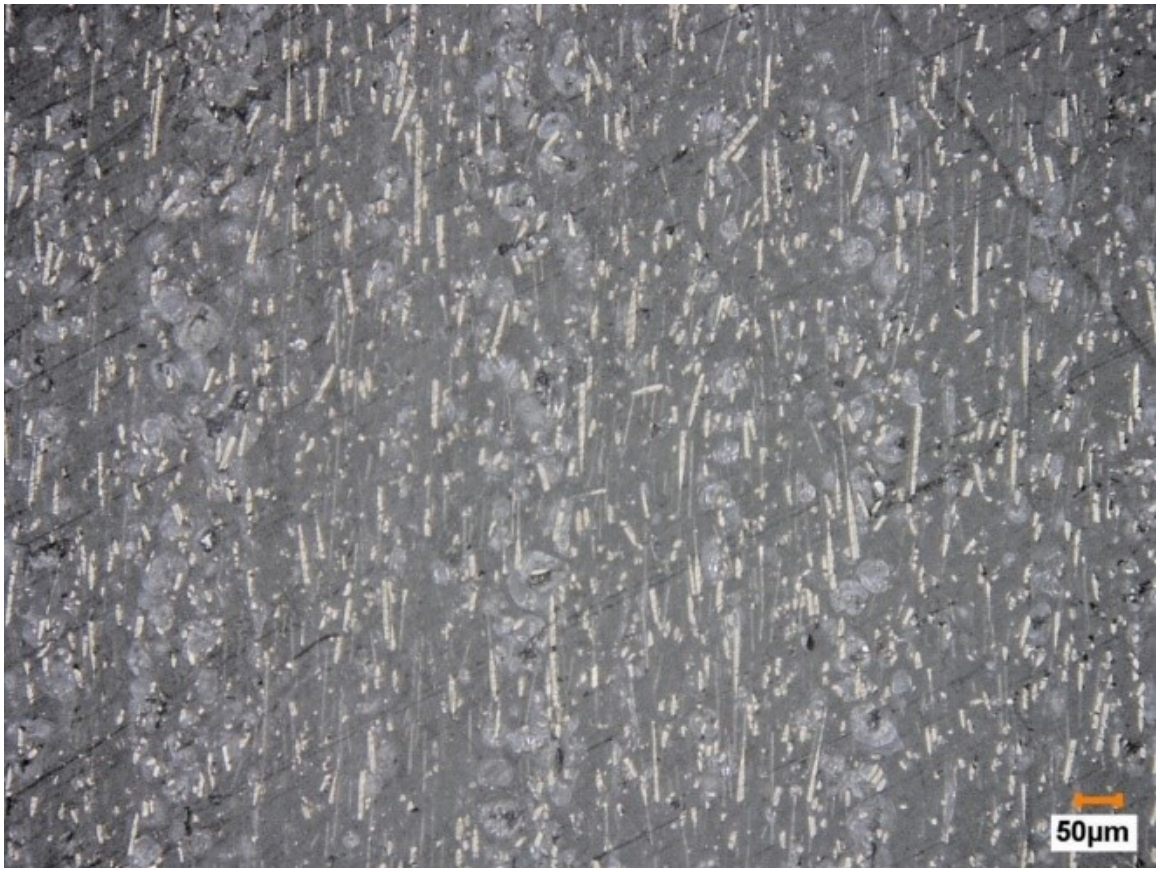

Figure 5.2: Cross section of the 90-degree sample showing the fibers length across the extruded filament (magnified ×250).

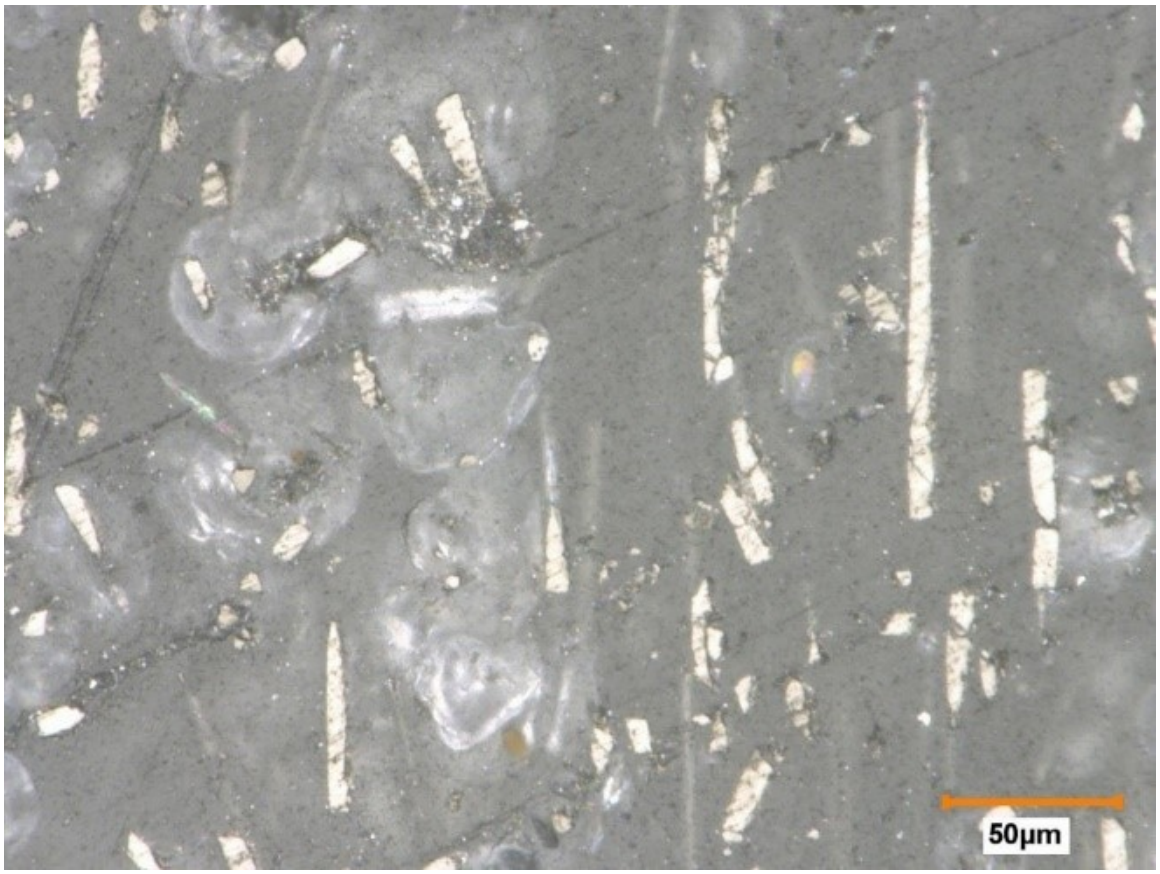

Figure 5.3: Further magnified image of the 90-degree samples cross section (magnified $\times 1000$).

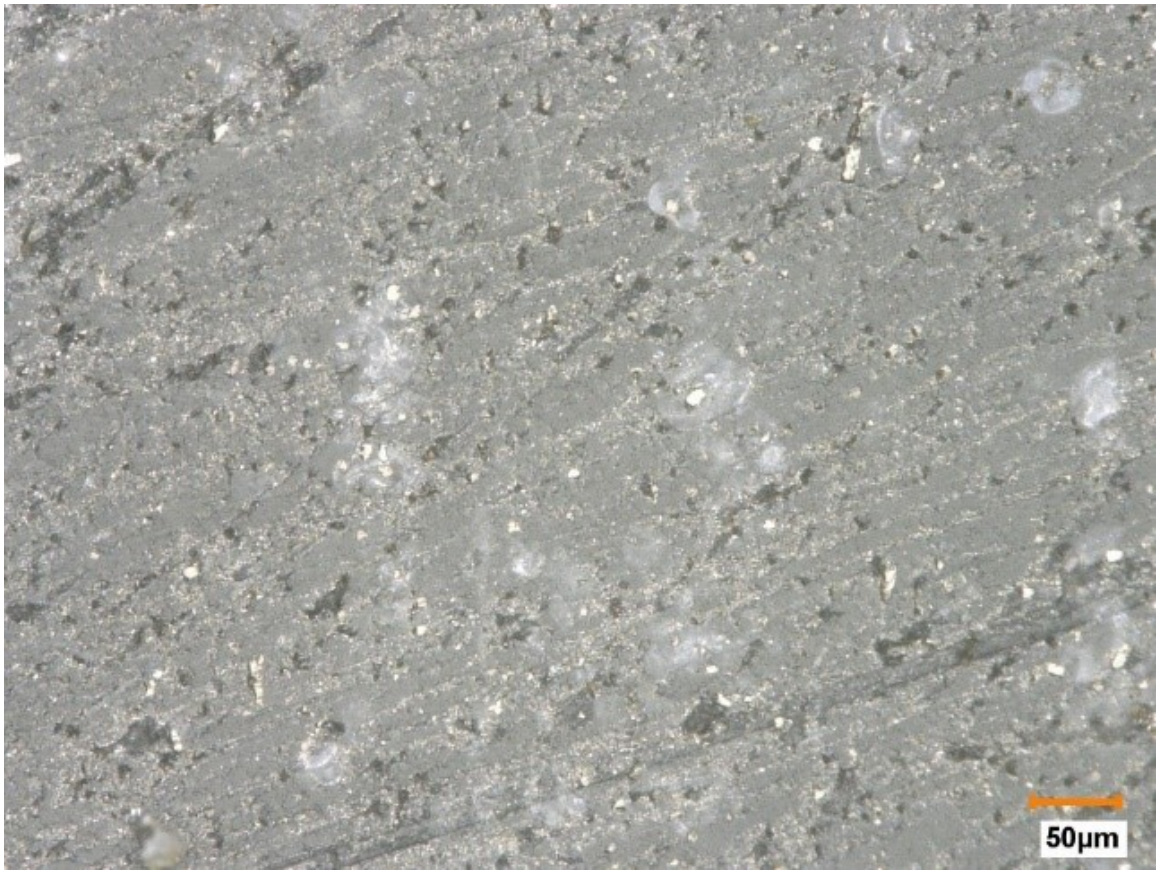

Figure 5.4: Magnified image of the 0-degree samples cross section showing only small reflective dots of carbon fiber (magnified ×500).

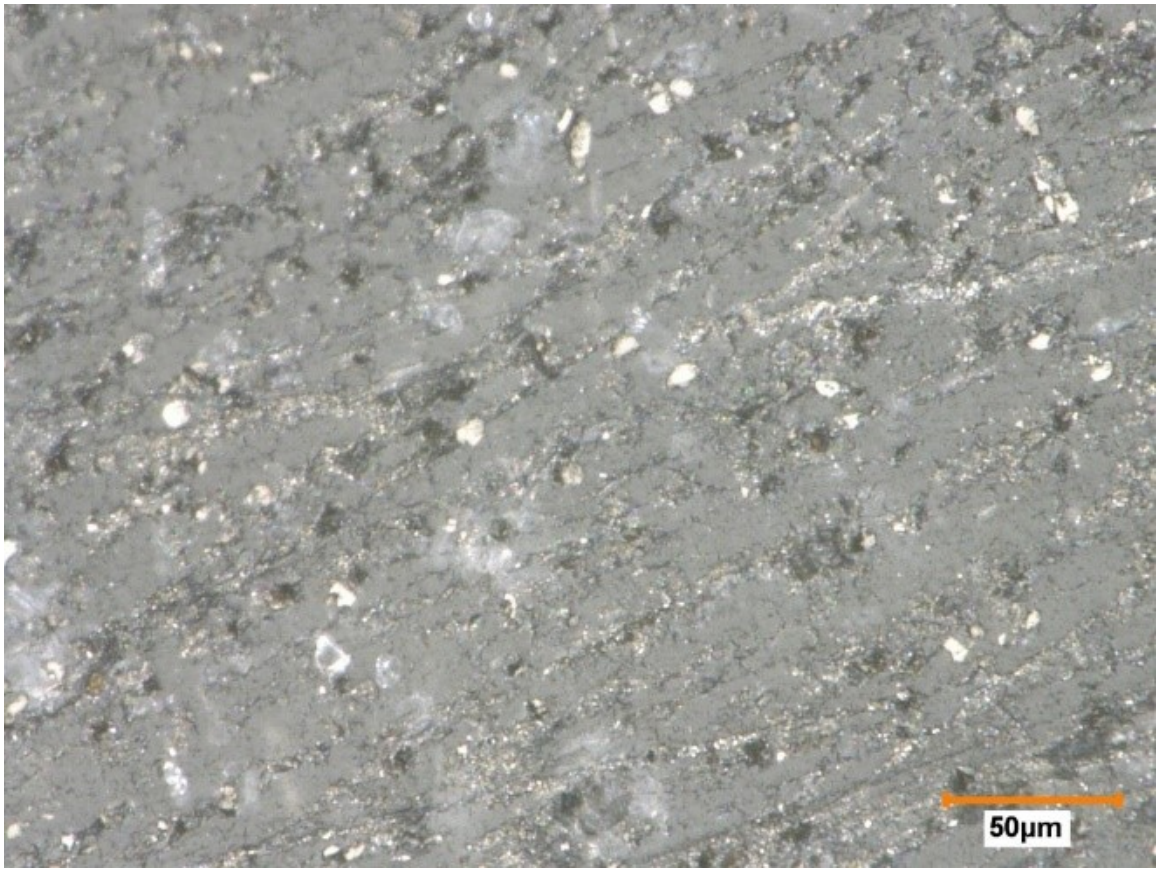

Figure 5.5: The further magnified cross section shows how the reflective carbon strands are dispersed can greatly vary in size (magnified ×1000).

5.3 Image processing

The image processing program ImageJ was then used to post-process the microscope images to determine what the percentage of filament was reinforcing fiber and some of the fiber's general dimensions. By importing one of the microscopic images and setting a threshold color, the reinforcing fibers can be separated from the matrix material due to its bright coloration from reflecting the light source (Figure 5.6). The 90-degree sample showed that approximately 9 percent of the surface of the sample was brightly reflective carbon fiber. Assuming the sample was homogeneous it could be stated that the samples showed to have an approximately 1/10 volume fraction though this is most likely not the case, instead it only shows that trying to find the

average length of the fibers would prove difficult to find. The fibers appear to be oriented along the vertical axis; however, the vast diversity in fiber lengths can be attributed to the samples being un-oriented in the axis out of the cut edge and resulted in truncated fibers. Another possibility is that the samples simply vary in length due to its method of manufacturing. Regardless the microscopic imaging software would not be able to give a reliable solution and more intrusive methods would need to be used to determine fiber dimensions (such as burning off the encasing matrix).

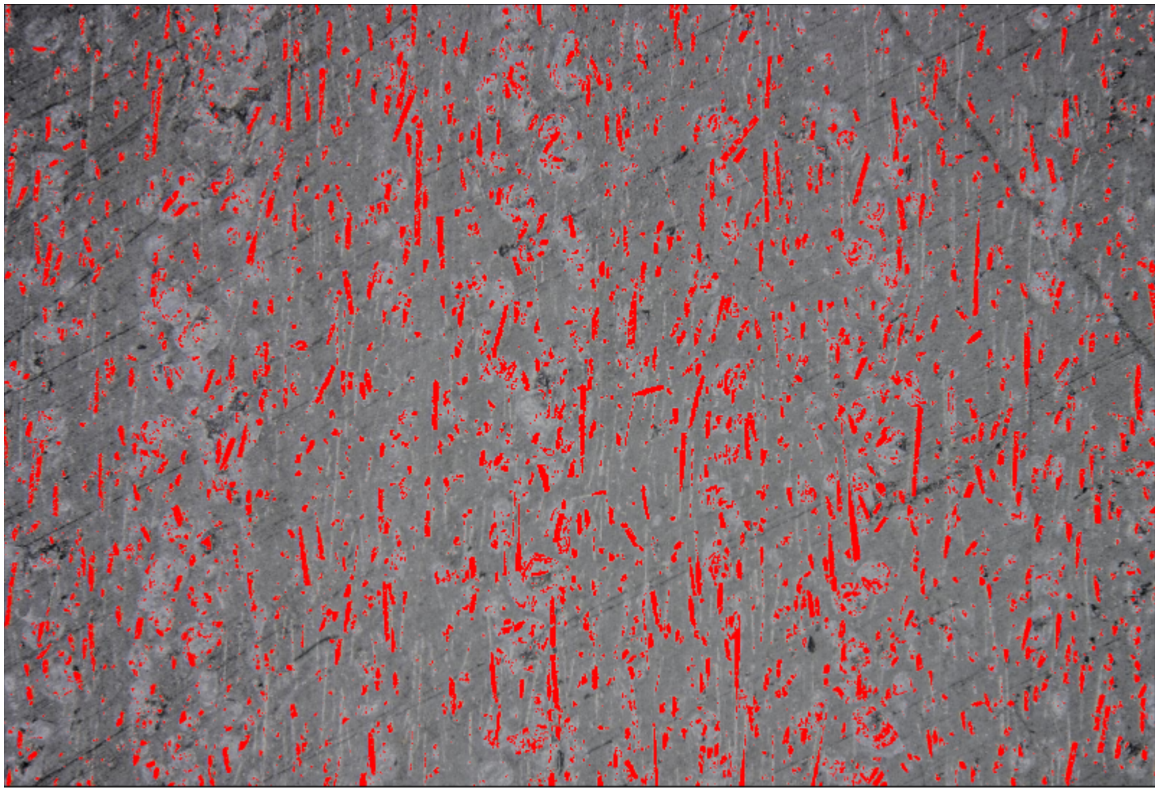

Figure 5.6: ImageJ altered microscopic image with the bright colored fibers selected due to their reflection of the microscopes light.

The imaging software was also used to assist in determining the diameter of the fibers using images of chopped fiber ends in Figure 5.7. Using the scale in the corner of Figure 5.5 found that 50 µm was 250 pixels in length, meaning a pixel represent approximately 0.2 µm (or 200 nm). Meaning a fiber with a diameter of 5 µm would have a minimum area of approximately 500 square pixels. A fiber with a diameter of

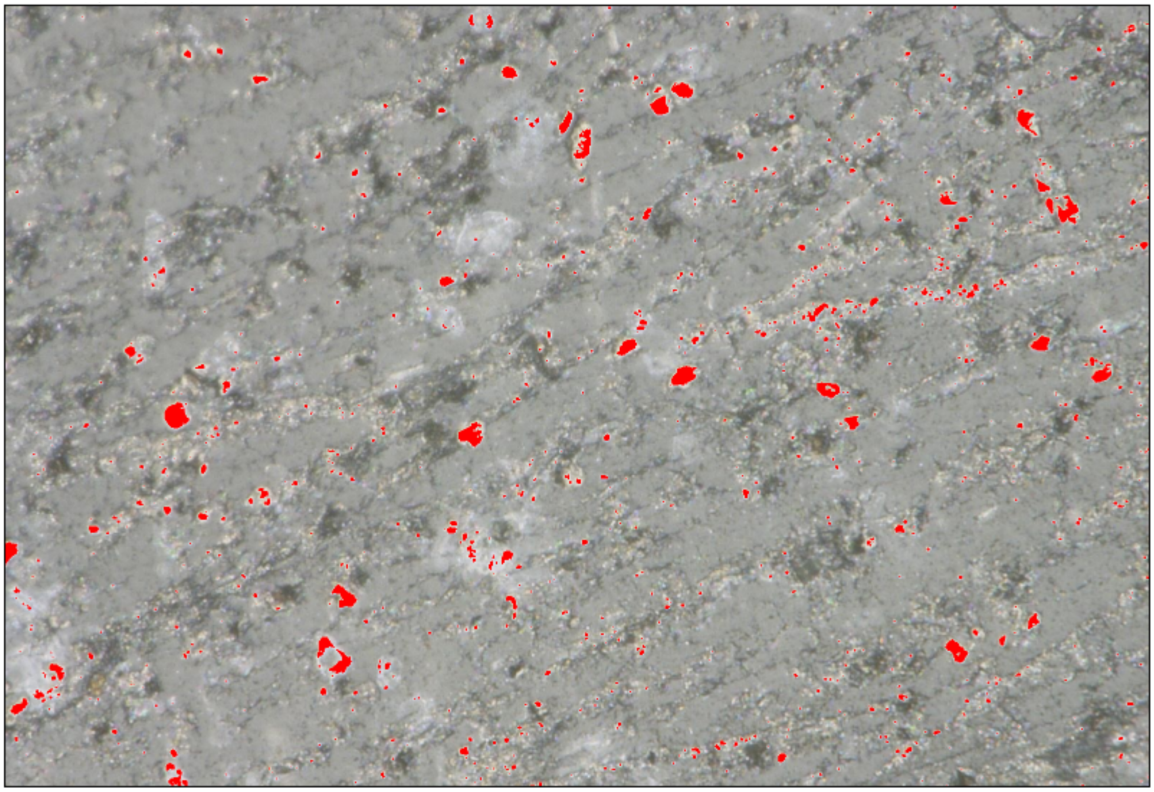

Figure 5.7: Image processed microscope image used to calculate the average size of fibers in the reinforced filament.

15 µm would have an area of approximately 2000 pixels. To ensure the minimization of noise in the images, the boundaries are set to ignore any particles smaller than 300 pixels (approximately 4 µm), and any particles over 3000 pixels (approximately 12 µm). The image processor reported a total of 17 fibers present in Figure 5.7 with an average diameter of 5.08 µm (507 pixels) and a fiber diameter standard deviation of .68 µm (140 pixels in area). These numbers imply that the actual diameter of the reinforcing fibers tends to be less than the minimum specified by the manufacturer after printing.

5.4 Materials and methods

Fiber reinforced 3D printer filaments for both commercial and industrial use do exist, the reinforcing fiber dimensions and content can vary by manufacturer in 3D printer

filament [72]. Thus custom filament was manufactured to ensure the quantity and aspect ratio of the reinforcing fibers are properly investigated. Pure ABS 3D printing filament was purchased from 3DXTECH in 1kg spools and chopped into pellets with a nominal dimension of 1-2 mm (Figure 5.8).

Figure 5.8: ABS filament into bulk material form after being chopped into 1-2mm pellets.

A 500g roll of a wound continuous wire of carbon fiber (Figure 5.9) was purchased from Markforged and fed into a set of gears shown in Figure 5.10 breaking the strands. The gears are designed to break the carbon fiber wire being fed into them into a specific length depending on the spacing of the gear teeth.

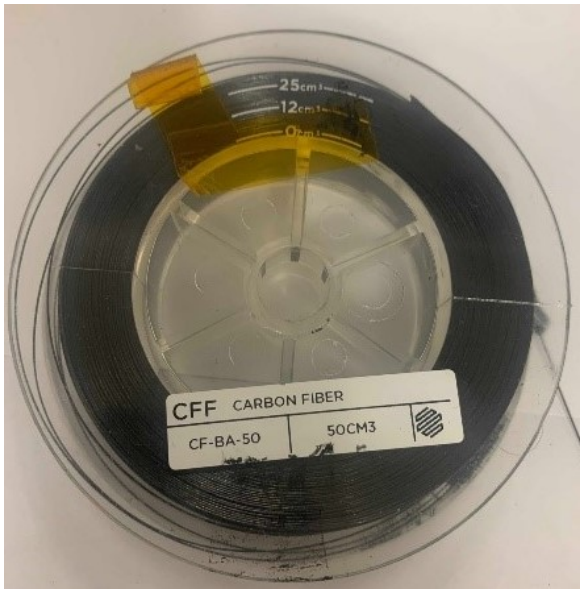

Figure 5.9: Roll of continuous carbon fiber from Markforge used to create discontinuous fibers with set aspect ratios.

Figure 5.10: Set of 3D printed gears used to dhear the carbon fiber wire to a specified length to determine aspect ratio.

Once broken into small strands, these fibers are combined with the ABS pellets and fed into the Wellzoom filament extruder (Figure 5.11). This extruder turns the pellet ABS, combines it with pre-cut fibers and creates a single continuous filament for use in the 3D printer. The filament extruder uses a single screw feed that pushes the ABS pellets into a heated die that melts the material into the filament diameter. Then an Arduino controlled roller winds up the extruded filament material into a roll used for traditional 3D printing applications. The fiber content of the filament can then be controlled by the quantity of the fibers inserted; the size of the fibers can also be controlled by cutting the fibers to different lengths using different sized gears.

Figure 5.11: Filament extruder and Arduino controlled auto-roller for creation of 3D printer filament with specified aspect ratio.

The two major contributing factors to short fibers composites are the volume fraction and aspect ratio [73]. The composite volume fraction is the percentage of reinforcing fibers inside the matrix creating a fiber reinforced composite matrix, and the aspect ratio is the ratio of the length to diameter of the short fibers used as reinforcement. This factor is controlled by chopping the reinforcing fibers to a fixed length with the diameter of the fibers given by the manufacturer. The fibers are chopped using a dual gear mechanism where the fiber is fed in and fibers in the desired length are chopped and collected. To calculate the aspect ratio the simple

Equation 5.1 is used where L is the length of the fibers and T is the thickness.

$$R = \frac{L}{T} \tag{5.1}$$

Methods to find the volume fraction of reinforcing fibers often involve removing the matrix material by use of acids or heat [74]. Since the filament material will be manufactured in-house, the volume fraction can be calculated and controlled by measuring the bulk materials before combining them in the extruder. The volume of the fibers can be difficult to find without altering its mechanical properties, thus the weight of the fibers and polymer matrix are measured, and the weight fraction is used [75]. The weight fraction of the fiber is the weight of the reinforcing fibers introduced into the composite vs the weight of the entire composite structure. This weight fraction can then be converted to the volume fraction based on the density of the materials used as seen in Equation 6. To create samples with a specific volume fraction, the quantity of reinforcing fibers and polymer matrix pellets need to be predetermined to be mixed in the extruder. Knowing the material densities of both the polymer and fibers, the volume fraction can be converted to a weight fraction and vice versa [76]. Once the weight of each material needed is calculated, they can be added to the extruder and the filament produced will have the desired volume fraction.

$$V_f = \frac{w_f \rho_m}{w_f \rho_m + w_m \rho_f} \tag{5.2}$$

Where w, ρ, v are the weight fraction, density and volume fraction, with the subscript f denoting the properties of the fiber and m for the matrix material.

Once the 3D printer filament has been manufactured it is then fed into the 3D printer for sample fabrication. The Mattercontrols PulseXE printer (Figure 5.12) was used along with the Simplify3D slicing software to produce oriented fiber samples.

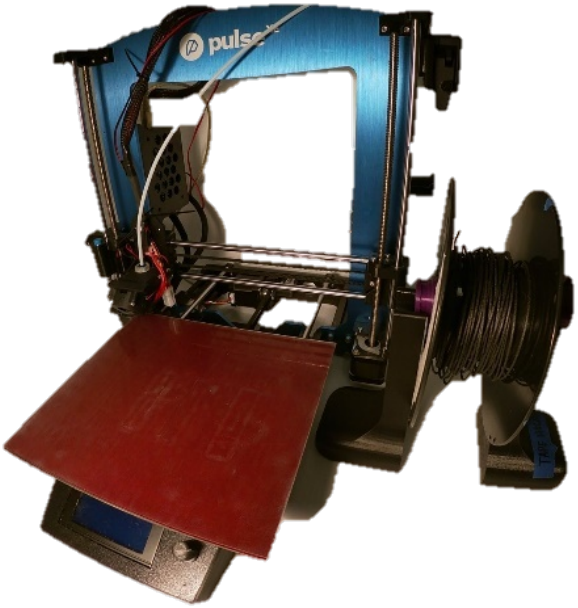

Figure 5.12: PulseXE FDM printer used for sample production coupled with a roll of reinforced filament produced using the filament extruder machine.

5.4.1 Slicing settings

Due to the control needed to create composite samples with variable infill fiber orientations, the Simplify 3D slicing software was used. The slicing software was designed to extrude material oriented in a single global orientation and thus orient the short fibers along with the filament based on the users input (Figure 5.13). These layers are then printed and combined one upon another creating a structure composing of individually oriented layers. Each of these layers can then be treated as individual lamina plies and the Classical Laminate Composite Theory (CLCT) can be applied to the 3D printed samples [77]. Just as fiber orientation can be controlled for each layer in hand-laying techniques, the slicing software can specify which global angle the fibers are oriented with in each layer of the entire composite. Based on the fiber's

direction, the forces applied to the final product can be more optimally distributed. To create these individually oriented layers, the filament material needs to be extruded in a way that the reinforcing fibers will face a certain direction. When the filament material is in a molten state the fibers are freely suspended in the molten plastic being fed through the extruder. Once the material begins to get extruded, the frictional forces of the plastic unto the nozzle as well as the viscus forces of the plastic align the fibers in suspension [78]. The material containing the aligned fibers is then extruded as a single strand through the nozzle with each strand combining to form a layer of material. In short, the slicing software directs the 3D printer in which direction to lay the strands of material to create a layer and the reinforcing fibers align with these strands. Thus aligned short-fiber composite layers are possible to construct using 3D printing technology.

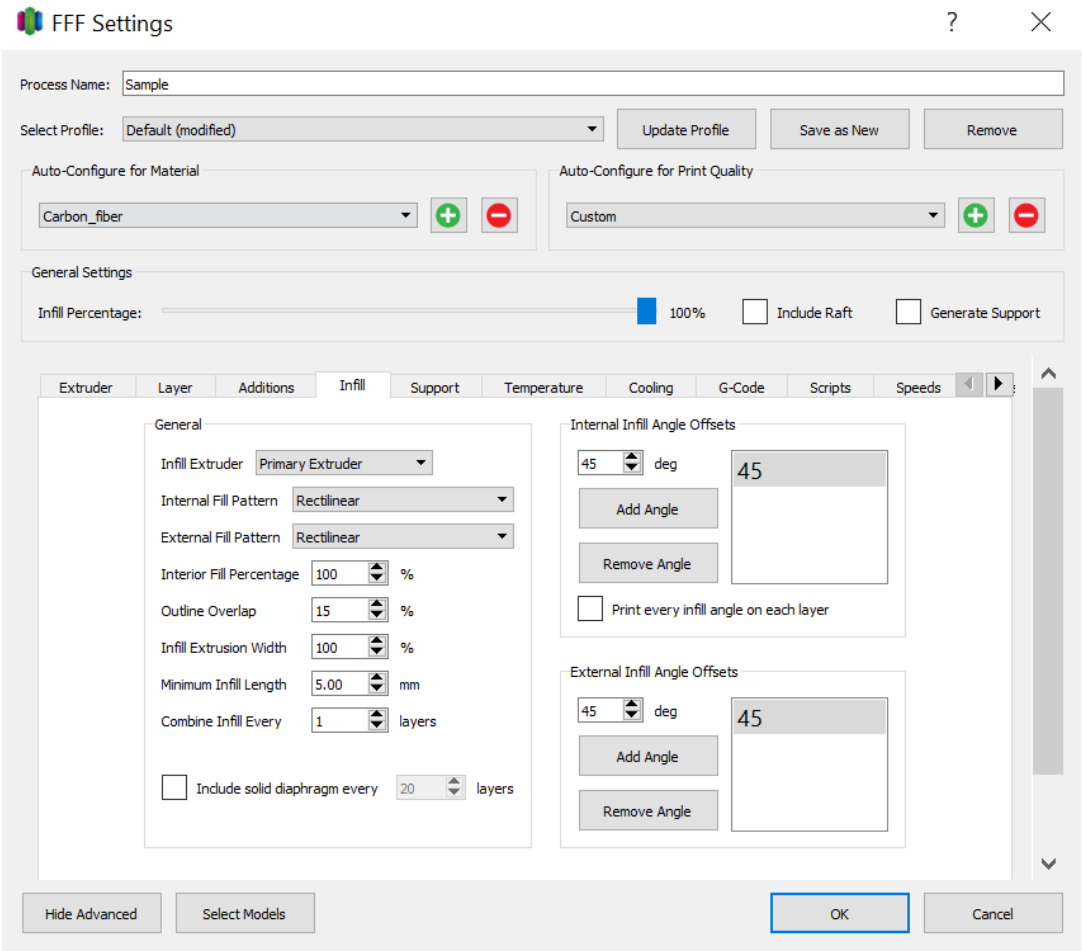

Figure 5.13: Layer-by-layer infill orientation specification in Simplify 3D used to create the oriented fiber reinforced test samples.

The process of extruding the material depends on adequately melting the polymer so the reinforcing fibers are free to align by the friction/viscus forces. Each extruded material has different thermal properties and the temperatures of both the extruding nozzle and heated bed need to be adjust for optimal performance [79]. For the ABS plastic used, the extruder was set to 260 degrees Celsius and the print bed to 105 degrees Celsius. These values are higher than the pure polymer versions as the material needs to be fully melted in a large portion of the extruder for the fibers to align [80]. The thermal conductivity of the reinforcing fibers can cause issues as well if the temperature of the block is not high enough to fully melt the polymer in the specified locations before it cools. Once the material is immediately extruded, the

fiber reinforced version has a higher thermal conductivity but like the pure version it still needs to be pliable to properly adhere itself to the bed [81] To accommodate for this the bed temperature is also raised.

5.4.2 Sample dimensions and testing

Rectangular bending specimens are manufactured with the nominal dimensions of 45 x 15 x 2.8 mm (length, width, height) consisting of 14 oriented layers .2mm each. The samples would be 3D printed one sample at a time in the center of the PulseXE print bed. Each sample will then be allowed to cure before being removed of the bed and the process repeats until multiple samples are ready to test. On a desktop computer, the PASCO Capstone software was installed and linked with the load and deflection sensors on the materials tester. Calibration proceeded by manually rotating the crank to move the force applicator on the materials tester. The Capstone software would then record the load and deflection measurements and plot them in real time as the samples are being tested. The crank was rotated until the sample snapped into two separate pieces and the software was stopped. The coupon fragments were removed from the tester and the load/deflection data was saved as a .cap file as well as a text file for subsequent analysis. Prior to testing the actual parts, each part was labeled by batch number and degree number on both ends to ensure each part could be matched once fragmented. Using the classical Euler-Bernoulli beam theory, the force and displacement data of the applicator can be converted to a tensile stress perpendicular to the neutral plane and a strain from the deflection of the neutral axis. This theory makes the assumptions that the beam bends into an arc shape and the neutral axis does not elongate during the testing process. To calculate the stress of the rectangular cross section at the location of failure, Equation 6.2 is used with the width and height variables. Note these simplified equations only relate to simple rectangular geometries and its stress/strain relations perpendicular to/on the neutral axis.

$$\sigma = \frac{3FL}{2bd^2} \tag{5.3}$$

Where F is the applied force, L is the length of the sample between the deflectors, b is the width of the sample and d its height. To calculate the flexural strain on the neutral axis, a different equation (Equation 6.3) is required with a new variable D, where D is the distance the beam has deflected from its original position [82] This value is represented by the distance the force applicator traveled during testing.

$$\epsilon = \frac{6Dd}{L^2} \tag{5.4}$$

5.5 Experimental results

The Halpin-Tsai model equations show how the aspect ratio of the fibers and the volume fraction of the reinforcing fiber can greatly alter the products mechanical properties [83] To experimentally investigate just how much these variables affect the final product and if the theoretical method is accurate, multiple aspect ratios and volume fractions are produced. As mentioned in the previous sections, the original printing fiber was chopped into small pellets and fed into the filament extruder. To investigate how this process affects the filament a control spool is manufactured without the introduction of reinforcing fibers. This filament spool with a volume fraction effectively being zero will be used to see if the secondary processing method has an effect on the products mechanical properties and be used to compare how the reinforcing fibers affect the samples. To investigate how the volume fraction affects the sample, two types of filament rolls are produced with varying quantities of carbon fiber strands. The first roll with attempt to replicate the fiber quantity of the commercial filament used in the dynamic analysis and the image processing. This fiber roll manufacturer states that the amount of carbon in the system should be approximately 15 percent, yet further investigation through testing and image processing implies this quantity is considerably less in small strands (about 5-10

percent) and the remainder might be scattered particles. Thus for the first set of samples, the rolls were produced with a fiber reinforcing quantity of 5 percent and 2.5 percent by mass. This should ideally be similar to the mass-produced version and the lower quantity will show how the increasing/decreasing quantities change the final products mechanical properties. The volume fraction of the filament can then be altered in increasing or decreasing quantities by adding or subtracting the quantity of fibers. The aspect ratio changes require a new set of gears to be produced for each length of fibers to be manufactured. The new gears will shear the fibers at a specific length and thus change the aspect ratio since the diameter is predetermined by the manufacturer. The smallest aspect ratio the gears can reliably shear at a consistent length is a value of 5. Beginning with the smallest consistent ratio the length that the fibers would be cut at could then be increased with ease and the varying aspect ratios can be investigated. As previously mentioned, the smallest aspect ratio of 5 was produced (with a fiber length of approximately 1.5mm) and increasing fiber lengths such as 2mm were also produced. These two aspect ratios and two volume fractions required 5 rolls of filament to be produced for preliminary results. Two rolls of 1.5mm length fiber rolls with varying fiber percentages, one at 5 percent and one at 2.5 percent. Then two more rolls with a fiber length of 2mm with fiber volume percentages of 5 percent and 2.5 percent. Finally a single control roll with no reinforcing fibers was also produced to set a "zero value" for theoretical analysis (Figure 5.14 & 5.15).

Filaments of varying volume fraction were produced and bending samples were manufactured and tested. For the 1mm samples, volume fractions of the following percentages were produced: 2.5%, 5%, 7.5%, and 1%. Each batch of samples contained samples with the 0, 45, and 90 degree infill orientations. Starting with the samples containing the lowest quantity of reinforcing carbon, the 2.5% samples showed that by adding the small amount of fiber drastically impacted the mechanical properties (Figure 5.16 & 5.17). When comparing to the 0% fiber control group, me-

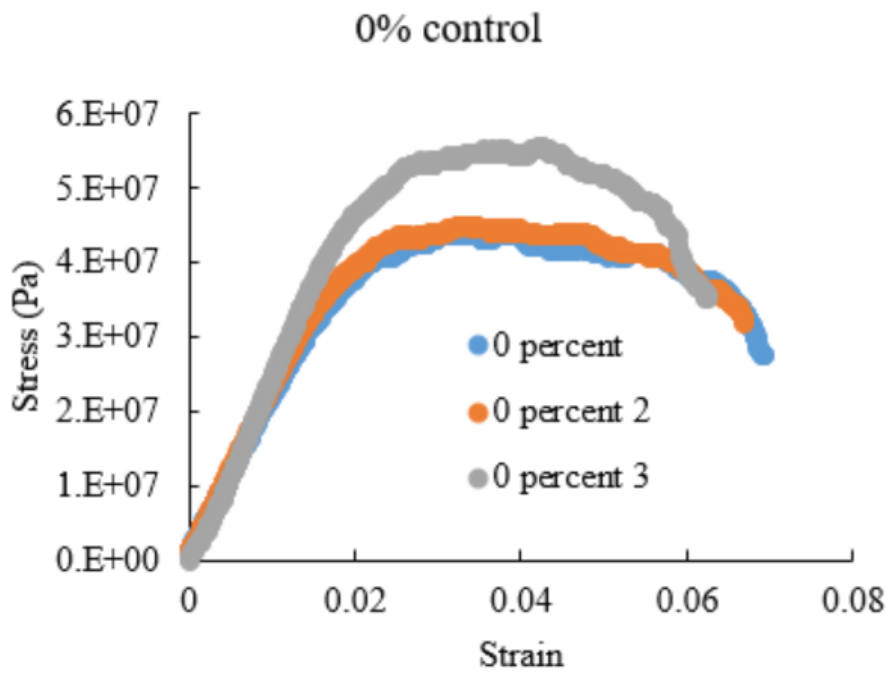

Figure 5.14: Stress/strain response of control samples with no fiber reinforcement.

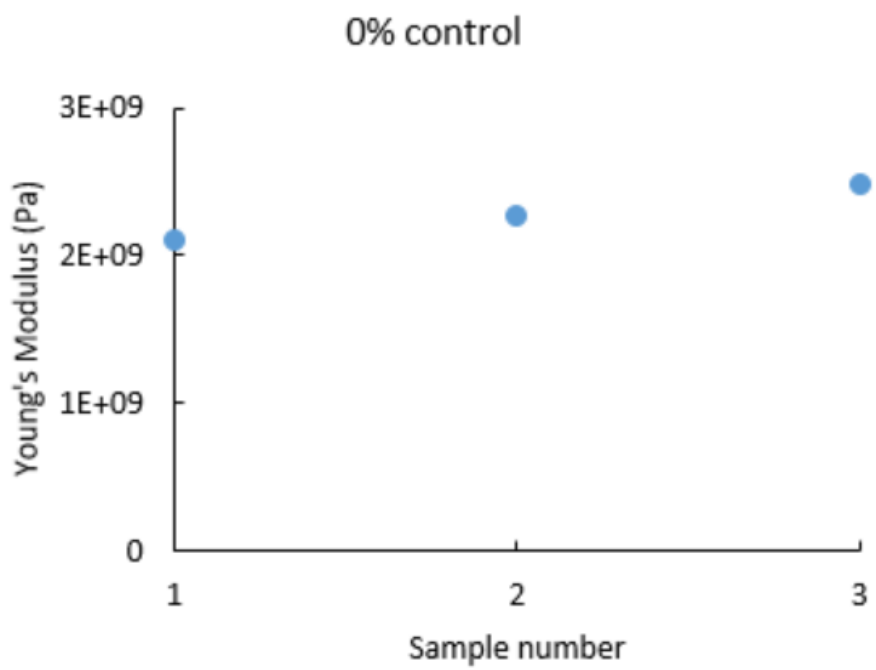

Figure 5.15: Young's modulus of each control sample without fiber reinforcement of the re-extruded pellet filament.

chanical testing showed that the fiber reinforced sample had a 30% higher modulus of elasticity. Interestingly the maximum stress the material endures remained constant, yet the fiber reinforced version had a 54% reduction in final product toughness. These results agree with the composite theory of increasing a materials modulus at the sacrifice of becoming more brittle. There is also the anisotropic properties in the fiber reinforced sample due to its orientation that are amplified by the inclusion of reinforcing fibers. By changing the orientation of the reinforcing fibers in the 2.5% 1mm samples, the change in the modulus of elasticity from the 90 degree samples (all fibers are perpendicular to the loading direction) to the 0 degree samples (all fibers are parallel to the loading direction) resulted in an average increase from 1.51 GPa to 3.13 GPa. A change of 108% due to the direction of the reinforcing fibers in reference to the loading condition.

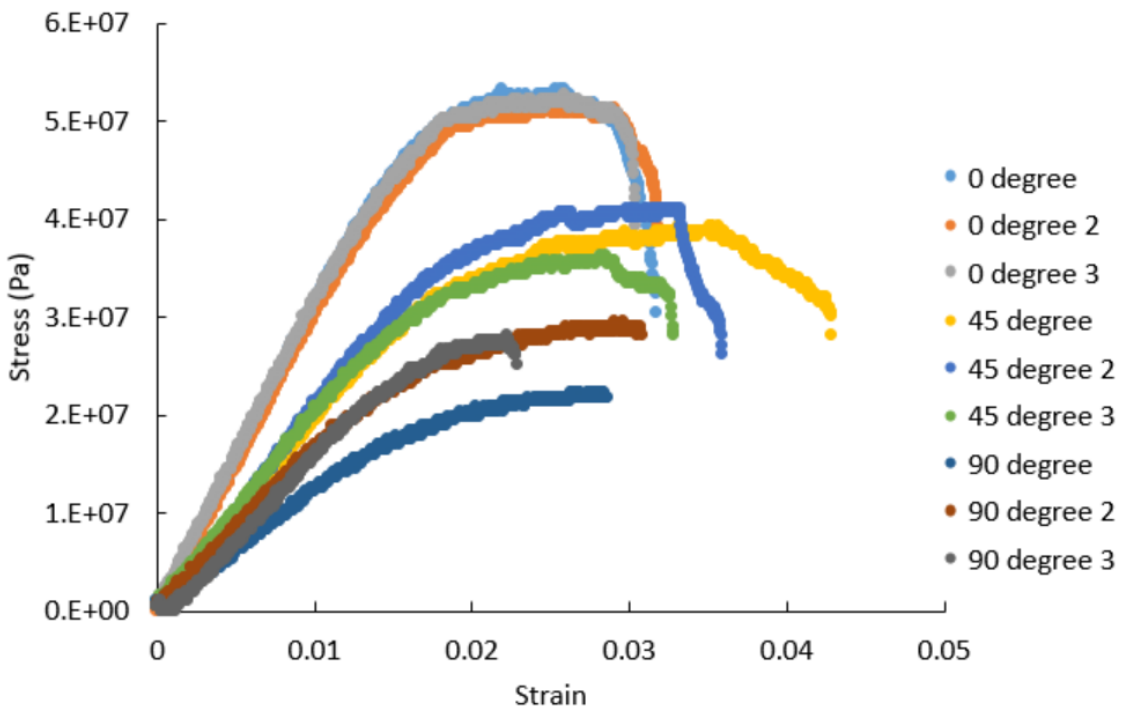

Figure 5.16: Mechanical response of 2.5% by volume reinforced samples in various orientations.

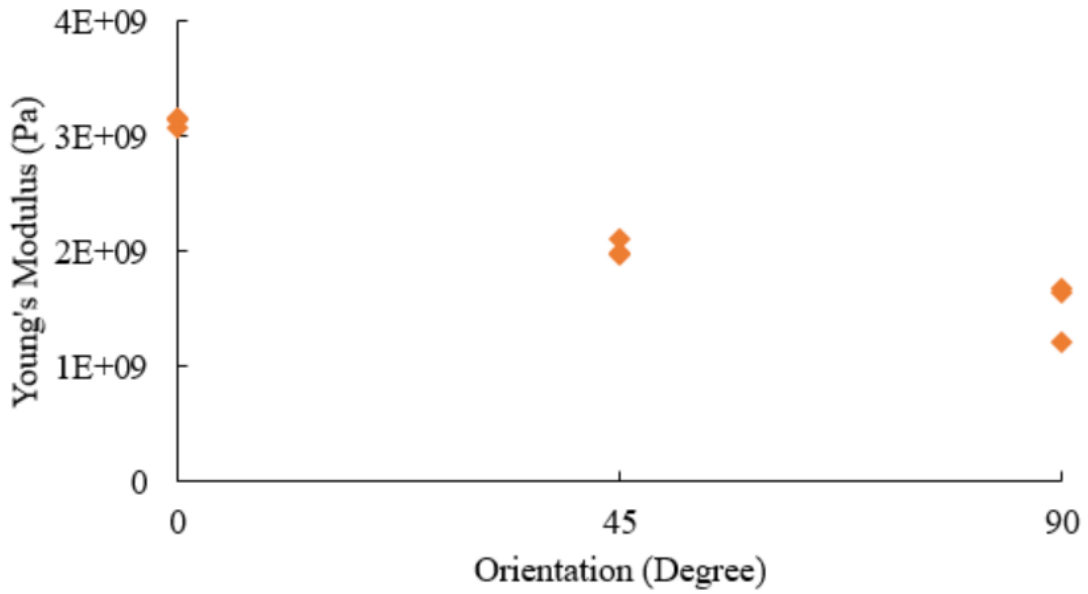

Figure 5.17: Young's modulus of the 2.5% samples based on orientation of reinforcing fibers.

Further increasing the amount of reinforcing fibers in the samples results in a larger gap between the 0 degree and 90 degree sample properties as seen in Figure 17. The change in the modulus of elasticity from the perpendicular fiber orientation and the parallel fiber orientation resulted in a 425% change from .428 GPa to 2.25 GPa (Figure 18). Interestingly enough the drop in the modulus is more drastic with moderate misalignments resulting in a 278% from the 0 degree to 45 degree infill orientations. This change in modulus from 0 degrees to 45 degrees is more than double the largest change in the 2.5% fiber reinforced samples. This implies that increasing the amount of reinforcing fibers in the 3D printer materials causes higher sensitivity in the change in mechanical properties due to fiber orientation. It should also be noted that the samples printed in the 0 degree orientation tend to have less variance in recorded results compared to the 45 and 0 degree orientations. This can be attributed to the fact that when the reinforcing fibers are aligned with the force of the direction, the mechanical properties are dominated by the material properties of the carbon fibers. In the misalignment orientations, the products with higher

quantities of reinforcing fibers are more greatly affected by the artifacts of the 3D printing process and thus have higher disparities.

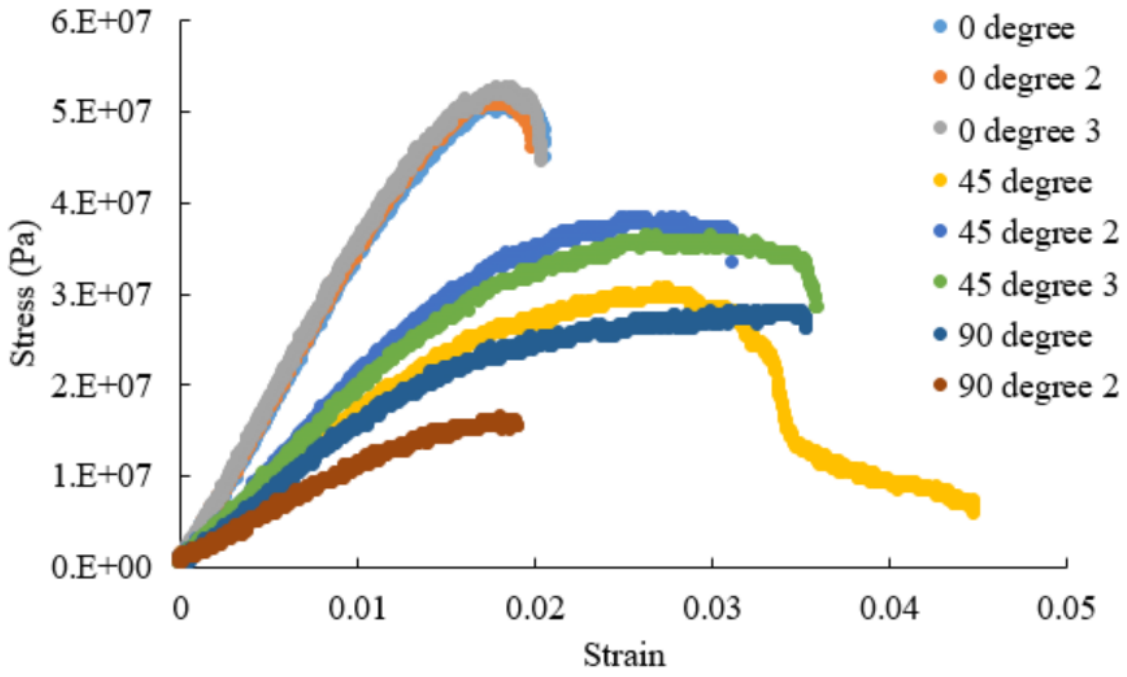

Figure 5.18: Stress strain responses of the further reinforced 5% samples with the same 1mm length reinforcing fibers.

Figure 5.19: Young's modulus of the 5% samples showing the drastic difference between the 0 degree and 90 degree samples.

In the 7.5% 1mm samples, similar results are recorded with the high sensitivity to misalignment and the higher modulus of the final products. The change in modulus from the 90 degree to the 0 degree samples resulted in a 468% change in the modulus which corresponds to the 5% results and follows the trend of increasing sensitivity due to the misalignment of the fibers.

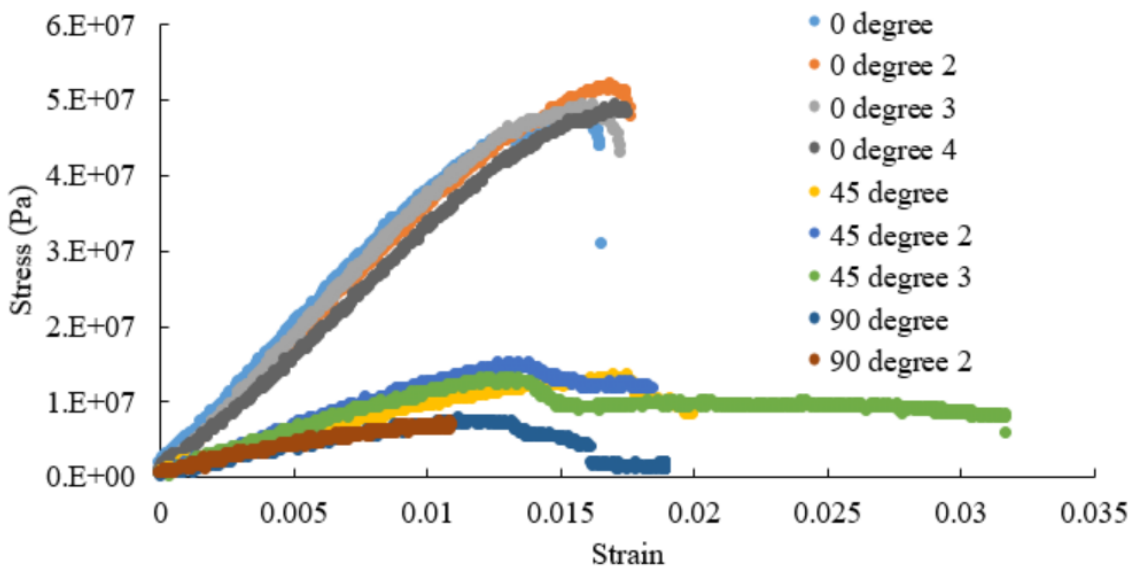

Figure 5.20: Stress/strain responses of the 7.5% fiber samples and the increase in its brittle mechanical response.

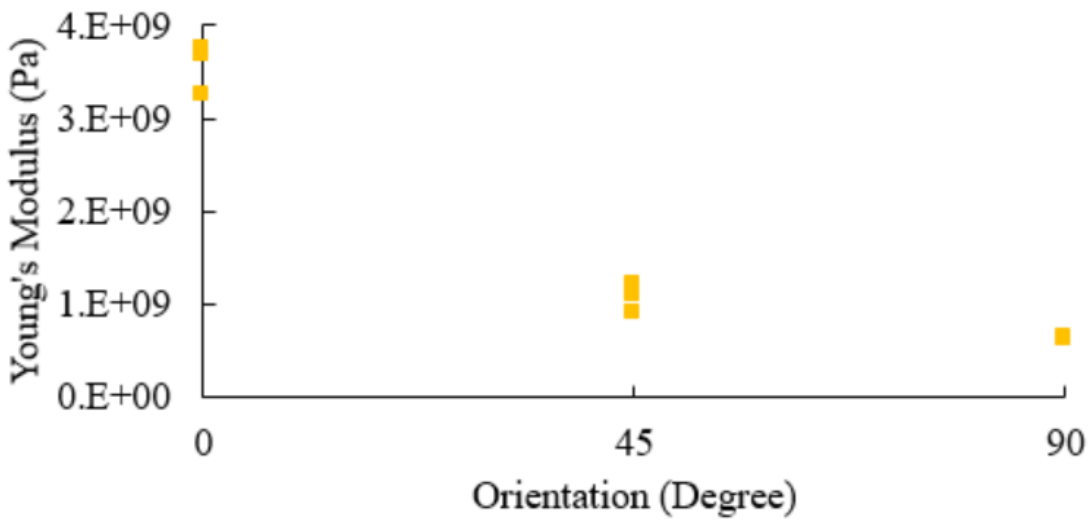

Figure 5.21: The 7.5% fiber reinforcement sample Young's modulus showing how drastic the change into a brittle response the samples exhibited.n

In the highest fiber volume fraction tested, the 10% samples only had a 311% increase in the fiber modulus from the 90 degree to the 0 degree orientation and

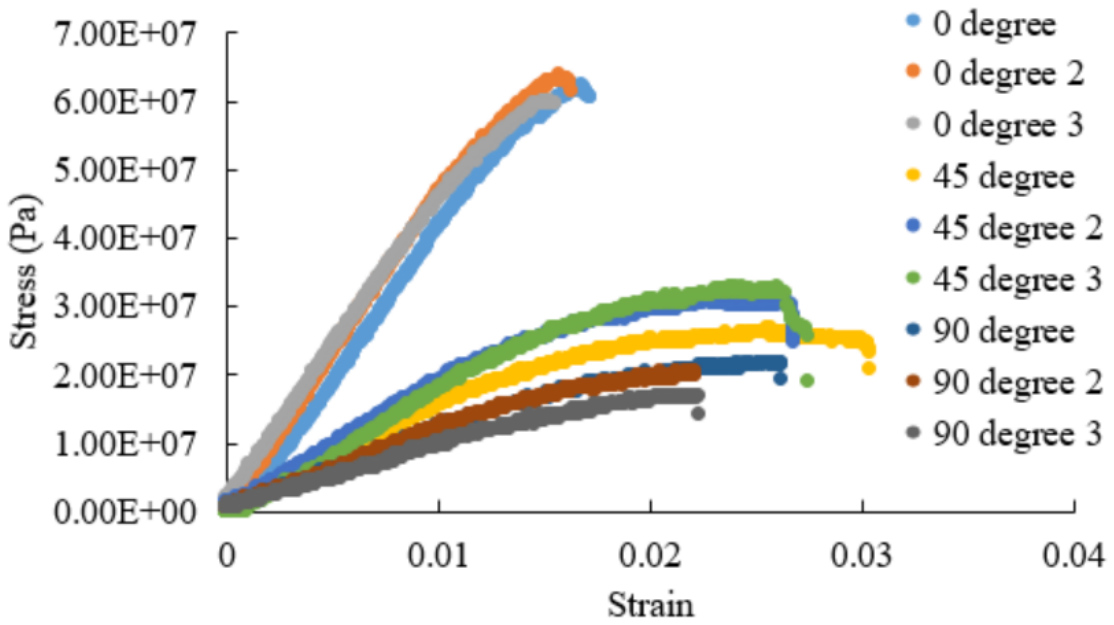

Figure 5.22: Stress/strain response of the samples containing the highest reinforcing fiber content volume ratio of 10%.

a 161% increase from the 45 to 0 degree orientations. One thing to note is that although the difference in the orientations is not as great as the lower volumes, the overall magnitude of the 0 degree 10% samples are significantly higher than all other fiber ratios. This implies that the highest fiber content results in the highest modulus of elasticity and agree with Laminate Composite Theory.

When comparing the overall results of each batch of samples we see how they compare to each other with respect to infill orientation and fiber content. It is shown how (with the exception of the 2.5% 1mm samples), there is a notable trend where the increasing fiber content results in a higher modulus for all infill orientation angles (Figure 5.24). Whilst it is uncertain why the 2.5% samples seemed to break this trend, it still performed better than the 0 percent control samples and followed the continual decline in magnitude with fiber misalignment.

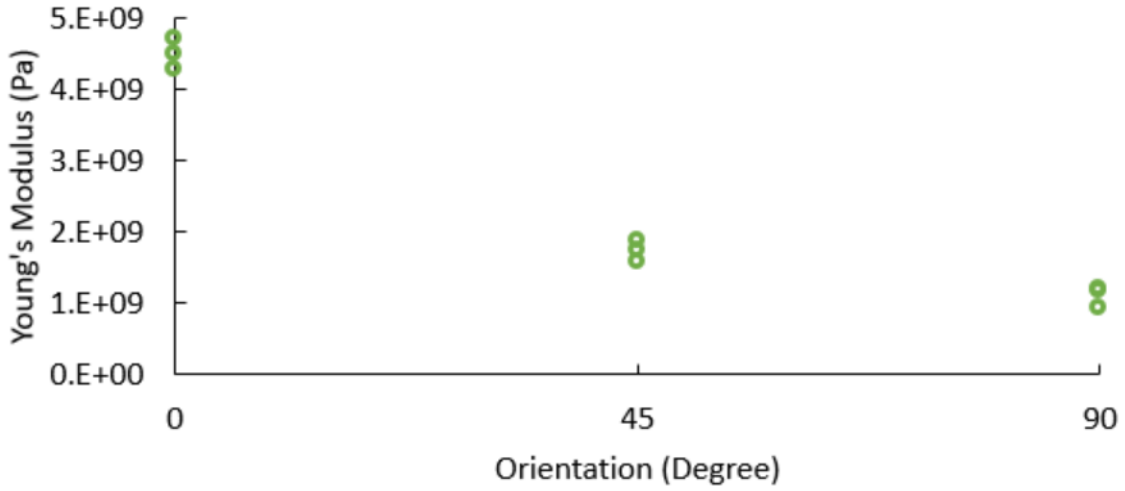

Figure 5.23: Young's modulus response of the 10% fiber content samples exhibiting the highest magnitude compared to the other sample sets.

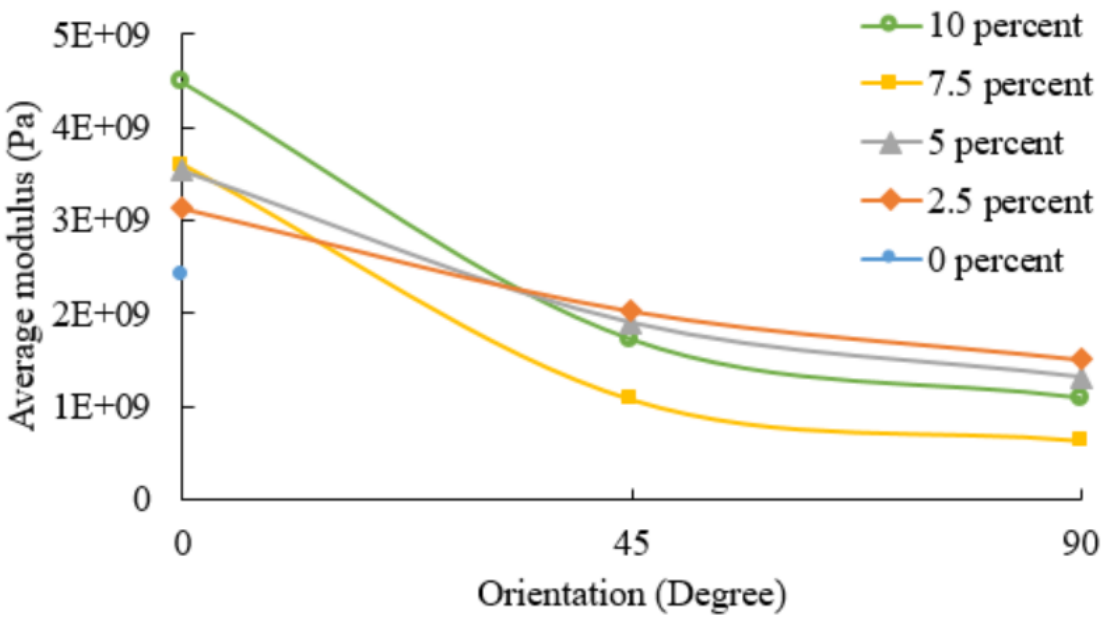

Figure 5.24: Summary of the average Young's modulus for each fiber percentage and infill.

With the Young's modulus of each the samples determined, it can be seen there is a varying level of "steepness" in the responses of each sample in relation to its 0 and 90 degree orientations. To better illustrate this relation a graph representing the

normalized modulus responses is plotted below (Figure 5.25). This graph shows how the increasing fiber content resulted in the samples becoming more dependent on fiber orientation as fiber content increased. As the fiber content increases, the variation of modulus vs orientation becomes greater, thus the anisotropic behavior also becomes greater. The only exception was the 10 percent samples slightly underperforming the 7.5% samples. This is mostly attributed to the 7.5% samples having an unusually low 90 degree response and thus further amplifying the normalized modulus quantity. The cause of this poor response could be attributed to a bad batch of samples with all three orientations exhibiting a lower modulus magnitude due to the manufacturing artifacts of using a non-enclosed 3D printer.

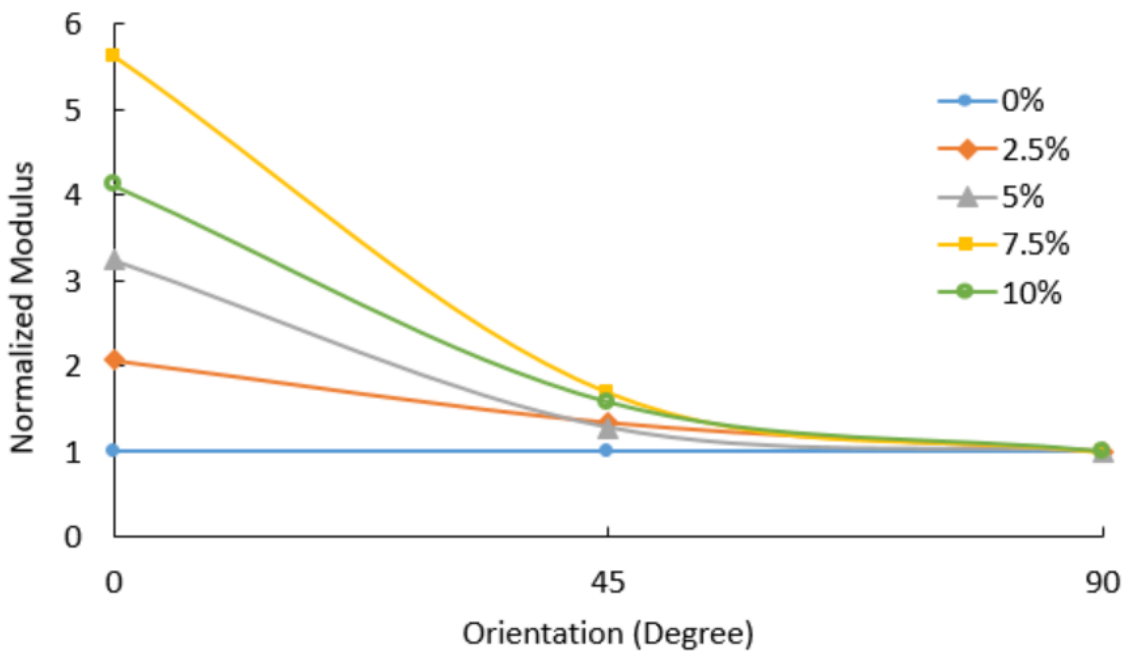

Figure 5.25: Normalized Young's modulus for each fiber content ratio compared to the 90 degree sample for each orientation.

With the volume fraction testing of the 1mm samples concluded, now the aspect ratio is observed with 1.5mm samples being tested at varying volume fractions. The same parameters and testing conditions were used with only the length of the reinforcing carbon fibers being changed to give a higher aspect ratio. In the previous

1mm samples, an aspect ratio of approximately 3.33 was used. This aspect ratio was increased to 5 due to the use of longer 1.5mm reinforcing fibers. In the previous subsection the effects of altering the fiber volume fraction were already explored and thus only the lower three infill orientations are observed instead of all four. The experimental results showed similar results to the shorter fiber counterparts with the main differences being the magnitude of its mechanical properties. Whilst the 2.5% samples both share a similar trend of decreasing modulus with increasing misalignment to the applied force, it is noted that the 1.5mm counterpart exhibited an average increase of 61% between the 90 degree samples and the 0 degree samples. The 1mm counterpart had a larger difference of 108% between the 0 and 90 degree infill orientations, yet the 45 and 0 degree difference is 54% which is smaller than the 104% difference for the 1.5mm samples.

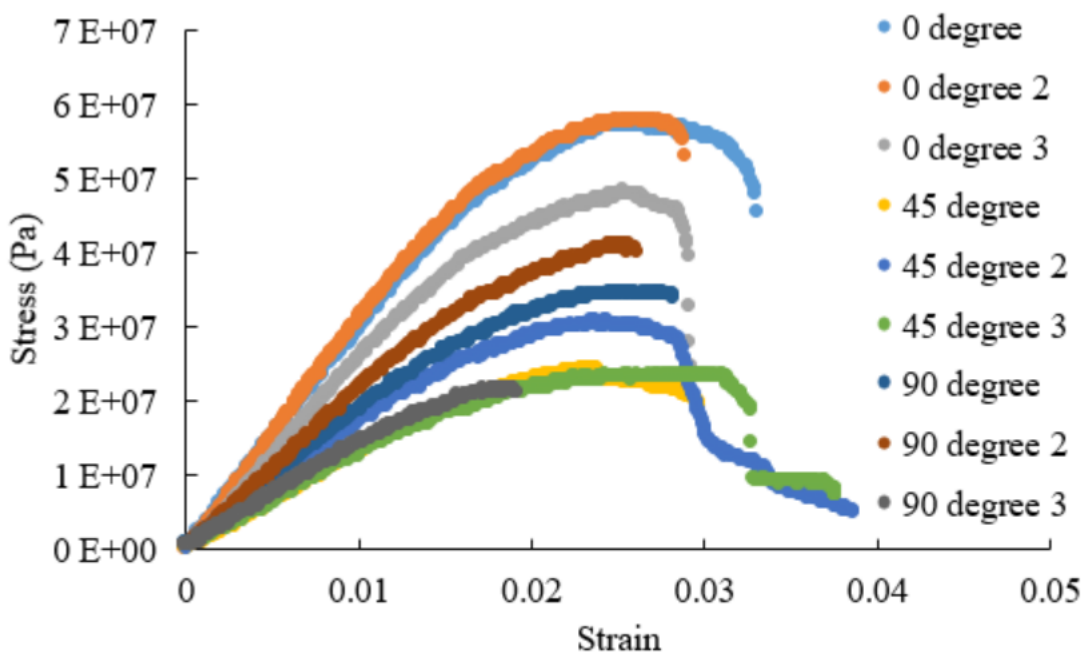

Figure 5.26: Varied stress/strain responses of the 2.5% low volume fraction reinforcing fiber samples with the longer 1.5mm fibers.

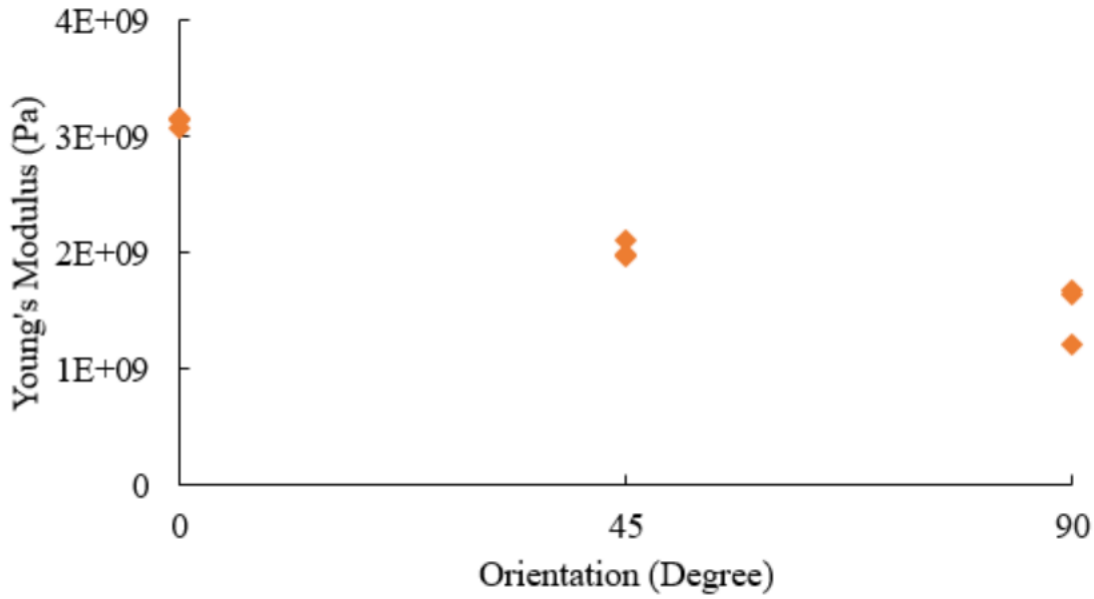

Figure 5.27: Young's modulus response of the 2.5% samples exhibiting varied results in the transverse 90 degree orientation.

The experiments are then repeated for the 5% samples with the longer 1.5mm reinforcing fibers and the data is shown in the Figure below. These results are consistent with the 2.5% samples with the exception of one of the 45 degree samples that exhibited a drastically higher toughness than the other samples. Despite this, it still performed similarly to the other 45 degree samples and is considered an anomaly due to the artifacts of inter-layer fusion of 3D printed layers. One thing to note is that although there is still a high sample disparity for each orientation (similarly to the 2.5% samples), there is a greater difference or "gap" between each infill orientation. Figure 5.29 shows how each infill orientation follows a steady trend of a decreasing Young's modulus with 2/3 samples consistently following the decline and having similar properties.

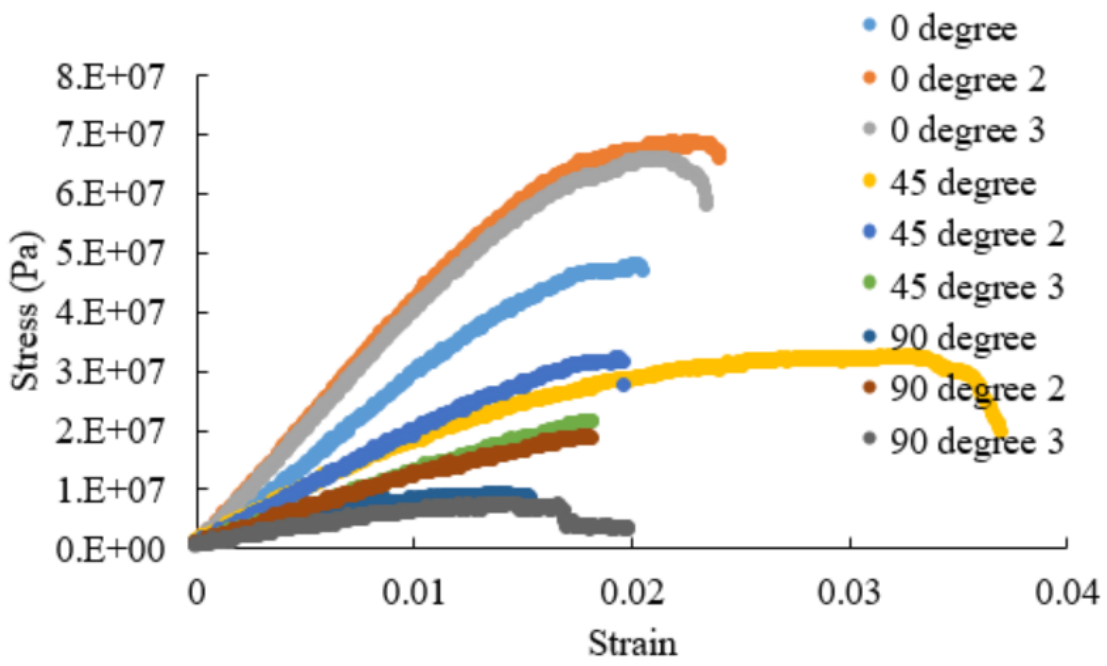

Figure 5.28: Stress/strain response of the 5% samples with two sample anomalies of the first 0 degree sample and the first 45 degree sample.

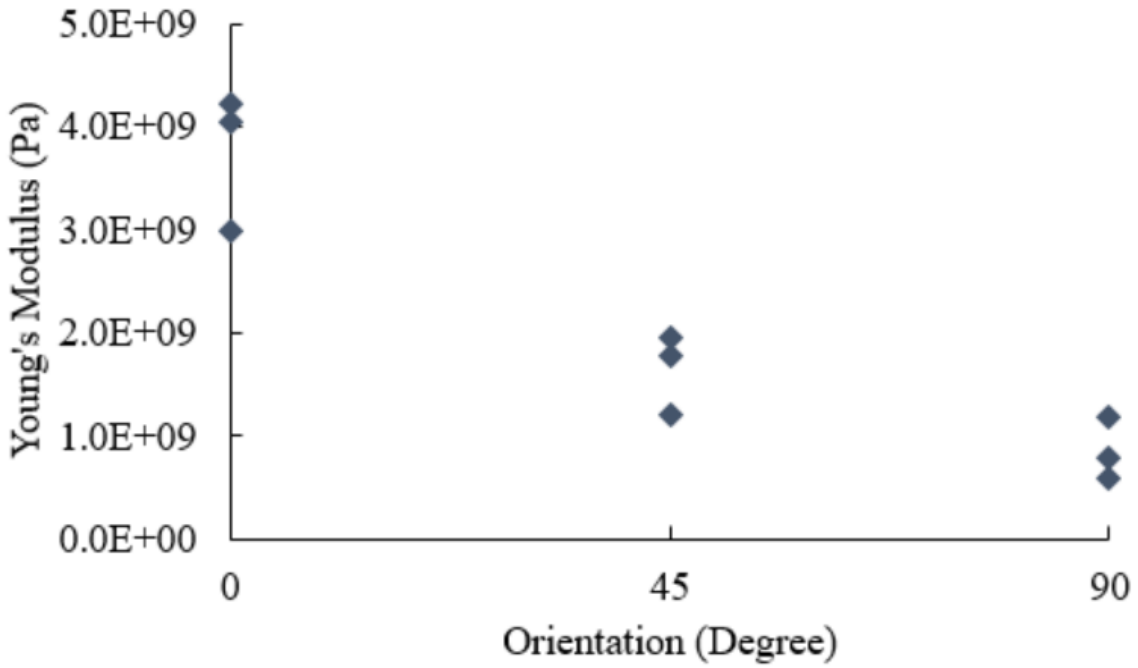

Figure 5.29: Young's modulus responses of the 5% samples further showing the 0 degree anomaly affecting the average value with a considerable drop.

Finally, the 7.5% samples show an increase in stability and consistency in the 3D printed samples stress/strain results and follow the same trend stated for the 2.5% and 5% samples. An increasing in alignment of the reinforcing fibers showed consistent gaps in the mechanical responses recorded and the orientation is shown to greatly impact its mechanical properties. Although the results appear to be more consistent than the 2.5% or 5% results, it still has a toughness anomaly with a 90 degree sample and further reinforces the statement that the 1.5mm samples are more susceptible to 3D printing artifacts.

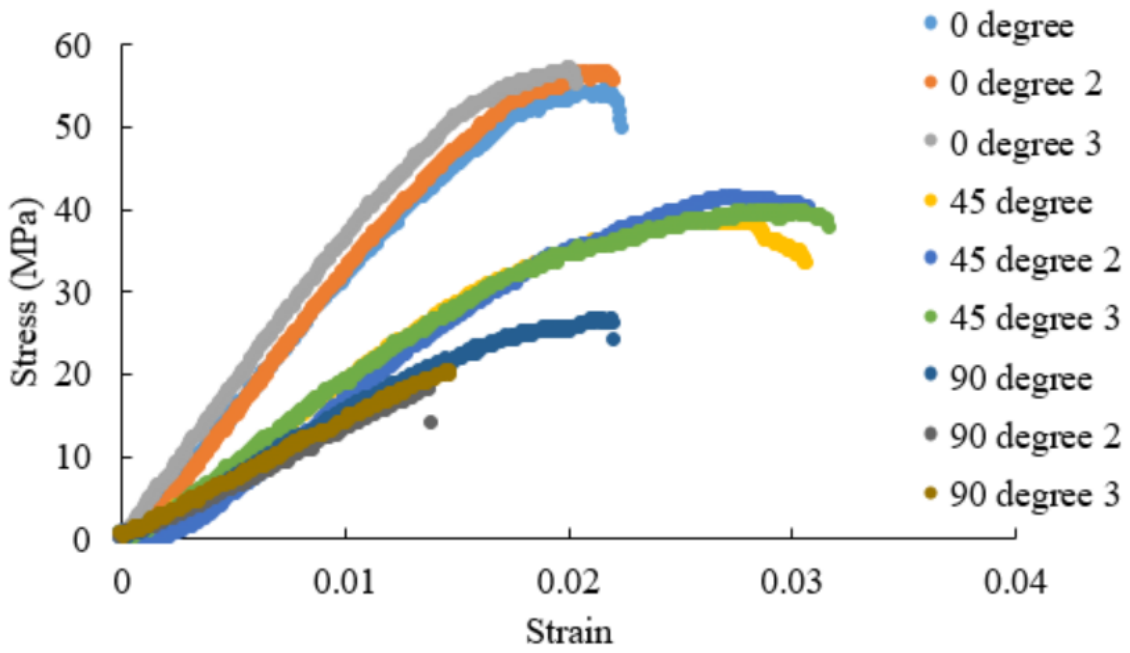

Figure 5.30: The 7.5% sample stress/strain response show more distinct separations between fiber orientation and sample response.

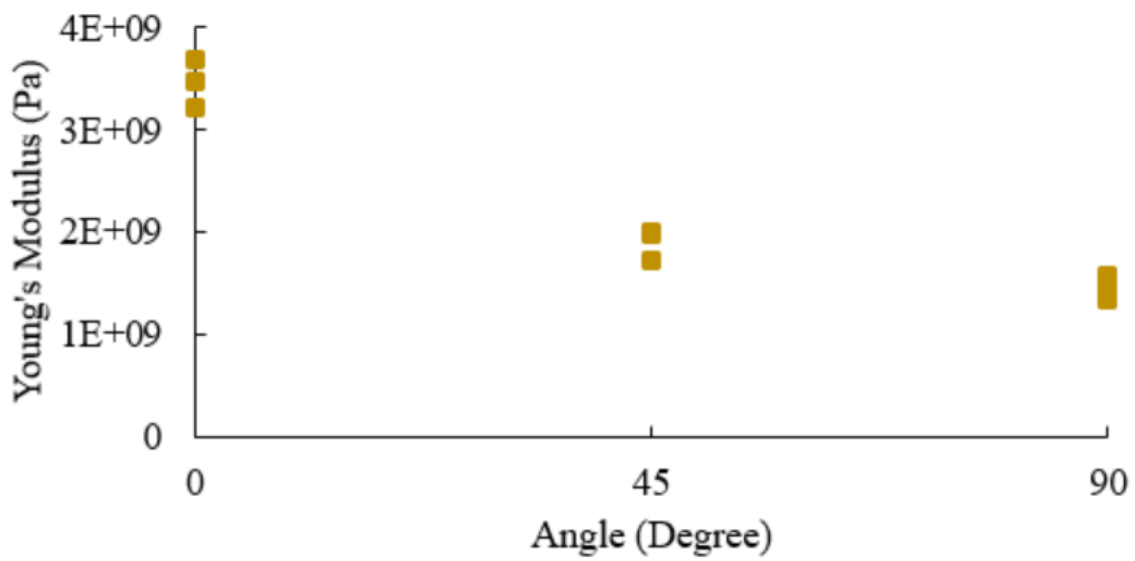

Figure 5.31: The Young's modulus for the 7.5% samples showed a more balanced distribution of values and seemed to be free of the anomalies seen in the 2.5% and 5% samples.

To the summarize the 1.5mm reinforcing fiber samples, Figure 31 shows the average change in the Young's modulus with respect to the filaments volume fraction for the fiber reinforced samples. The results show how the fiber orientation is still the dominating variable when comparing the 0 degree samples, yet with the misaligned samples this no longer holds true. With the fibers not aligned with the direction of loading the mechanical responses become less predictable with the longer fiber samples compared the shorter 1mm samples.

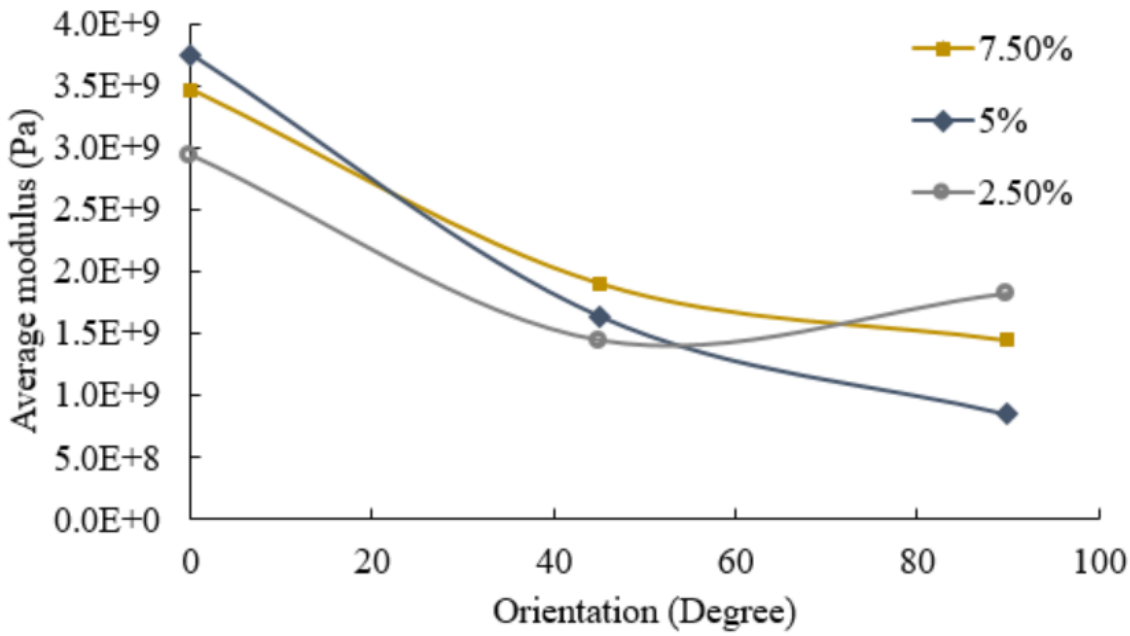

Figure 5.32: Mechanical response of the 1.5mm samples which behave more chaotically with the misaligned fiber orientations compared to the 1mm samples.

When normalizing the Young's modulus for the 1.5mm samples we see how anisotropic the response of the samples can be based on the fiber content and orientation. One thing interesting to note is how much more distributed the values appear to be for the 1.5mm samples compared to the 1mm samples. It is theorized that the longer fibers might not have the same aligning properties as the 1mm samples and as a result are more diverse in their responses.

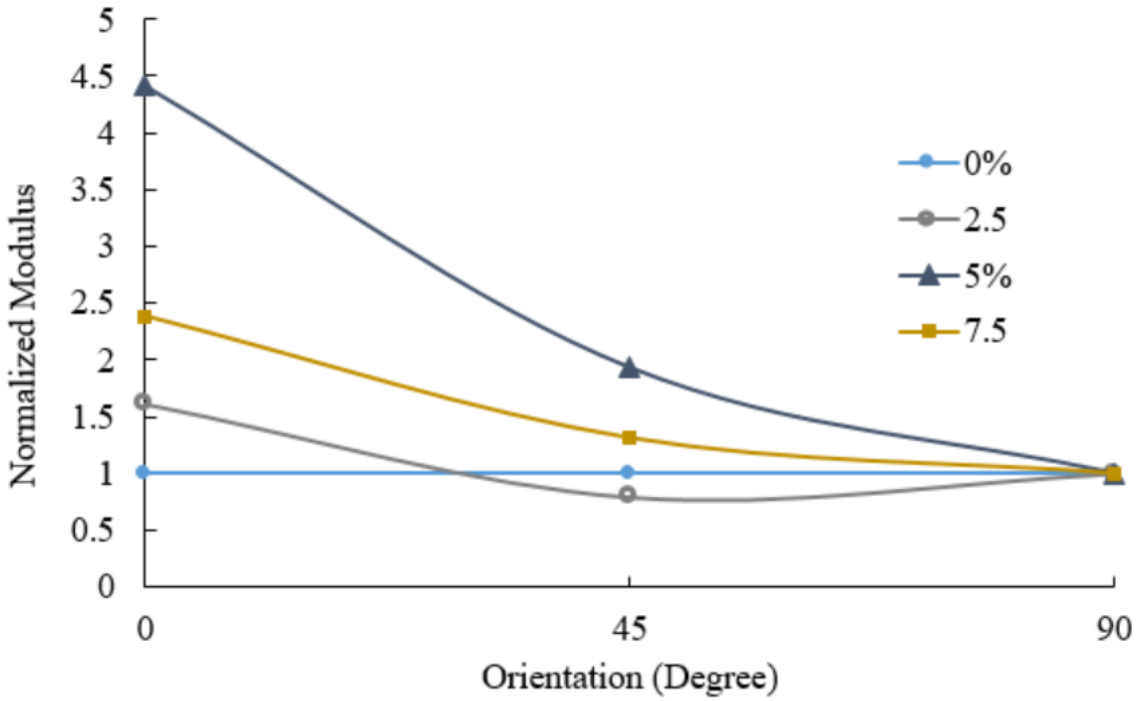

Figure 5.33: Normalized modulus response of samples with 1.5mm reinforcing fibers.

5.6 Theoretical analysis (Haplin-Tsai)

As mentioned in a previous section, the aspect ratio and volume fraction of the reinforcing fiber plays a considerable role in the mechanical properties. The Halpin-Tsai model is a popular theoretical analysis model used to predict the mechanical properties of composites, specifically short fiber composites [84]. The Halpin-Tsai model is often used as an empirical method to solve for the micromechanics of discontinuous (short) fiber composite laminas for both the aligned and randomly distributed fiber orientations. For the case of the aligned fibers, the two major moduli that need to be determined are the longitudinal and transverse modulus. Equation 5.5 represents the equation to solve for the longitudinal modulus while Equation 5.6 represents the transverse modulus. These equations share a few constant values that repeat and are thus shown as Equations 5.7 & 5.8 to simplify the moduli equations.

$$E_1 = \frac{1 + (2R\eta_1 c)\, E_m}{c\eta_1} \tag{5.5}$$

$$E_2 = \frac{1 + (2\eta_2 c)\, E_m}{c\eta_2} \tag{5.6}$$

Where c is the volume fraction contribution of the fiber and R as mentioned before is the aspect ratio. Constants η_1 and η_2 are defined by fiber properties calculated using Equations 5.7 & 5.8 where Ef and Em are the elastic modulus for the fiber and matrix respectively.

$$\eta_1 = \frac{E_f/E_m - 1}{E_f/E_M + 2R} \tag{5.7}$$

$$\eta_2 = \frac{E_f/E_m - 1}{E_f/E_M + 2} \tag{5.8}$$

For instances with randomly distributed fibers a new equation is used to determine the modulus for the whole matrix (Equation 5.9) using the previous equations for a single lamina.

$$E = \frac{3}{8}E_1 + \frac{5}{8}E_2 \tag{5.9}$$

For the Halpin-Tsai approximations, the mechanical properties of the manufacturing materials are used. The modulus of the bulk ABS used as the polymer matrix was used based on the manufacturer specifications of 2.41 GPa. For the reinforcing fibers the manufacturer specified 60 GPa and thus the ratio of the fibers modulus to the matrix modulus would be 60 GPa/2.41GPa or a ratio of 24.7 [85] The aspect ratio is then determined by using the manufacturer specified thickness of .36mm and the length of the reinforcing fibers varied between 1mm and 1.5mm to replicate the experimental testing. With the aspect ratio and material properties defined, the only remaining variable still needed is the volume fraction of fibers to matrix. This is varied similarly to the physical samples tested with reinforcing fiber quantities between

1.25% and 10% volume fractions. Figure 5.34 shows the computational longitudinal modulus for both the 1mm and 1.5mm fiber lengths with respect to the volume fraction of reinforcing fibers. The results appear to be mostly linear in the ranges tested with the 1.5mm having an increase in the modulus at a slightly faster rate than the 1mm.

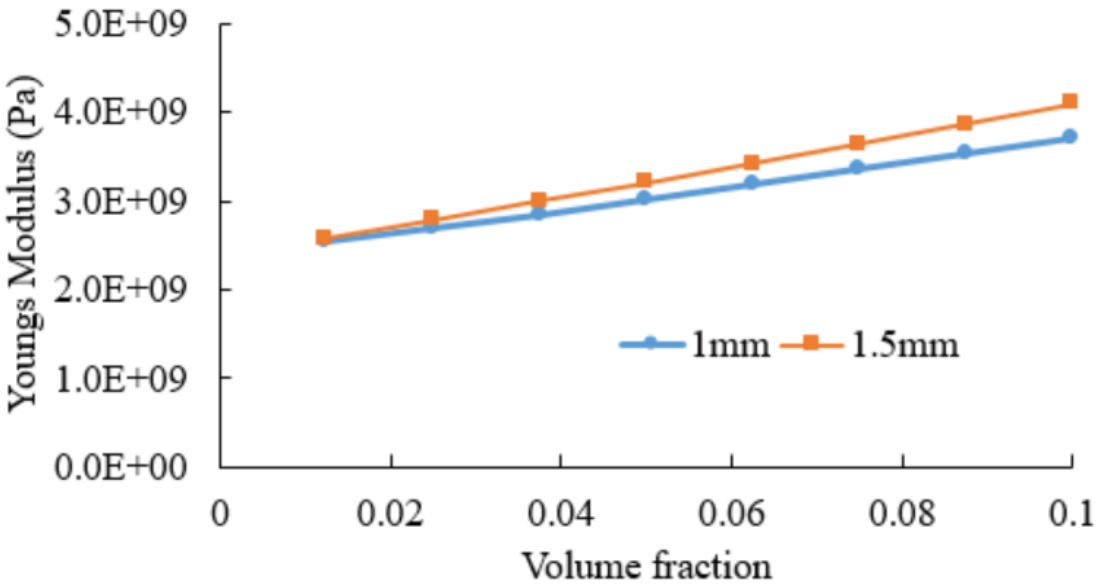

Figure 5.34: Theoretical longitudinal Young's modulus response for varying infill percentages and fiber length.

For the transvers modulus, the Halpin-Tsai equation only use the fiber volume ratio and ignore the aspect ratio. According to the Halpin-Tsai criteria, the 90 degree orientation is perpendicular to the fiber direction and the length of the fiber is irrelevant for this failure method. This can be seen in Figure 5.35 where both the 1mm and 1.5mm calculations overlap.

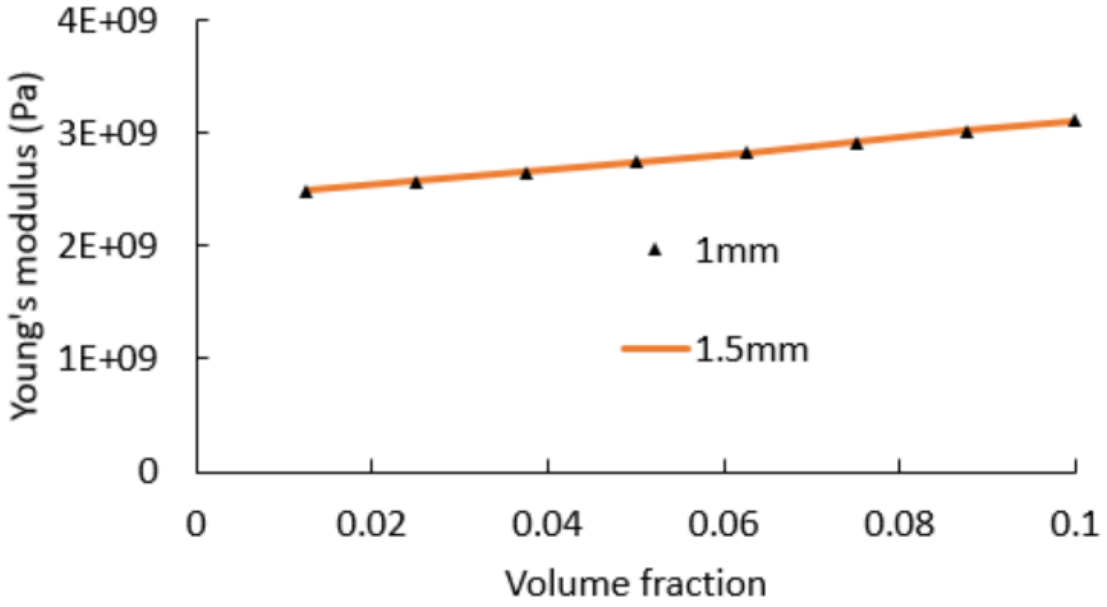

Figure 5.35: Theoretical transverse modulus for varying fiber content despite varying fiber lengths.

The results from the Halpin-Tsai approximations are then compared to the experimental results shown from the previous sub-sections. Figure 35 shows the ratio of the 0degree sample modulus with respect to the unreinforced modulus of the plastic matrix for both the experimental results and the Haplin-Tsai calculations. The results show a trend of an increasing longitudinal modulus with comparable magnitudes for the actual vs theoretical results. This gives credibility to the idea of using short fiber laminate composite theories to predict the mechanical responses of 3D printed short fiber composites.

The same analysis was then conducted for the 1.5mm samples and the results are plotted in Figure 5.37. The results appear to be similar to the 1mm samples with a steeper increases per fiber content with the 5% being an anomaly as stated in the previous subsection.

Finally for the transverse samples, the 1.5mm and 1mm transverse (90 degree) moduli are compared to the constant Haplin-Tsai values (Figure 37). These results

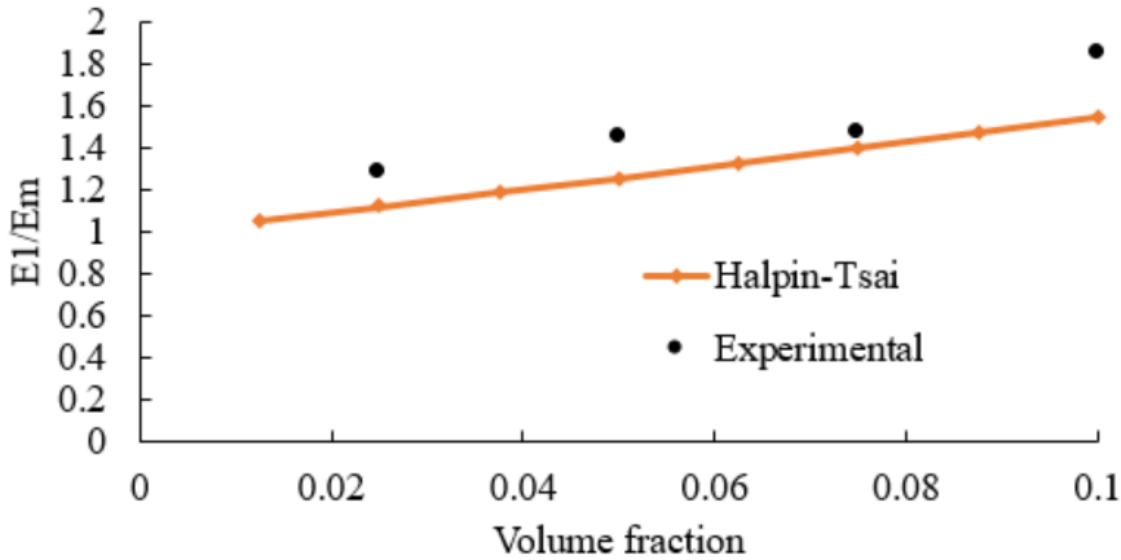

Figure 5.36: Comparison of the 1mm fiber length samples vs the Halpin-Tsai theoretical values.

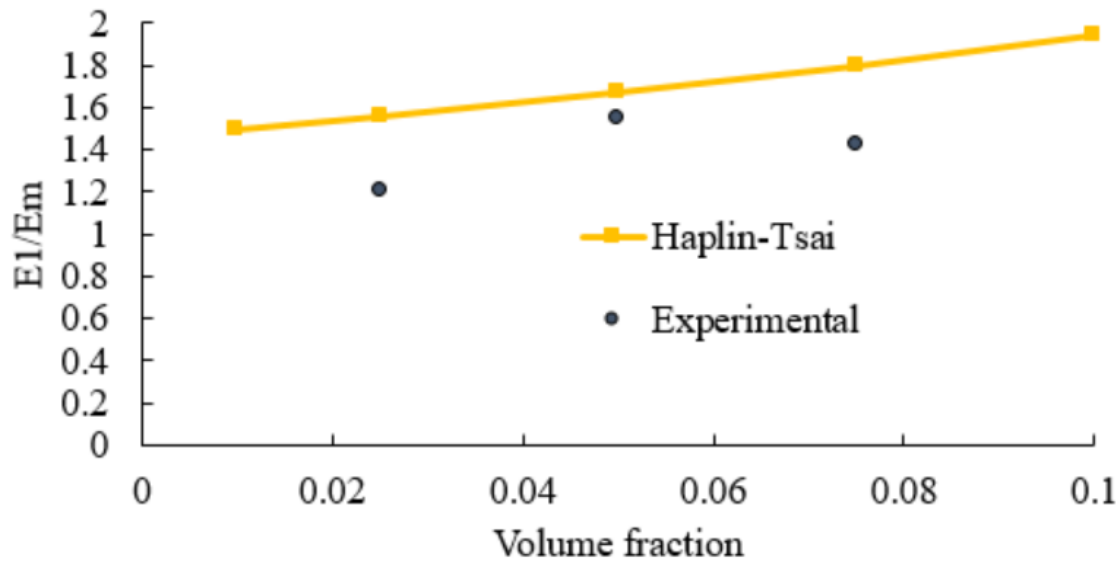

Figure 5.37: Comparison between the theoretical and measured values of the 1.5mm samples and the Halpin-Tsai calculations.

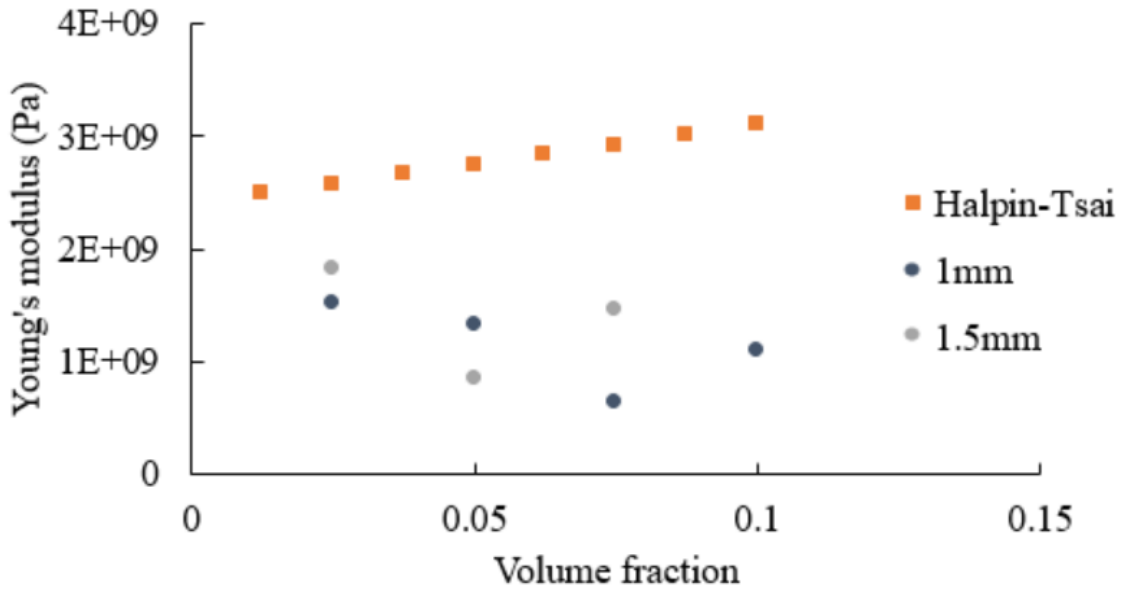

Figure 5.38: The transverse responses of the samples showed no correlation to fiber content as expected with the Halpin-Tsai calculations and was dominated by artifacts of 3D printing instead of fiber content/length.

show the chaotic responses of the samples and how they are considerably more susceptible to 3D printing artifacts. For the 90 degree samples, the failure mode is the separation between the extruded strands and inter-layer delamination which is dependent on the physical movements of the printer and the dimensional quality of the input filament.

5.7 Conclusion

The results show how a 3D printed objects mechanical properties can vary greatly based on its fiber volume fraction, fiber aspect ratio and orientation of reinforcing fibers. By studying the microstructure of commercially available carbon-fiber reinforced 3D printer filament, it is seen that there can be a considerable variance in carbon content and fiber aspect ratio in a printed part. This study used custom filament with discontinuous reinforcing fibers to control the content and length of these

fibers in an effort to capture the effects of these parameters on a 3D printed object in bending. The findings showed that increasing the fiber volume fraction can greatly increased the longitudinal modulus of the final part when comparing to the transverse modulus. This is especially noticeable when looking at the normalized modulus. The Halpin-Tsai model is used to predict the mechanical behavior of short fiber reinforced composites and compared to short fiber 3D printed composites. When the theoretical results were compared to the experimental results a correlation is noticeable. These results however do have anomalies present. The shorter fibers tended to outperform the theoretical analysis and the longer fibers tended to underperform. It was also noticed that the longer fibers tended to have more variance in the results compared to the shorter fiber counterparts. This is likely due to the longer fibers having a more considerable and detrimental impact on the parts final mechanical properties. The fibers could become entangled or extruded in a non-linear direction. There is also the ever present variation due to the nature of 3D printing. As the transverse results show, in theory the fiber aspect ratio should have no effect on the transverse mechanical properties. The experimental data shows that although there is no clear distinction between the two, there is much variance in the Young's modulus regardless of fiber length. This is attributed to artifacts of the 3D printing process overwhelming any relation that the fiber volume fraction may have imposed.

Copyright© Jordan Garcia, 2023.

Chapter 6 ANISOTROPIC BEHAVIOR OF 3D PRINTED CONTINUOUS FIBER COMPOSITES

Continuous fiber composites traditionally have the best mechanical properties but can difficult or costly to manufacture, especially when attempting to use additive manufacturing methods. Traditionally, continuous fiber composites used specialized equipment such as vacuum enclaves or labor heavy hand layering techniques. An attractive alternative to these costly techniques is modifying discontinuous fiber additive manufacturing methods into utilizing continuous fibers. Currently there exist commercial systems that utilize finite-deposition (FD) techniques that insert a continuous fiber braid into certain layers of the composite product. One of these machines, (known as the Mark Forge), has the fiber being introduced into the composite through the nozzle and a saw-like mechanism cuts the long fiber after it is extruded between layers. This method does not produce products with fibers homogenous through the entire product. As a result, traditional Laminate-Composite-Theory (LCT) does not apply to these composites without implementing further modifications for this inconsistency. Just as in the discontinuous fiber composite samples, LCT is implemented to predict the anisotropic mechanical responses of continuous fiber 3D printed samples.

6.1 Materials and methods

For continuous fiber 3D printed samples, the Markforged mark II 3D printer was used with its manufacturer recommended materials. The OnyxTM filament polymer matrix and a continuous carbon fiber reinforcement strand. The OnyxTM filament is a carbon micro-fiber reinforced nylon material with a manufacturer specified tensile modulus of 2.4 GPa and density of 1.2 g/cm3. The continuous fiber strand is the same material used in Chapter 4 for the discontinuous fiber reinforcement. It has a manufacturer specified tensile modulus of 60 GPa and a density of 1.4 g/cm3. The

main difference between the samples of this chapter and the previous chapter is the use of a polymer matrix that is already reinforced with micro-fibers and the reinforcing fiber strand is continuous for the entire laminate; however, the LCT should be able to capture the mechanical responses of these materials similarly to the discontinuous fiber samples.

6.1.1 Slice settings

The MarkForge composite printer uses a proprietary software called Eiger.io slicing software, this software was used to specify the orientation of the internal reinforcing fiber and convert the geometry into G-code for the printer. The default settings of the slicing software is set to use a repeating 0,45,90,-45 degree fiber orientation infill, with the top and bottom 4 layers absent of any fiber reinforcement. Meaning in a 3mm rectangular cross section with .125mm thick layers, the bottom 0.5mm and top 0.5mm are not fiber reinforced and only the center 2mm has continuous fiber reinforcement. The layers without any fiber reinforcing and only the OnyxTM are then printed at alternating 45,-45 degree orientations for the top and bottom layers only. These are the default settings that are used on any imported geometry into the Eiger.io slicing software. The focus is the application of CLCT thus only the orientation of the infill and reinforcing fibers will be modified from the default slicing parameters. As seen in Figure 6.1, the geometry is imported into the slicer and then the printing material needs to specified. The default OnyxTM was set up in the machine and Carbon fiber was used for material reinforcement. It should also be noted that both of these materials were enclosed in a humidity controlled container to minimize variation in prints due to changes in humidity in the environment.

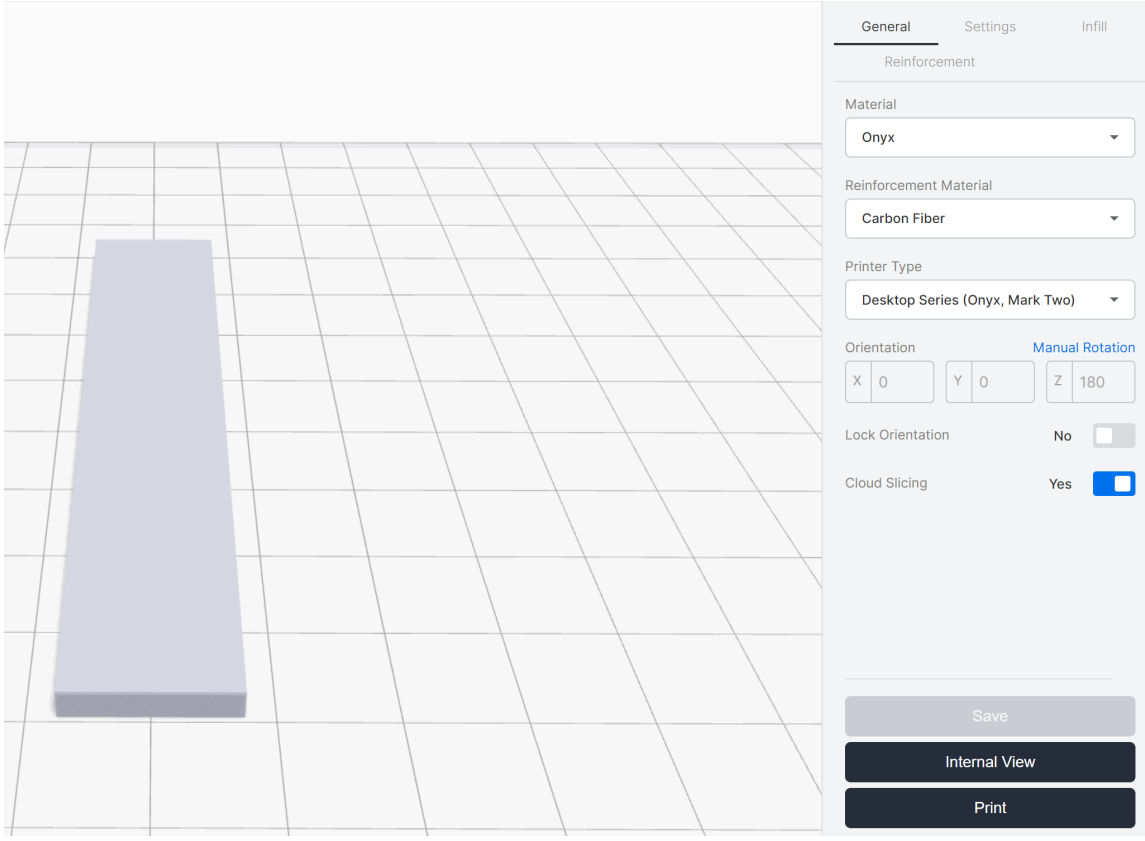

Figure 6.1: Eiger.io slicer with materials specified on the right side of the user interface. The materials specified are the OnyxTM as the polymer matrix and carbon as the reinforcing fiber.

With the printing materials specified, the only parameter changed for each printed batch was the orientation of the reinforcing carbon fiber; this was done by specifying the fiber content and orientations in the reinforcement tab. The fiber is set to create solid parts while minimizing the number of exterior polymer only walls to capture the change in properties based off the fiber orientation only. Figure 6.2 then shows how the reinforcing fiber can be specified by increasing the quantity and specifying the orientations used for each layer. Combinations of layers can be specified by the user to set repeating patterns if desired. For this case all fibers are universally oriented in a singular direction to capture the oriented lamina properties for each angle.

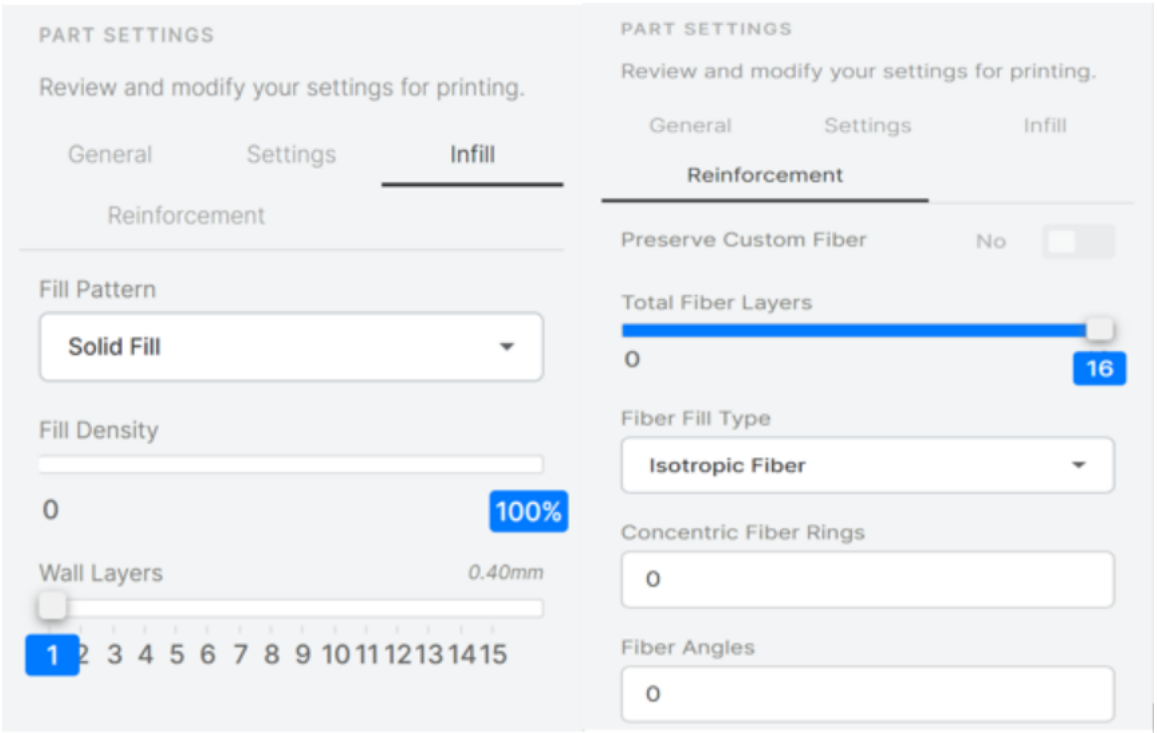

Figure 6.2: The polymer infill is specified (Left). The Fiber content is then specified using the reinforcement tab (Right).

The internal view component is used to visualize the orientation of the reinforcing fibers as well as the quantity of reinforced layers. As previously stated, unless the code is manually overridden a minimum of 0.5 mm on both the top and bottom of the samples must be polymer only. As seen in Figure 6.3 the blue lines on the sample depict the fiber reinforcement being placed for each layer while the white depicts the polymer being laid around the fibers to assist with adhesion.

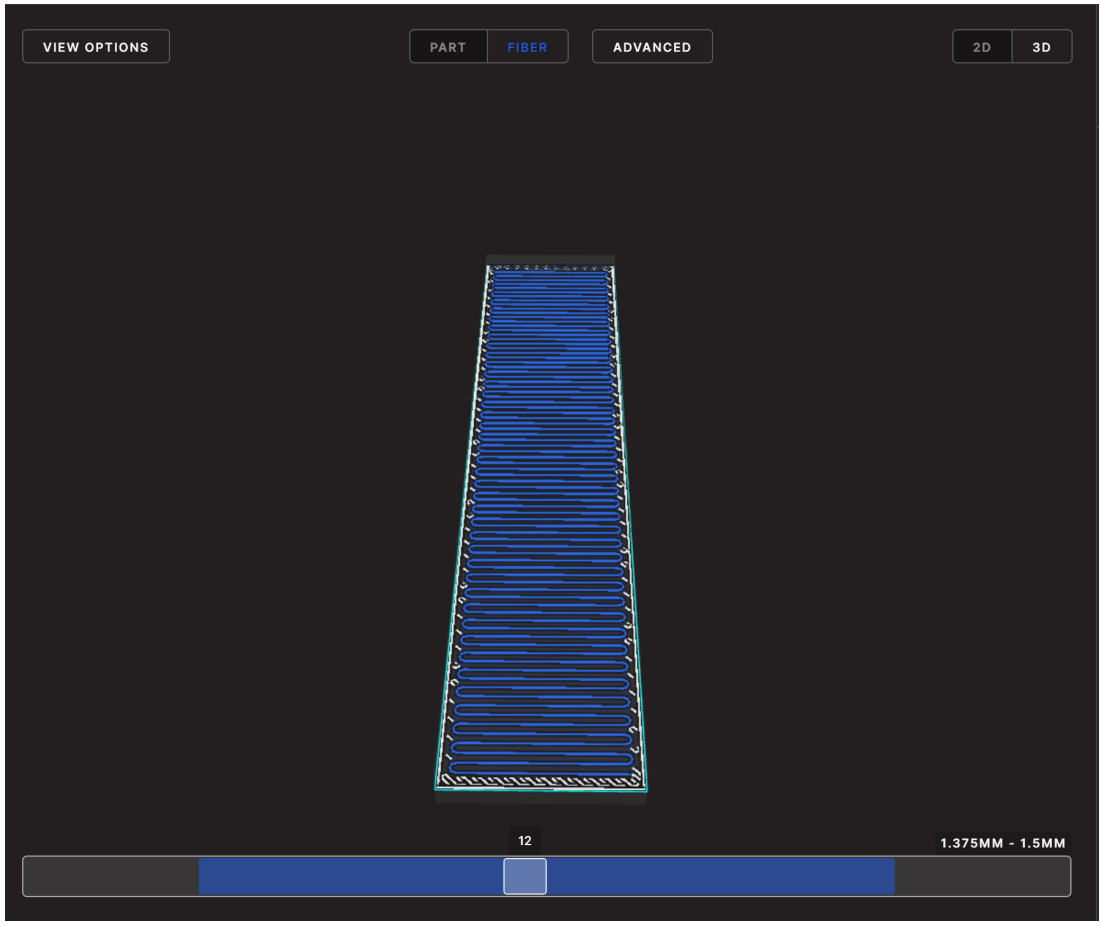

Figure 6.3: Internal view component of Eiger.io slicing software were the fiber orientations are specified by the user. This image depicts a cross section of the 0 degree angle fibers shown in blue with the polymer reinforcement shown in white.

First the orientation of the reinforcing fibers will be oriented to all face a single direction and the entire sample will be composed of continuous carbon fiber reinforced onyx filament. By testing samples whose fibers are entirely oriented in a singular direction, (such as longitudinal or transverse), the mechanical properties of a single composite laminate can be determined. The 0 degree oriented fiber samples would be used to calculate the longitudinal properties and the 90m degree oriented samples are used to calculate the transverse properties. The 45 degree orientation is then used in conjunction with the 0 and 90 degree samples to calculate the shear modulus using Equation 6.1. The end goal of these tests is to find the individual properties for each laminate orientation and implementing the CLTC equations to find the products

anisotropic macroscopic responses using the Tsai-Wu criterion. Once these properties are calculated they can then be inputted into ANSYS simulations to determine the products response by treating each layer of the 3D printed part as a laminate. Then by combining each laminate into the final geometry, the overall response is calculated for both structural and modal responses of theoretical parts.

$$G_{12} = \frac{1}{\frac{4}{E_{11}^{45}} - \frac{1}{E_{11}} - \frac{1}{E_{22}} + \frac{2\nu_{12}}{E_1 1}} \tag{6.1}$$

6.1.2 Sample fabrication and testing

Geometrically identical rectangular bending specimens to those in chapter 4 were produced to compare to the short fiber composites from the previous chapter. With nominal dimensions of 15x75x3mm, the rectangular samples are printed in batches of similarly oriented fibers of increasing misalignment from 0 degree to 90 degree. The batches also include a control batch of only alternating 45 degree OnyxTM filament with no continuous carbon fiber reinforcement. The first set of batches were printed in random order with the final outcome being 0 degrees, control with no fiber, 90 degree, and 45 degrees. As previously stated, the printing parameters are left to default values from the Eiger.io printing software to simulate manufacturing with the machine "out of the box" and no modifications. This means the top and bottom layers are polymer only and the slicer is set to print solid parts. To test the samples, the PASCO materials tester was used similarly to the discontinuous fiber samples from chapter 4. The materials tester would collect the force applied data from the load cell and the deflection data of the applicator.

To calculate the stress of the rectangular cross section at the location of failure, Equation 6.2 is used with the width and height variables. Note these simplified equations only relate to simple rectangular geometries and its stress/strain relations perpendicular to/on the neutral axis.

$$\sigma = \frac{3FL}{2bd^2} \tag{6.2}$$

Where F is the applied force, L is the length of the sample between the deflectors, b is the width of the sample and d its height. To calculate the flexural strain on the neutral axis, a different equation (Equation 6.3) is required with a new variable D, where D is the distance the beam has deflected from its original position

[19]. This value is represented by the distance the force applicator traveled during testing.

$$\epsilon = \frac{6Dd}{L^2} \tag{6.3}$$

Using the averaged stress/strain responses of the samples, the average stress/strain curve can be plotted from the calculated data. From this plot, the Young's modulus, max stress/strain, and toughness of the material can be calculated based on the response curve. The Young's modulus would be calculated using the stress/strain slope of the first .1mm/mm of strain experienced by the sample. The max stress/strain of the samples would be calculated by finding the maximum values of each before complete failure of the sample (often meaning separation of more than half of the products layers. The toughness of the samples would be approximated by integrating the area under the stress/strain response curves. The combination of these three properties are used to assess how brittle or ductile each orientation response is when compared to the other orientations.

6.2 Experimental results

The control samples with no continuous carbon fiber reinforcement were tested and the results were plotted in Figure 6.4. The data from the control samples shows that the overall response of the samples remained consistent with a gradual elastic response initially, a mid range plastic response and a ductile failure in the end. The control responses also showed that using the same printer, print location, and filament still

resulted in considerably varied mechanical responses (Figures 6.5& 6.6). The Young's modulus varied up to 18% from the highest and lowest mechanical responses while the max stress varied similarly with a 15% variance. Also of note it appears that the highest and lowest Young's modulus and max stress correlate with the same samples, this implies that the mechanical response of a test sample would either be consistently better or worse based on the sample. Taken into effect, it appears that there will always be a considerable error margin due to the nature of the printer with "good" and "bad" samples being periodically produced. Therefore a change of over 20% would imply that the results are not simply due to an artifact of the 3D printer but actually a change in the mechanical response of the samples. To predict the mechanical properties of the non-continuous fiber portions of a sample, the average Young's modulus between the samples is used instead of the manufacturer's technical data to adjust for the specific printer in use.

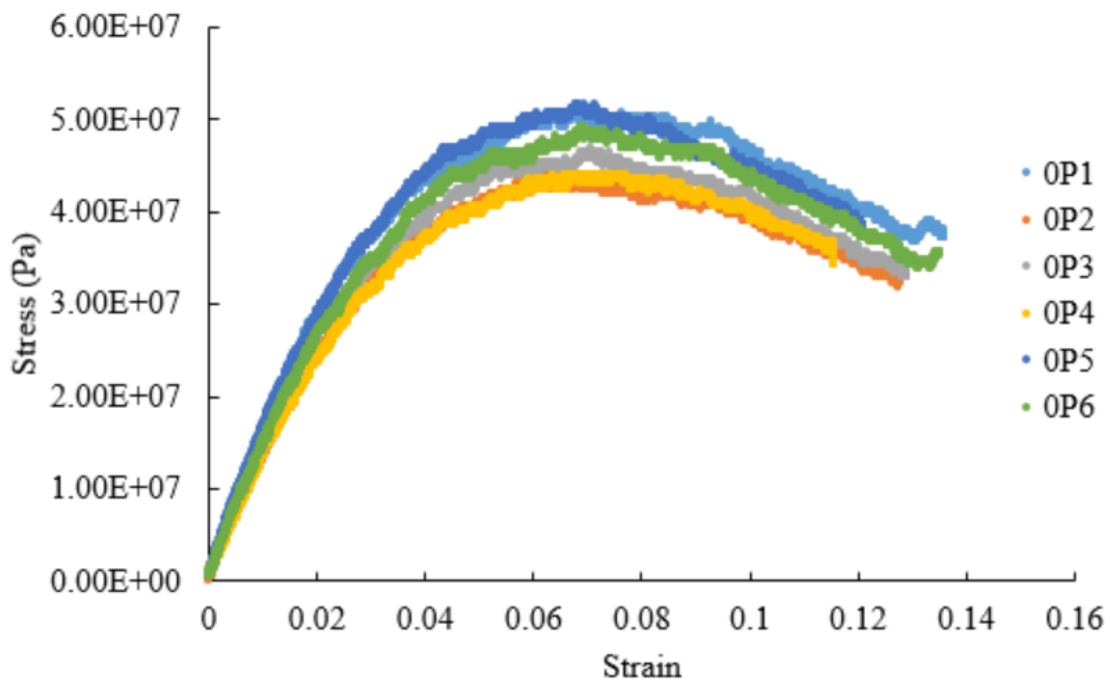

Figure 6.4: Mechanical responses of the Onyx only control samples with no continuous fiber reinforcement from the MarkForge printer.

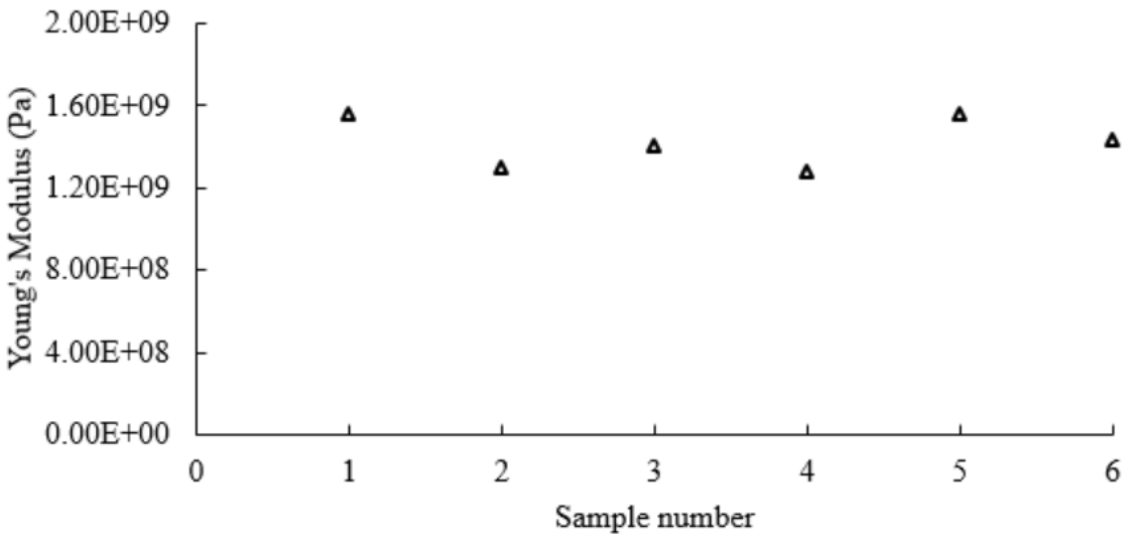

Figure 6.5: The calculated Young's modulus of the control samples based on sample data set using Equation 6.2 & 6.3.

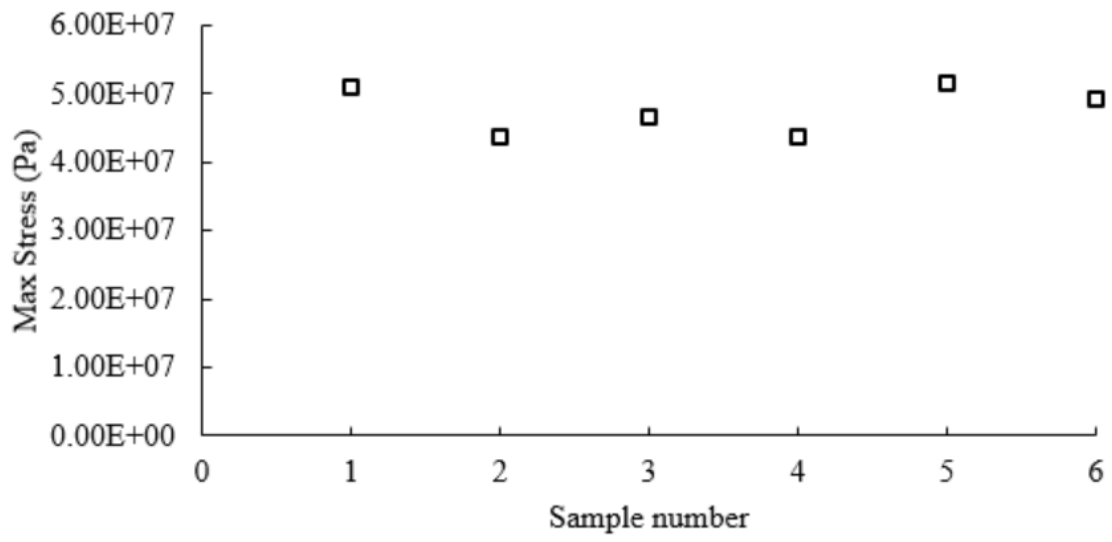

Figure 6.6: The max stress of the samples using the same data set numbering as the Young's modulus data.

The continuous fiber reinforced samples are now investigated using samples printed by the same machine. In order to calculate the longitudinal, transverse and shear moduli, the 0, 45, and 90 degree samples are used. Each sample was tested until

failure, often meaning the sample would "snap" and each half of the sample would eject itself in an opposite direction. The exception to this would be the 90 degree samples which simply separated both halves when the force applicator would reach its maximum displacement. Three sets of samples were produced and tested, each set consists of one sample with the fibers aligned to be perpendicular with the direction of the loading applicator (0 degree) and increasing misalignment until the fibers are parallel with the load applied by the loading applicator. The data sets were not produced in order but assigned to a set based on order of testing with the first 0 degree sample being "0 degree" and once the second 0 degree sample is tested it is assigned the second set as "0 degree 2". The samples were tested at random and number assigned based on the order of testing alone. The three total sets were tested and had their mechanical properties calculated with the results shown in Figures (6.7& 6.8 & 6.9).

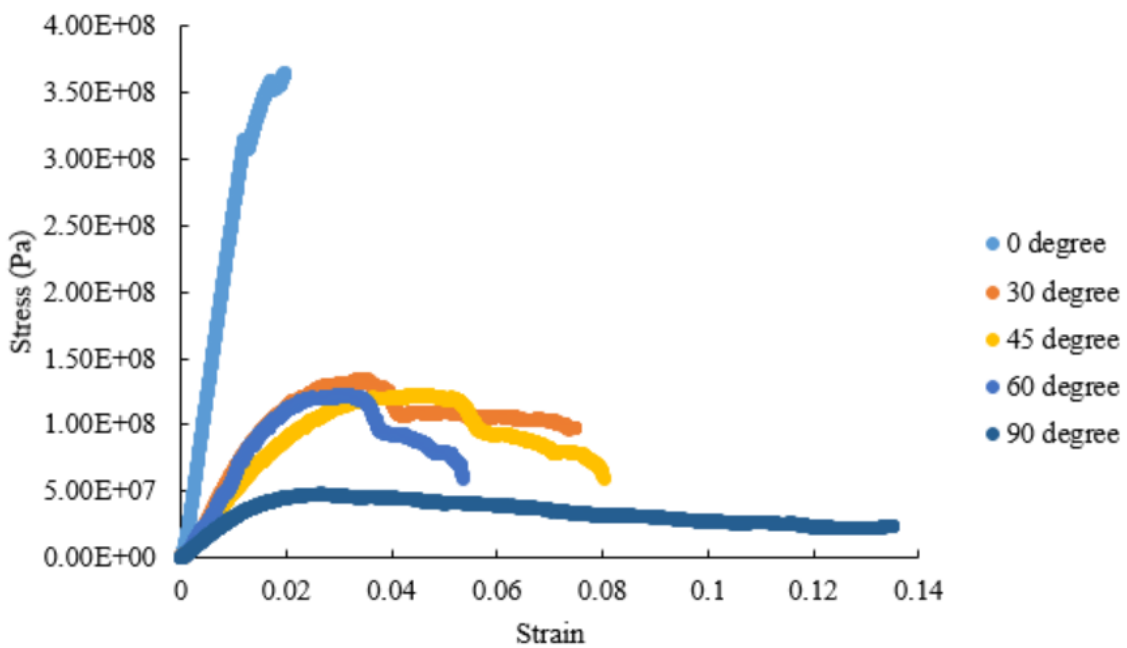

Figure 6.7: First set of data for the continuously reinforced samples and their calculated responses.

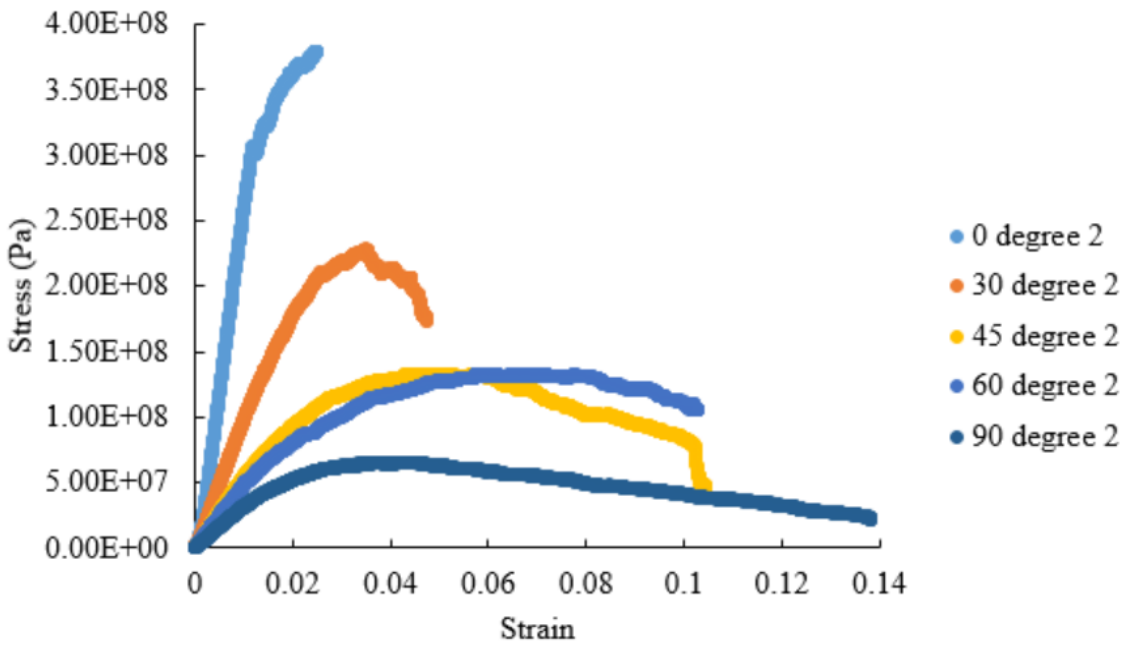

Figure 6.8: Stress/Strain response from the second set of samples tested from the Markforge printer.

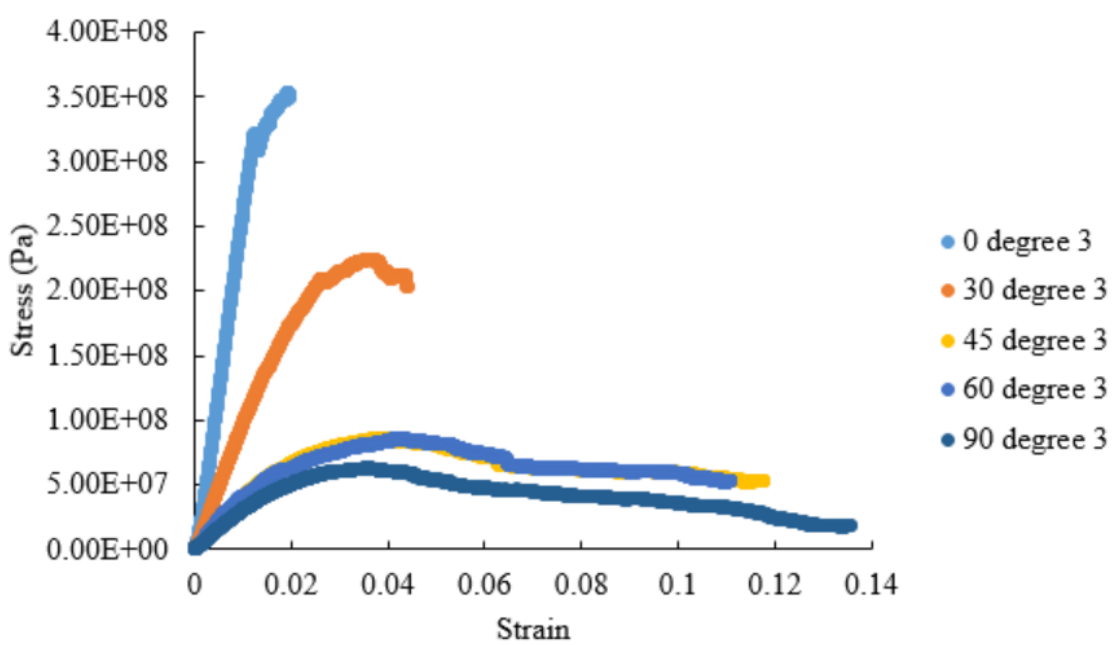

Figure 6.9: Third and final set of data from the continuously reinforced samples tested.

The calculated results showed a dramatic change in the stress/strain curve from the 0 degree to the 30 and 45 degree samples. The 0 degree samples showed a very brittle response with a steep Young's modulus and a sudden abrupt failure. The Stress response of the 0 degree sample dwarfed all other samples by almost an order of magnitude; however, the failure strain of the 0 degree samples were 80% smaller on average than the max strain of the 45 degree samples. This shows that the 0 degree samples have improved stress performance at the cost losing considerable plastic deformation, hence becoming more brittle. The results also show how slight misalignment's with the fiber loading direction can cause drastic changes on the overall mechanical responses. A misalignment of 30 degrees causes a drop of the Young's modulus by 66% on average, and a drop in the maximum stress by 45%. These drops are drastic and show just how dependent continuous fiber composites can be based on the direction of loading, it also shows how much of the materials mechanical properties can underutilized if not properly oriented. There does appear to be one possible benefit in misalignment in that the materials behave in a much more ductile manner. By rotating the fibers to be 30 degrees off from being perpendicular to the loading direction, the toughness of the material increased by 50% on average. This could be used when optimizing fiber orientations for builds to avoid any brittle failures which may not be preferable depending on application. With the testing of the samples concluded, the data is then used to calculate the mechanical properties of a single oriented lamina ply. In order to calculate the needed values for representing 3D printed parts as a composite lamina, the 0 degree, 45 degree and 90 degree samples are further investigated (Figure 6.10). The longitudinal, transverse and shear moduli are needed to calculate the mechanical properties of a single lamina ply and can be found using these three orientations. This is further covered in the theoretical analysis section. The data from the samples also shows how the 0 degree samples remain more consistent in magnitude while the 45 and 90 degree samples showed higher levels of variation. The 0 degree samples would only have a maximum difference in Young's

modulus of 1.7% and max stress of 6.8%. These samples showed extremely varied results based on how closely the fibers are oriented with the loading condition, since the loading was perpendicular to the length of the par the 0-degree sample would be considered longitudinal. The change in the products Young's modulus can be as drastic as 737% when comparing the longitudinal 0-degree samples vs. the transverse 90-degree samples. The more misaligned samples from 45-degrees and on-wards would have very little difference in their elastic response compared to the much more brittle response of the 0 degree samples.

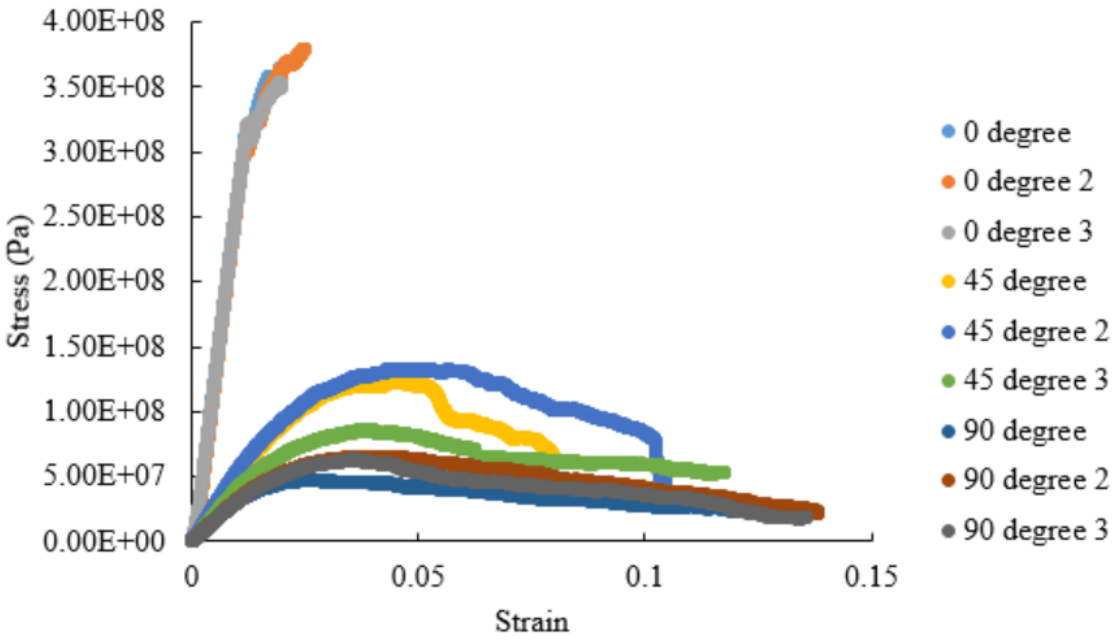

Figure 6.10: Focused results comparing the 0, 45, and 90 degree samples from each batch for CLCT calculations.

The maximum stress of the samples also directly correlates to the Young's modulus having a 687% increase from the 90-degree sample to the 0-degree sample. The following misalignments have a considerable affect between the 30-degree and 45-degree samples, yet any further misalignment appears to have a negligible effect. This is most likely attributed to the failure mode of the reinforcing fibers switching from a tensile failure to a more shear-based type of failure.

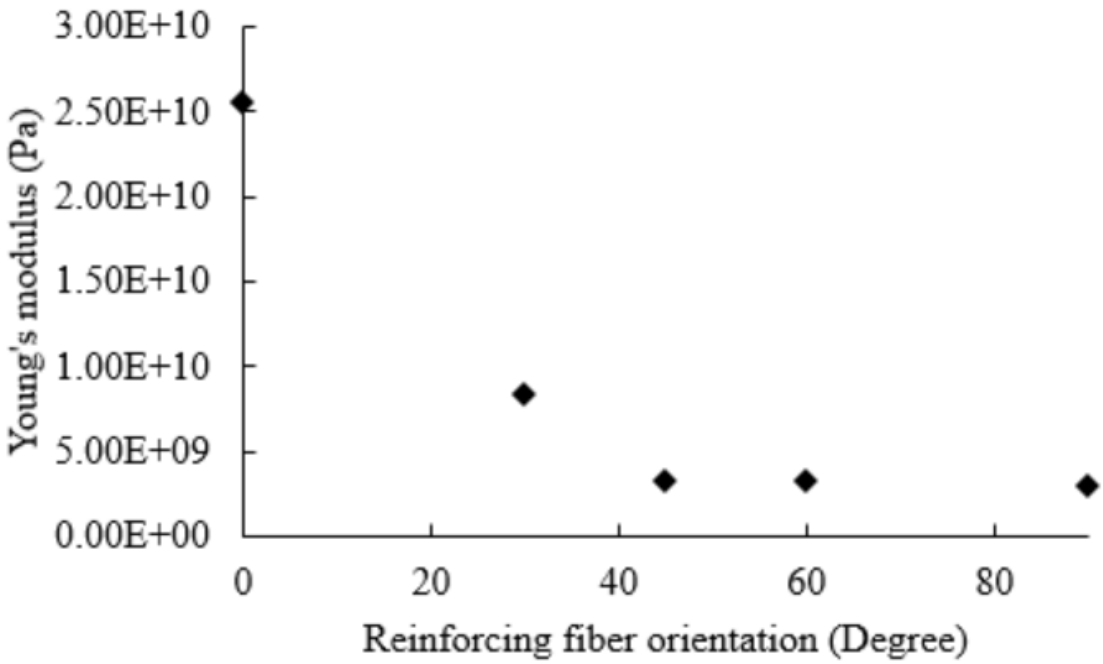

Figure 6.11: Change in Young's modulus based on fiber orientation for continuous fiber bending samples.

The effect of the fiber orientation for the continuous fiber samples appear to be much more drastic than the discontinuous fibers. Although the magnitude of the Young's modulus for continuous fiber samples outperformed the discontinuous samples, the moduli were normalized and compared to focus on the effect of the fiber orientation only. Comparing the normalized results between the two types of fiber, we see how the use of continuous fibers magnifies the effects of proper fiber placement based on loading conditions (Figure 6.13). These results show how both the continuous and discontinuous samples had the greatest mechanical response when the fibers were oriented perpendicular to the loading direction. Furthermore the continuous fiber samples had similar trends with an even greater sensitivity to fiber misalignment compared to the discontinuous fibers. This appears to agree with the Mori-Tanaka theory used in chapter 4 for the discontinuous fiber and increasing aspect ratio. Another explanation for these results is the possibility of the discontinuous fiber

samples having the short fibers "mostly" aligned with the print direction while the continuous fibers have more control over the direction of the fiber.

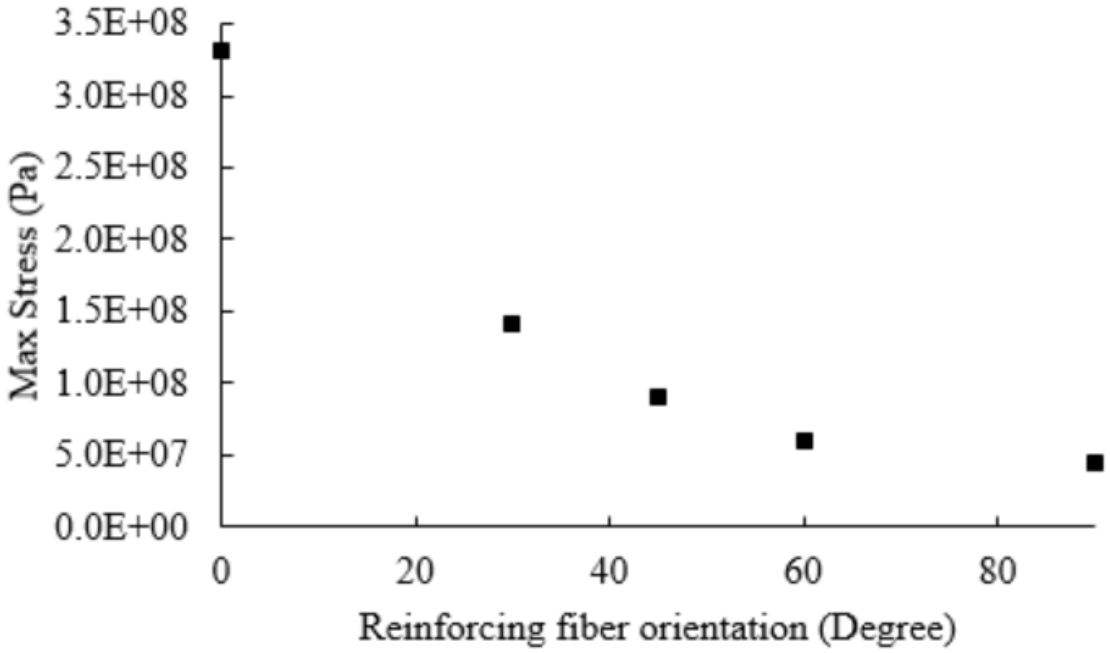

Figure 6.12: Comparison of average max stress based on reinforcing fiber orientation.

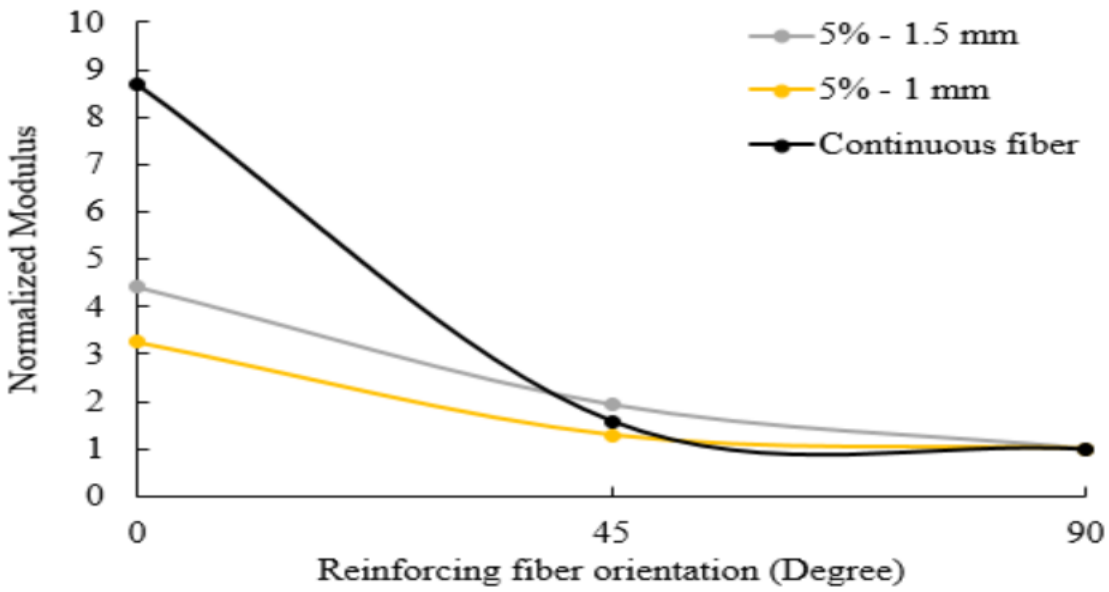

Figure 6.13: Comparison of the continuous and discontinuous fibers (2.5% and 5% 1mm samples) normalized Young's modulus.

6.3 Theoretical Analysis Tsai-Wu

Using the Tsai-Wu failure criteria for unidirectional continuous fiber composites are investigated and applied for the data gathered. These composites are constructed by combining multiple multidirectional laminates composed of individual oriented laminas. The single layer laminas are orthotropic and are stacked one atop another and combined to create a composite laminate. These laminates can be optimized for certain applications by changing the orientation or thickness of the individual unidirectional laminas. For a single layer composite lamina, when the reinforcing fibers are aligned parallel to one-another this is considered the lamina's longitudinal direction as seen in Figure (6.14). Perpendicular to the direction of the reinforced fibers is called the transverse direction; the properties of the composite lamina are dominated by the bulk matrix material instead of the reinforcing fiber.

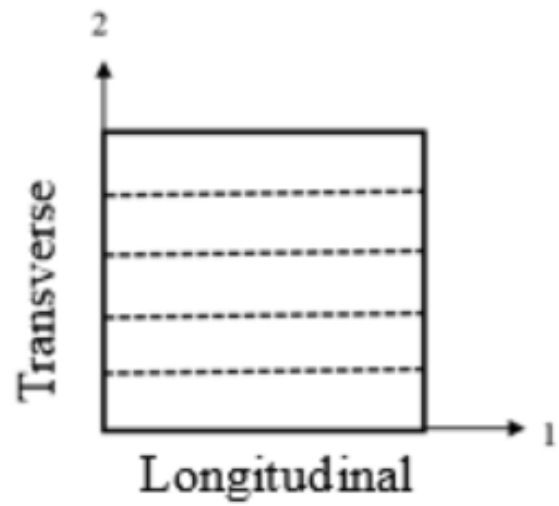

Figure 6.14: Sketch of an un-oriented lamina with its reinforcing fibers drawn to be aligned with the dotted lines

According to the Classical Lamination Theory, the strain-stress relation of an un-oriented, single-layer unidirectional lamina or ply is defined by Equation6.4.

$$\begin{bmatrix} \epsilon_{11} \\ \epsilon_{22} \\ \gamma_{12} \end{bmatrix} = \begin{bmatrix} S_{11} & S_{12} & 0 \\ S_{21} & S_{22} & 0 \\ 0 & 0 & S_{66} \end{bmatrix} \begin{bmatrix} \sigma_{11} \\ \sigma_{21} \\ \tau_{12} \end{bmatrix} \tag{6.4}$$

Where S_{11}, S_{22}, S_{12}, and S_{66} are the directional compliance's, defined by the fundamental material constants E_{11}, E_{22}, G_{12} and γ_{12}. For the engineering constants, ϵ is the strain experienced by the lamina and σ is the axial stress applied, γ is the shear strain and τ is the shear stress. The subscripts refer to the principle directions, $_1$ being the longitudinal direction, $_2$ being the transverse direction and $_6$ being in plane. To calculate the compliance, certain mechanical properties need to be used. One such property being E, where E is the Young's modulus (note the subscripts are the same as in the engineering constant where $_1$ and $_2$ refer to the longitudinal and transverse directions respectively). The symbol ν represents the Poisson's ratio and G denotes the shear modulus. The $_{12}$ and $_{21}$ subscripts refer to a combination of

loading and strain directions; the first number depicts the direction of the loading, while the second number depicts the direction of the strain.

$$S_{11} = \frac{1}{E_1} \tag{6.5}$$

$$S_{22} = \frac{1}{E_2} \tag{6.6}$$

$$S_{12} = s_{21} = -\frac{\nu_{12}}{E_1} = -\frac{\nu_{21}}{E_2} \tag{6.7}$$

$$s_{66} = \frac{1}{G_{12}} \tag{6.8}$$

For the unidirectional lamina, the variables s_{11}, s_{22}, s_{12}, and s_{66} all represent the compliance due to loading in the longitudinal direction, transverse direction, Poisson's effect, and shear loading respectively. It should be noted that due to symmetry the Poisson's effect compliance relation holds true for both Poisson's ratios so long as its divided by its respective modulus.

These relations are used for a lamina with no orientation dependencies and assuming the loading is perfectly in the longitudinal, transverse or shear directions. In real applications, the applied loads or subsequent strains can vary in directions, thus an orientation is used to describe these new directions as seen in Figure (6.15). The angle of the x direction of the orientation with respect to the longitudinal direction of the lamina is labelled as θ, and the y direction is perpendicular to the x direction. The strain-stress relation of an arbitrarily oriented, single-layer lamina or ply with arbitrary loading conditions is defined by Equation where now the compliance matrix accounts for varying types of shearing.

$$\begin{bmatrix} \epsilon_{xx} \\ \epsilon_{yy} \\ \gamma_{xy} \end{bmatrix} = \begin{bmatrix} S_{xx} & S_{xy} & S_{sx} \\ S_{xy} & S_{yy} & S_{ys} \\ S_{sx} & S_{sy} & S_{ss} \end{bmatrix} \begin{bmatrix} \sigma_{xx} \\ \sigma_{yy} \\ \tau_{xy} \end{bmatrix} \tag{6.9}$$

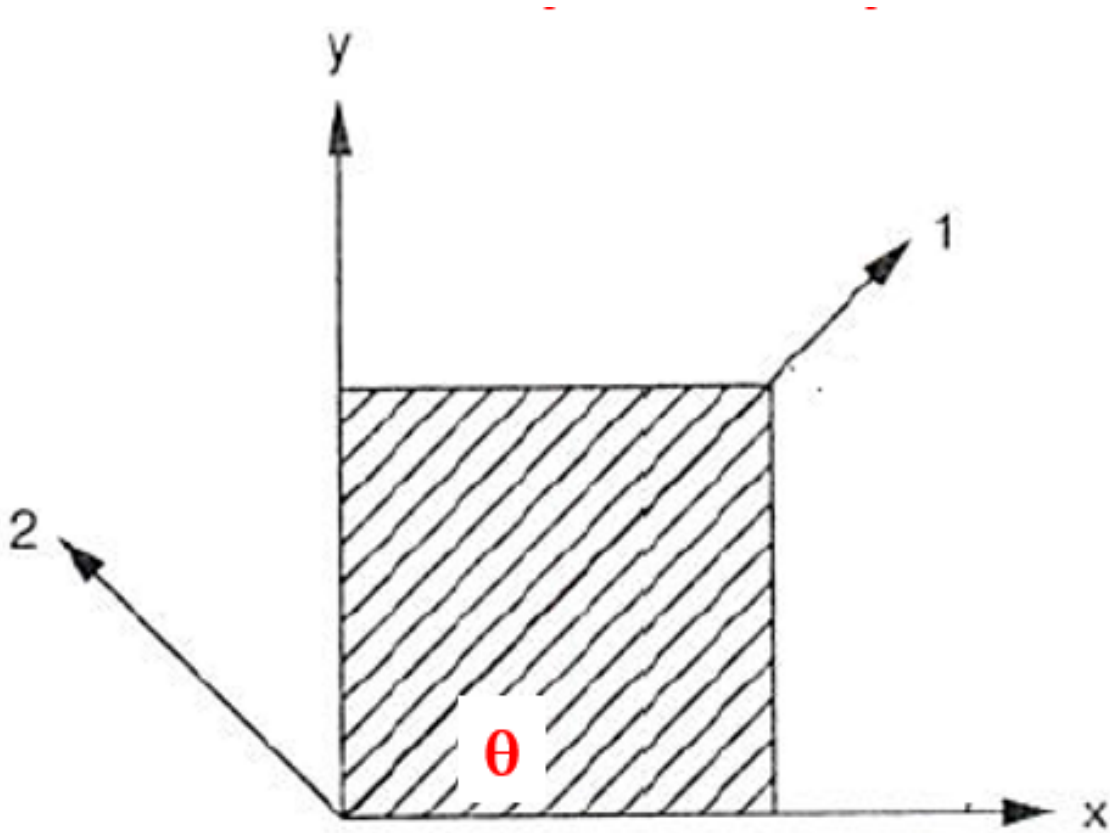

Figure 6.15: Orientation of infill fibers with respect to θ with the longitudinal and transverse directions in the 1 and 2 directions respectively.

The values for the compliance components of the oriented lamina use the same un-oriented lamina mechanical values but incorporates the orientation effects m and n. The trigonometric function Cos(θ) is represented using m and Sin(θ) represented by n.

$$S_{xx} = m^4 S_{11} + n^4 S_{22} + 2m^2 n^2 S_{12} + m^2 n^2 S_{66} \tag{6.10}$$

$$S_{yy} = n^4 S_{11} + m^4 S_{22} + 2m^2 n^2 S_{12} + m^2 n^2 S_{66} \tag{6.11}$$

$$S_{xy} = m^2 n^2 S_{11} + m^2 n^2 S_{22} + (m^4 + n^4) - S_{12} + (mn^3 - m^3 n) S_{66} \tag{6.12}$$

$$S_{xs} = 2m^3nS_{11} - 2mn^3S_{22} + 2(mn^3 - m^3n)S_{12} + (mn^3 - m^3n)S_{66} \tag{6.13}$$

$$S_{ys} = 2mn^3S_{11} - 2m^3nS_{22} + 2(m^3n - mn^3)S_{12} + (m^3n - mn^3)S_{66} \tag{6.14}$$

$$S_{ss} = 4m^2n^2S_{11} + 4m^2n^2S_{22} - 8m^2n^2S_{12} + (m^2 - n^2)S_{66} \tag{6.15}$$

As an arbitrarily-oriented single layer lamina is placed in a xy-plane and subjected to a load, the moduli of the lamina can be computed from the compliance values.

$$E_x = \frac{1}{S_{xx}} \tag{6.16}$$

$$E_y = \frac{1}{S_{yy}} \tag{6.17}$$

$$G_{xy} = \frac{1}{s_{ss}} \tag{6.18}$$

$$\nu_{xy} = -\frac{S_{xy}}{S_{yy}} \tag{6.19}$$

As seen from the compliance equations, the moduli of the lamina will be dependent up the orientation angle of the lamina layer. The longitudinal modulus (E_x), the transverse modulus (E_y), and the shear modulus (G_{xy}) are determine by the un-oriented lamina compliance values (Equations 6.10 - 6.15) which are determined by using the 0, 90, and 45 degree samples in conjunction with Equations 6.5-6.8.

Markforge provides the longitudinal modulus of its extruded carbon fiber material to be 60GPa; however, the transverse and shear properties are not specified and thus the experimental results are used to approximate these values. The 90 degree oriented samples are used for the transverse response and the shear is calculated using

Equation 6.1. The final values are calculated to be the following: the longitudinal modulus is given from the manufacturer E_x=60GPa, the transverse modulus uses the data from the 90 degree samples E_y= 3.06 GPa, and the shear modulus is calculated using a combination of the other factors G_{xy}= 2.08 GPa. With this data the mechanical responses of a single oriented lamina are calculated using the Tsai-Wu criterion. Figure 6.16 shows just how the change in orientation can cause a significant drop in the Young's modulus for a single lamina of continuous carbon fiber especially in the first 5-15 degrees of misalignment. As the theory predicted the transverse modulus would then mirror the longitudinal modulus an increases with orientation angle. This is due to the fibers orienting themselves with the direction of the loading as the fiber angle increases. As the fibers rotate the 90 degree transverse response is essentially the longitudinal 0 degree and the longitudinal 90 degree is the transverse 0 degree (Figure6.17).

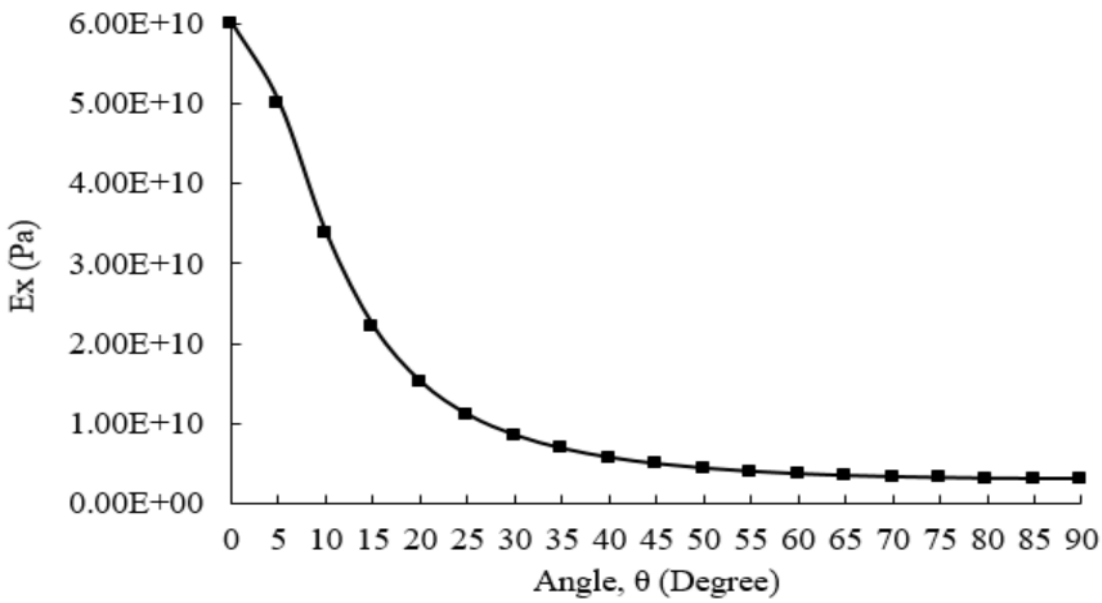

Figure 6.16: Longitudinal modulus prediction using the Tsai-Wu criterion for a single layer continuous fiber reinforced composite lamina.

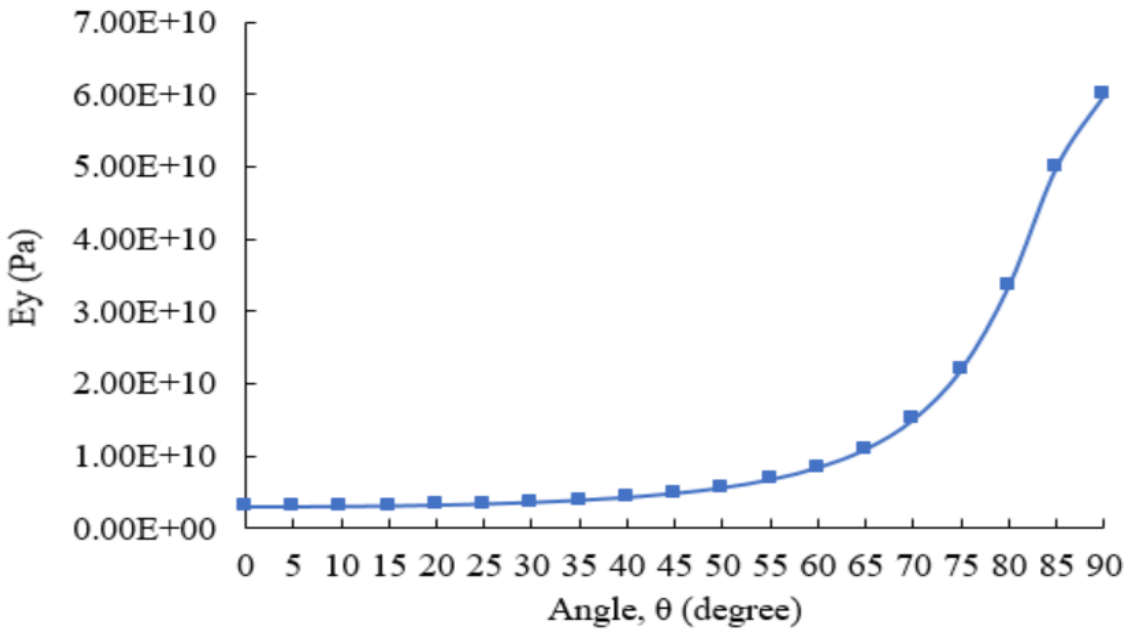

Figure 6.17: Lower transverse modulus of an oriented lamina ply for the continuous fiber reinforced lamina ply which mirrors the longitudinal modulus.

The shear modulus and effect of the Poisson's ratio instead show their own unique behavior with the lowest values at the 0 and 90 degree responses. Instead the shear modulus has its maximum value at the 45 degree orientation. This is when all the fibers would be oriented in a way that the shear force would be most translated to a longitudinal force for the reinforcing fibers, while the 0 and 90 degree samples would rely only on the shear properties of the carbon fiber and polymer matrix. The Poisson's ratio then also has the greatest effect on the 45 degree samples for similar reasons. As the shear force distributes unto the fibers, the material elongates in the axial direction of the fibers and results in the higher shear stress observed for the same angles.

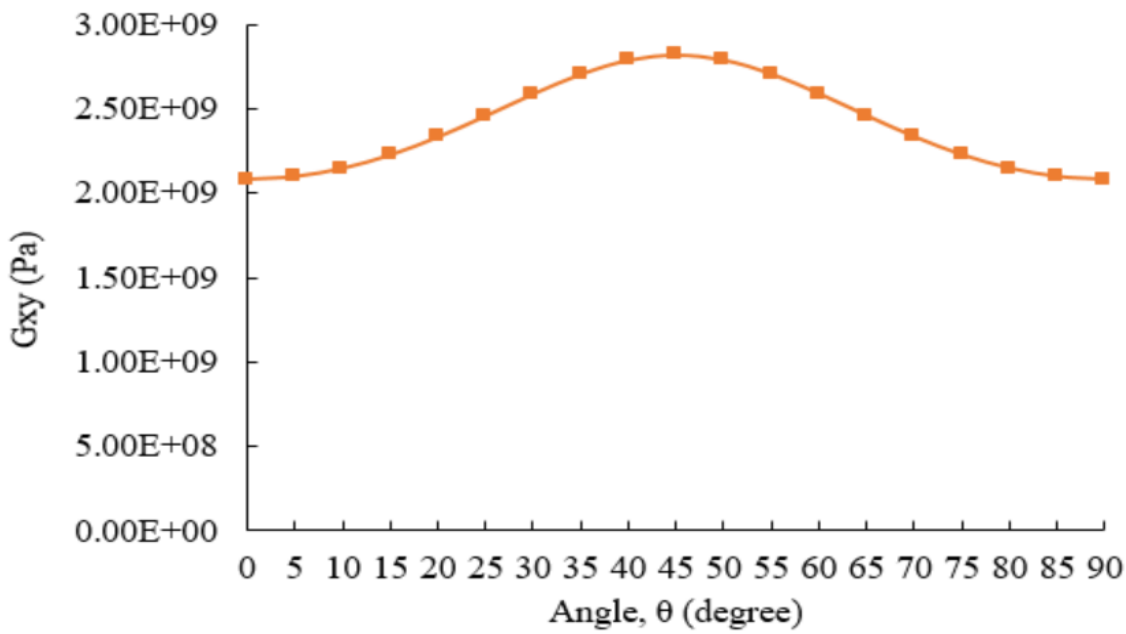

Figure 6.18: Shear modulus calculated using the Tsai-Wu criterion for the oreinted single play lamina based on reinforcing fiber angle.

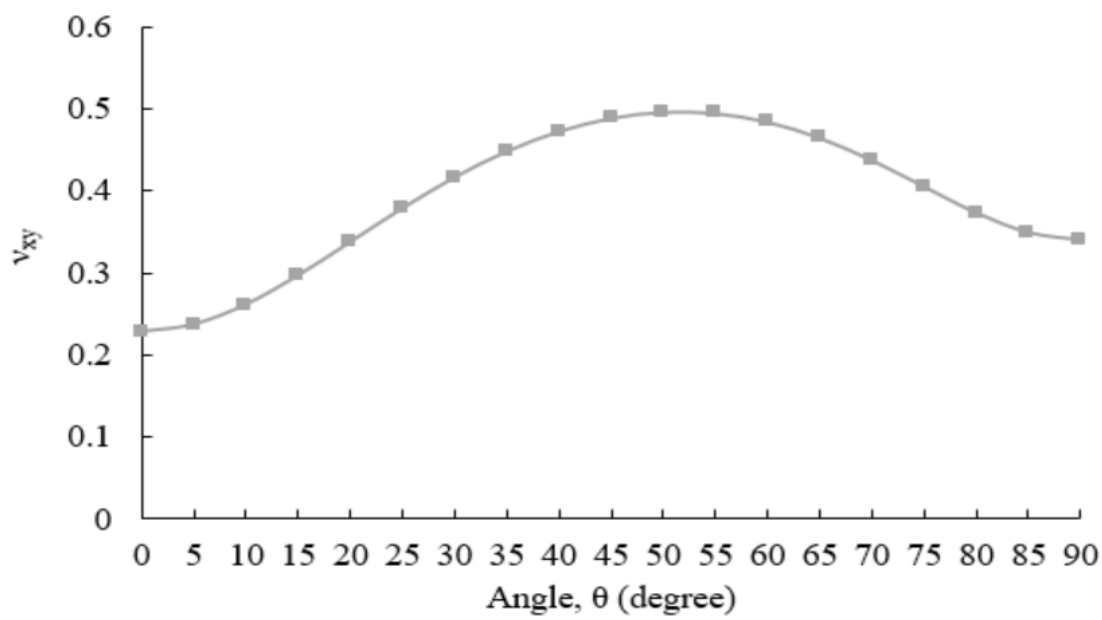

Figure 6.19: Change in effect of Poisson's ratio with respect to orientation angle resulting in the shear force being distributed more along the axial direction of the fibers.

Using the Tsai-Wu criterion the macroscale mechanical response of an oriented lamina is determined for each fiber orientation. Having the ability to predict the mechanical properties of the lamina based on fiber orientation can then be used as an input for CLC. As previously stated CLC gives the ability to predict the macro response of the final product of any combination of these laminas and orientations based on the mechanical properties calculated using the Tsai-Wu criterion. The equations for CLC were used in chapter 2 for the discontinuous fibers assuming a homogenous material. Yet for the continuous fiber samples with 4 top and bottom unreinforced layers, this assumption is no longer valid as these layers would consist of their own type of lamina response different from the layers with continuous fiber reinforcement. As a results the mechanical properties of the extruded matrix material alone must be used to compensate for these unreinforced layers and get accurate results of combined multi-lamina laminates. To summarize the Markforge printer can create continuous fiber reinforced 3D printed samples; however, the fiber is not present in all layers. Each layer has anisotropic mechanical properties independent of fiber content. The polymer only samples follow the classic 45 & -45 degree orientation when extruding while the sections with fiber reinforcement are specified by the user. To accommodate for these layers with different mechanical properties, the data from the control samples with no continuous fiber reinforcement were used. Using this data the average Young's modulus for the polymer only layers was found to be 1.42 GPa, and seeing as the orientation will not change this value is assumed for the transverse modulus as well.

By using the Tsai-Wu criteria any lamina orientation the Markforge printer follows can have it results predicted. With the properties of each lamina known, the properties of the complete laminate can be predicted and subsequently the actual final product/structure. This method can predict the mechanical response even if the fiber content is not homogenous through the laminate. This is valid as long as the mechanical properties of each material lamina type is known such as the polymer

only laminas and the fiber reinforced laminas. With this data the Tsai-Wu theory can then be applied to any combination of lamina plies to predict the mechanical response of the final structure. Several composite laminate solvers currently exist, especially in academics; however to assist in application to industry use, a commercial solver is used instead. One commonly used commercial solver with capabilities of simulating multiple lamina orientations and materials is by using the ANSYS WORKBENCH Composite Post/Pre (ACP) module. Using data from the manufacturer, and extracting data from the rectangular bending samples explained earlier in the chapter, the ACP module can simulate the responses of the composite material using CLCT.

6.4 ANSYS simulations

With the laminate mechanical properties determined from the test specimens, the theory can then be applied to a composite simulator, in this case ANSYSWORKBENCH is used. AnNSYS has a component titled the ANSYS Composite PrepPost (ACP) that allows the user to input the laminate properties for the composite material to simulate. The geometry is then modeled layer-by-layer with each layer having a defined thickness and material. The solver then combines all these layers using CLCT and simulates the mechanical responses of the entire structure. To begin, the materials for the laminates are inputted as having orthotropic elasticity using the values calculated previously (longitudinal/transverse/shear moduli and poisons ratio). The geometry of the sample is then modeled in the Geometry Modeler component using the samples nominal rectangular dimensions of 75X15 mm as seen in Figure 6.20. A simple rectangle is created using the sketch feature, then the rectangular sketch is used to create a surface.

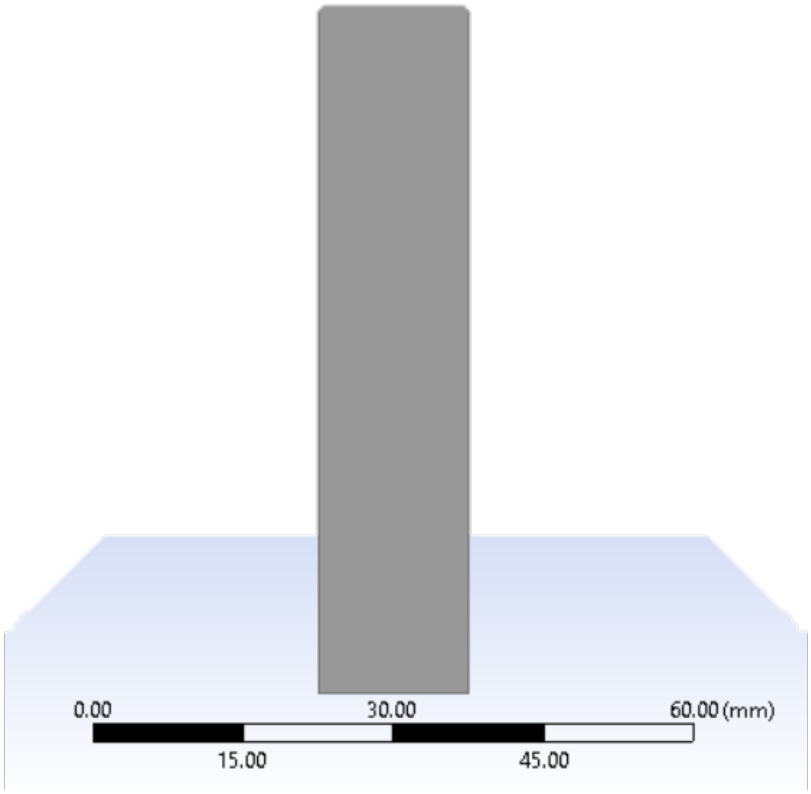

Figure 6.20: Geometry representation of sample with nominal print dimensions using a surface element in the ANSYS geometry modeler.

This surface is then used as a mid-plane for the laminates to orient around, with the thickness of the sample being determined by the number of layers and each layers respective thickness. In the ANSYS workbench ACP, the number of lamina and their associated materials/orientations can be inputted into the worksheet defining the physical part. Below in Figure 6.21 we see the actual laminate layering of a sample with unmodified 100% infill with a specified fiber orientation of 0-degrees. This inclusion of the polymer only layers captures how the Markforge actually produces solid parts if you specify the reinforcing fiber orientation with maximum carbon content. The top and bottom layers are polymer only and thus if the entire composite is assumed to be fiber reinforced, the predicted results would be considerably greater than the actual mechanical response of the samples.

Layer	Material	Thickness (mm)	Angle (°)
(+Z)			
24	Onyx_polymer	0.125	45
23	Onyx_polymer	0.125	-45
22	Onyx_polymer	0.125	45
21	Onyx_polymer	0.125	-45
20	Carbon fiber	0.125	0
19	Carbon fiber	0.125	0
18	Carbon fiber	0.125	0
17	Carbon fiber	0.125	0
16	Carbon fiber	0.125	0
15	Carbon fiber	0.125	0
14	Carbon fiber	0.125	0
13	Carbon fiber	0.125	0
12	Carbon fiber	0.125	0
11	Carbon fiber	0.125	0
10	Carbon fiber	0.125	0
9	Carbon fiber	0.125	0
8	Carbon fiber	0.125	0
7	Carbon fiber	0.125	0
6	Carbon fiber	0.125	0
5	Carbon fiber	0.125	0
4	Onyx_polymer	0.125	45
3	Onyx_polymer	0.125	-45
2	Onyx_polymer	0.125	45
1	Onyx_polymer	0.125	-45
(-Z)			

Figure 6.21: Worksheet of each specified individual laminate and its respective material, thickness, and reinforcing fiber orientation

The next step is then to mesh the geometry, due to the simplicity of the geometry a structure mesh is used. To ensure that the refinement of the mesh is not affecting the simulation results a grid independence study is conducted. Beginning with a course mesh of 30X6 elements along the geometric edges is applied as seen in Figure 6.24. The 75mm side contains 30 elements along the length of its edge and the 15mm sides have 6 elements running along the side of its edge. For a finer mesh the number of elements along each edge is doubled, 60 on the long sides, 12 on the shorter sides. This results in the finer mesh having a 300% increase in the number of elements. Both meshes neatly align with quadrilaterals filling in the space in-between the edges of the geometry, this will assist with gradient reconstruction accuracy and minimize discretization error in the simulations.

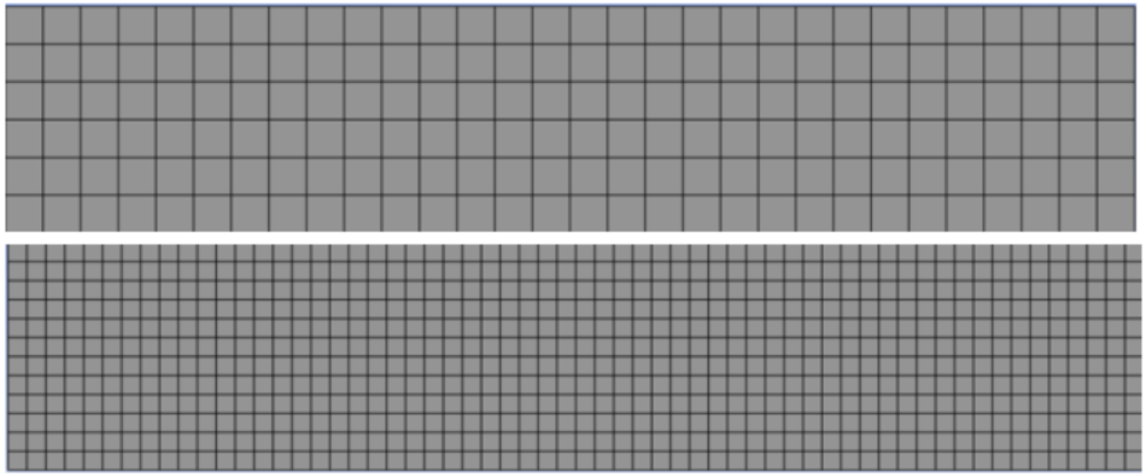

Figure 6.22: The two types of mesh are used to conduct a grid independence study to ensure the mesh is not affecting the simulation results.

The center of both the geometries is then loaded with a 10N force while the edges have a fixed displacement parallel to the load, this allows any displacement due to the load to occur without the simulation giving a translation error; (If the tested object is not sufficiently fixed the object is assumed to accelerate/translate indefinitely in the direction of the load). The solution outputs are recorded and compared, these values include the Von-Mises stress, Elastic Strain, and total or Z-directional displacement. Figure 6.23 shows a graphical result of the displacement of the beam for both meshes with a 10N force applied at the center. Despite the coarse mesh having a third of the number of elements the results were very similar and the largest change in value being the stress at 1.8% difference. With a 300% increase in elements having less than a 2% difference in the results, the mesh is considered converged for the rectangular geometry.

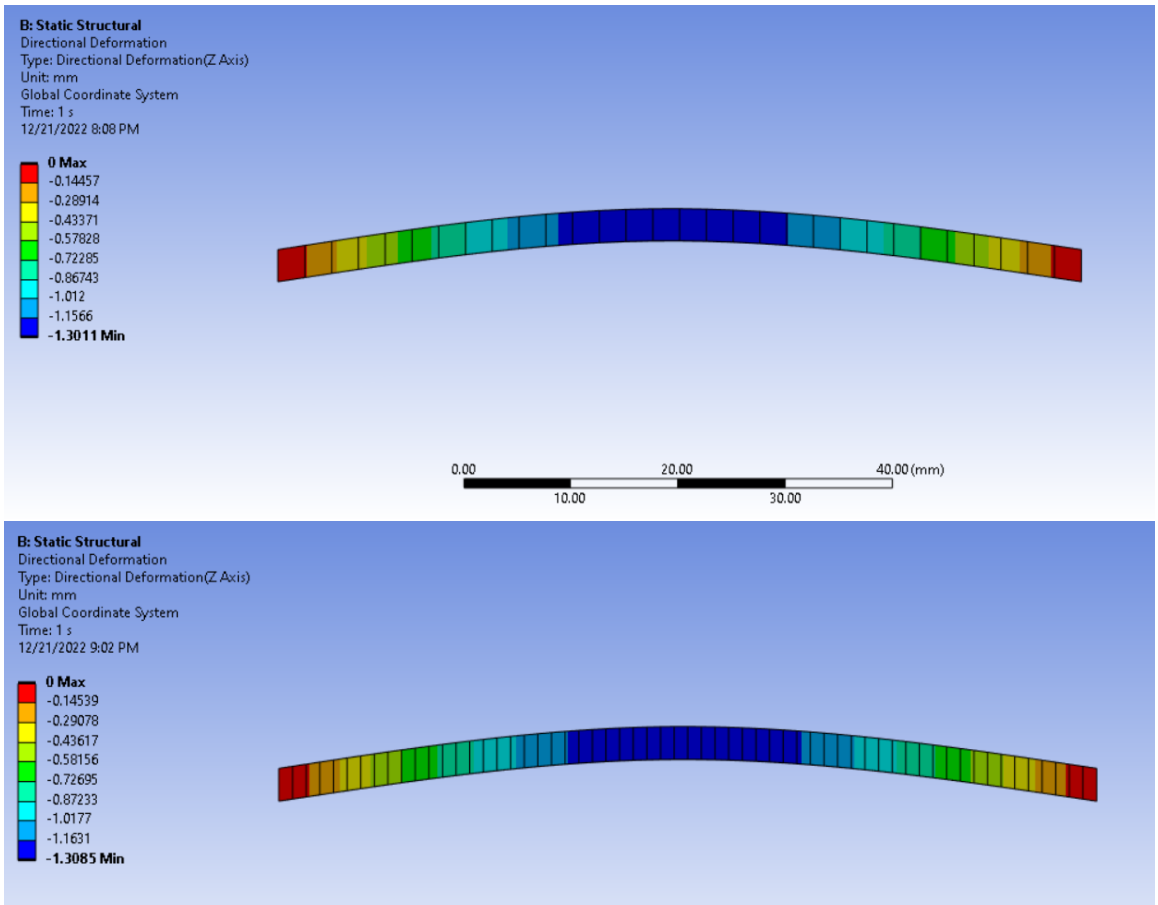

Figure 6.23: Displacement in the Z direction for the coarse mesh with a 10 N force applied at the center (top) and the same force applied at the center for the fine mesh (bottom).

As the simulations are not computational expensive due to the simple geometry, the finer mesh is used for further study. The simulator theoretically only uses the 0 and 90 degree orientations as a start and end point and calculates all the values in-between. Therefore the 30, 45, and 60 degree orientations would need to be simulated using ANSYS and CLTC to compare the simulated results with the tested samples. For the mechanical testing of the printed samples, the force and displacement data was recorded by the tester and used to calculate the stress and strain responses. For consistency the same will be done with the simulation results, the force is designated while the displacement is recorded. Both values are then inputted to the same av-

eraging equations used to calculate the stress strain curve to find the final products Young's Modulus (Equations 6.2-6.3). On the lower end of the modulus calculations a value of 17N would cause .1mm/mm of strain which was used to calculate the Young's modulus. Therefore a value of 15N was applied to the simulation specimens to be on par with the weakest samples responses to avoid any bias due to larger force values being used for the simulated samples. The results for the simulated samples using 15N of force on the center of the sample and averaging the strain compared to the experimental results can be seen in Figure 6.24.

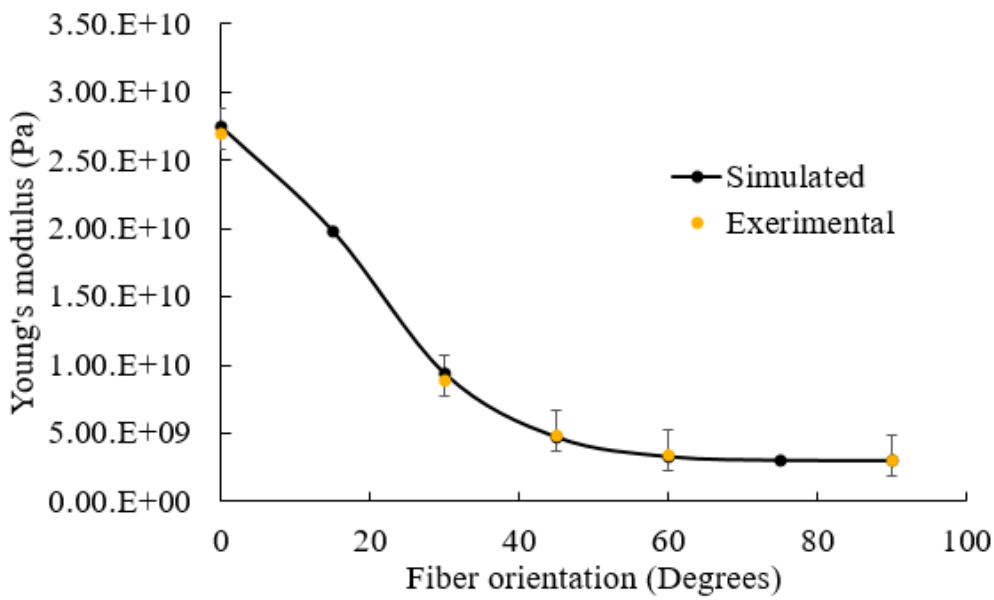

Figure 6.24: Comparison of ANSYS simulation results and physical test samples using the same averaging methods for calculation stress and strain based on force and displacement.

The simulation results showed a surprising match to the statistical average of the experimental results. The greatest disparity between the Ansys simulations and the experimental results was the 30 degree angle with a less than 5% difference. This is likely due to the 30 degree angle having the most variation in the mechanical responses of its test samples. That being said the simulation method very accurately captures the average response; however as seen in previous sections the samples do tend to

vary due to the nature of the 3D printer. Utilizing this simulation method would then come with an admonition; while this method can give the statistical average of the mechanical response, it is up to the user to incorporate the variations of their own machines and consider this when designing final products for use.

6.5 Conclusion

As previously stated the 0 degree orientation consistently had the best stress responses at the cost of behaving as a brittle material. This may not be preferable when designing structural components as an abrupt failure can cause harm to the user or attached components. It may be preferable to sacrifice the products stress response by purposefully misaligning the fibers to allow more gradual and noticeable failures. This is left to the engineer designing the component to contemplate when deciding on the fiber orientations to use. With the ACP settings and test values inputted into ANSYS workbench, more complex geometries and more abstract orientation combinations can be simulated without the need for further sample/material testing. According the CLCT more complex orientations can produce non-anisotropic final products that additive manufacturing techniques are notorious for. Certain lamina combinations can product final products that have limited isotropic properties down to the more complex quasi-isotropic laminates. Another theoretical use for this simulation method using CLTC is by testing simple rectangular bending specimens, the solver can also simulate other types of responses such as a force applied in the tensile direction or even the dynamic responses of these materials. In closing, the simulation can give the statistical average of the products final mechanical response yet the printing process itself may cause variation away from this average. Minimizing variation between printed parts is a widely studied topic although this is not the focus of this study and therefore this section is concluded.

Copyright© Jordan Garcia, 2023.

Chapter 7 SUMMARY AND FUTURE WORKS

Literature has shown that 3D printed composites have highly anisotropic mechanical properties for both continuous fiber and short fiber composites. While there is no universally accepted method for calculating/predicting the mechanical properties of 3D printed parts, it has been proposed to use laminate composite theory which is already used for composite products. Ideally the choice of a manufacturing method should not alter the mechanical properties of a finished product; however, this is not the case with 3D printing. As a mold-less, pressure-less manufacturing method, 3D printing produces parts by depositing successive layers in an open environment. As a result, the 3D printed parts often contain "voids" and have poor adhesion between strands/layers, which lead to anisotropic structure and mechanical properties.

Starting with the analysis of comparing the printing orientation of premanufactured carbon fiber reinforced filament, the mechanical properties of 3D printed objects are examined. The 3D printed sample results from chapter 3 show that using the default slicing software settings the mechanical properties can change not only due to which 3D printer is used but how the sample is oriented along the printing bed. The results also show that even the best samples obtained by 3D printing methods fail to meet the mechanical properties of samples produced by a more conventional compression molding technique.

The analysis then continued with looking at the dynamic properties of 3D printed composites. This included printing significantly larger samples and attaching a load cell. The vibrational data was analyzed and the modal frequencies are recorded. The data showed that the direction of the extruded strands altered the modal frequencies even for a sample with the same geometry. Further implying that the fiber directions significantly influence the mechanical properties of a 3D printed part, for both the static and dynamic loading types. With the direction of the extruded strands affecting

the mechanical properties, the composition of these strands is also shown to affect the mechanical properties of 3D printed composites. For commercially available fiber reinforced filaments, it was found through microscopic analysis that the fiber content stated by the manufacturer is not very accurate. In order to apply CLCT the fiber volume fraction and aspect ratio need to be known for the necessary equations. This lead to the creation of custom filament with the desired fiber content and geometry. Using this custom filament it was observed that the fiber content did result in more brittle behavior in the 3D printed composites. The Halpin-Tsai model is used to predict the mechanical behavior of short fiber reinforced composites and compared to short fiber 3D printed composites. When the theoretical results were compared to the experimental results a correlation is noticeable. These results however do have anomalies present and the longer aspect ratio samples tended to have higher variance in results.

Finally the mechanical properties of continuous fiber composites are examined. The continuous fiber samples showed that the orientation of the fibers had an enormous effect on the mechanical properties of the 3D printed composite. The 0 degree orientation significantly out performed the other fiber orientations with a drastic drop in Young's modulus even with slight misalignment in fiber direction. This did however result in very brittle responses which may not be preferable. Then using experimental data from simple testing methods to fill in information not given by the manufacturer, CLCT is applied using the simulation software ANSYS WORKBENCH. With the ACP settings and test values inputted into ANSYS workbench, more complex geometries and more abstract orientation combinations can be simulated without the need for further sample/material testing. The results showed considerable correlation for each orientation and can be an accurate predicting method for 3D printed continuous fiber composites.

Overall 3D printing for composites still has many other variables and artifacts that need to be investigated for more complex applications before a universal method

is accepted; however, this paper proposes a method to use already existing methods for defining composites currently used for both research and industry purposes. Future works are planned to further capture these variables and apply them in 3D printed composites. These variables include investigating the effect of fiber in non-solid infill patterns. Often a solid part with 100% infill may not be the most desired manufacturing method, and in its current state CLCT would need further refinement to better capture these types of composites. Sandwich composites which consist of multiple layers of different materials are also produced and the current model has only been used for single-material purposes. Repeating the testing and analysis for multi-material composites is a future work which can help further the design and production of these types of 3D printed composite materials.

Copyright© Jordan Garcia, 2023.

Appendix

Traditional 3D printer extrusion systems are not capable of producing products filled with continuous fibers. To manufacture 3D printed samples that use a continuous strand of carbon fiber, the extruding mechanism needs to be modified. In order to design a modification to fit most 3D printing applications, an investigation into the main components of the extruder is conducted. Beginning from the bottom of the extruder assembly is the print nozzle, heat block, heat break and heat sink. The print nozzle is the narrow exit pathway for the extruded filament to lay on the print bed (Figure A.1). The heat block is used to hold the heating element and thermistor in the extruder assembly (Figure A.1). The heating element is a high-temperature resistive heating element that causes the heat block to reach a temperature capable of turning the polymer material molten. The thermistor measures the temperature and controls the voltage sent to the heating element to maintain a constant temperature. The two are secured in the pre-cut channels and held in place via setscrews. The heat break is a threaded extension of the heat block used to create a thermal barrier between the molten material in the extruder nozzle and the polymer filamnet being fed into the system. The extruder system depends on the stiffness of the polymer filament to push the molten material out of the nozzle; if the filament was entirely molten this would cause the material to pool itself in the assembly and seek other exits to relieve the pressure. By keeping the entry to the extruder assembly relatively cold, the polymer material only remains molten at the end of the assembly. This is why the heat break (Figure A.2) is attached to the heat sink ensuring the entry remains at a lower temperature than the nozzle. The final assembly of all the components can be seen in Figure A.3.

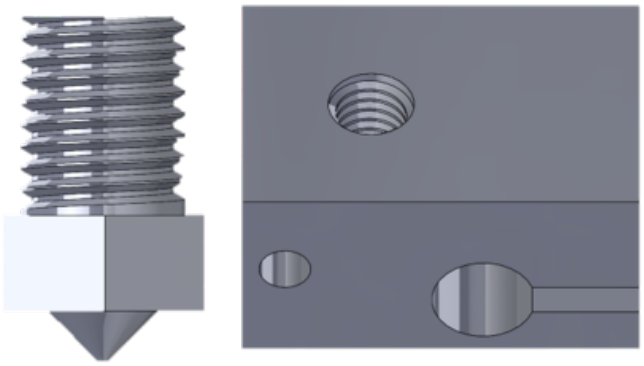

Figure A.1: CAD representation of the extruder nozzle (Left) and heat block (Right) of the extruder assembly.

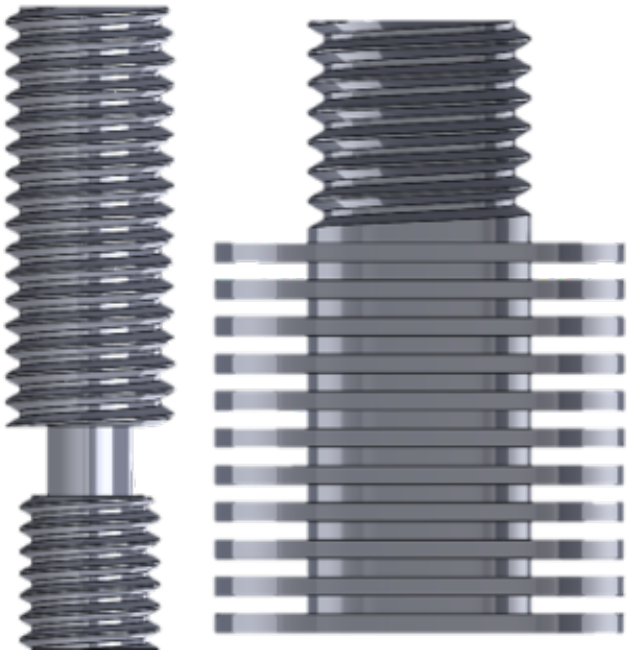

Figure A.2: CAD representation of the heat break (left) and heat sink (Right) of the extruder assembly.

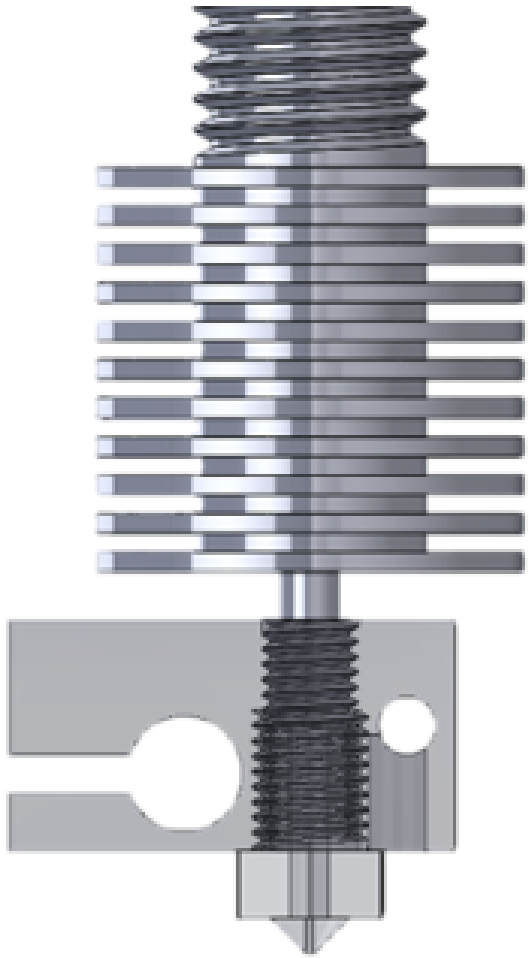

Figure A.3: CAD assembly of an E3D extruder assembly

By observing the assembly and understanding the function of the components, it was determined that any modifications to the assembly need to be made from the heat break above. As the lower assembly contains a pool of molten polymer, any modification to this section would cause the material to seep through any cracks or defects caused by the modifications. Due to the limitations, a passive gravity and friction-controlled system is implemented by inserting the carbon strands directly into the extruder assembly via a 22-gauge hypodermic needle (Figure A.4). The needle would be used as a guide for the continuous fiber strands to travel into the extruder assembly into the pool of molten polymer. This would cause the continuous strand to be extruded along with the polymer material when the driving filament pushes

the material through. To implement this, a milling machine was used to drill a small hole through the heat sink into the heat block and heat break to allow the needle to be inserted. This method involved the least amount of modification to the extruder assembly and allow the continuous fiber to be fed into the assembly (Figure A.5). With the reinforcing fiber being introduced into the extruded material, the nozzle tip was expanded via drilling to allow the same amount of polymer to be extruded as in the polymer only system.

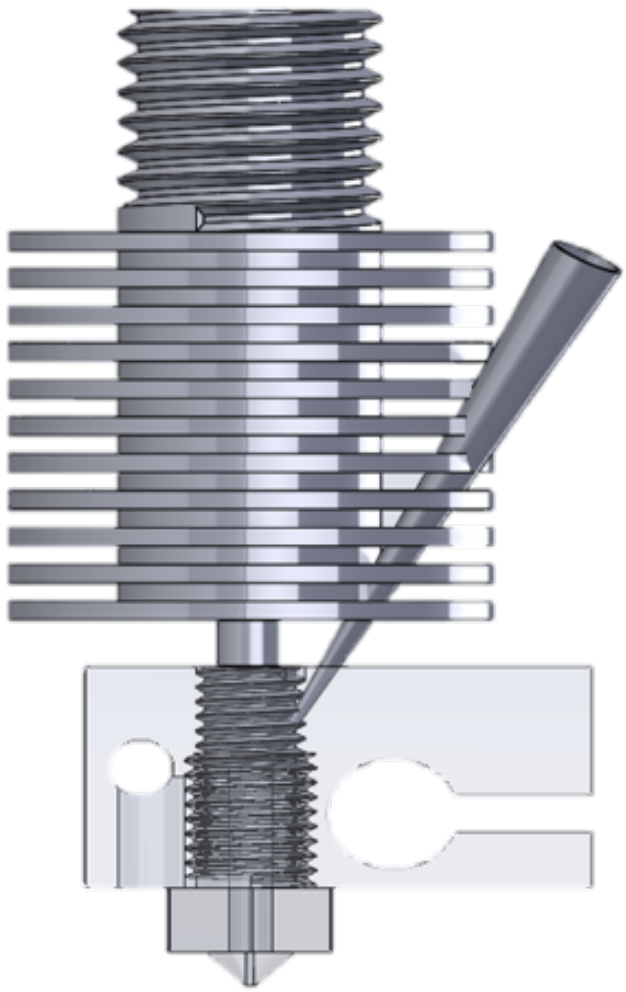

Figure A.4: CAD assembly of modified E3D extruder assembly with a continuous fiber injector for coaxial extrusion used for planning needle placement before machining existing assembly

Figure A.5: Machined extruder assembly with angled injection needle for continuous fiber extrusion for coaxially extruded composites

With hardware modifications made to the printer, it is logical that the software of the printer is also going to need to be modified to accommodate its new functionality. First the placement of the strands was modified to accommodate for the new extruding diameter, and the speed of the process was slowed to ensure more predictable friction/viscus force interactions. To accommodate for the new nozzle diameter and fiber extrusion, the slicing software parameters were modified accordingly and its movements were reduced to minimize opportunities for the fiber to shear. The G-

code of the initial printing script was modified to remove priming actions and instead a leveling code was added to assist in the bed leveling to minimize errors.

For mechanical testing, the same rectangular bending specimens used for the short fiber composites were used in the continuous fiber composites. White ABS 3D printer filament is being used to assist in differentiating the carbon fiber optically and should have no affect on the mechanical response of the samples. This assisted in seeing the path taken by the dark continuous fiber inside the 3D printed pat (Figure A.6). These samples were produced with an oriented infill for directional support and an outside shell to assist with adhesion of the first layer. While this system showed some promise it was ultimately left as future work due to the speed of the printing process being tremendously slower and the tendency to break the continuous fiber strand during the 3D printing process. The Markforge printer was used for the paper as a substitute.

Figure A.6: Coaxially extruded continuous carbon fiber samples from modified extruder with white ABS polymer filament.

Copyright© Jordan Garcia, 2023.

Bibliography

[1] Md Ali, Anuar Abilgaziyev, and D. Adair. 4d printing: a critical review of current developments, and future prospects. *The International Journal of Advanced Manufacturing Technology*, 105:1–17, 11 2019.

[2] Ankit Gupta, Ismail Fidan, Seymur Hasanov, and Aslan Nasirov. Processing, mechanical characterization, and micrography of 3d-printed short carbon fiber reinforced polycarbonate polymer matrix composite material. *The International Journal of Advanced Manufacturing Technology*, 107:3185–3205, 2020.

[3] Jun Wang, Bin Yang, Xiang Lin, Lei Gao, Tao Liu, Yonglai Lu, and Runguo Wang. Research of tpu materials for 3d printing aiming at non-pneumatic tires by fdm method. *Polymers*, 12(11):2492, 2020.

[4] Mahdi Mohammadizadeh and Ismail Fidan. Tensile performance of 3d-printed continuous fiber-reinforced nylon composites. *Journal of Manufacturing and Materials Processing*, 5(3):68, 2021.

[5] Chia Hung Yeh, Chia Man Chou, and Chien Pang Lin. Design of experiment for optimization of 3d printing parameters of base plate structures in colostomy bag for newborns. *Journal of Industrial and Production Engineering*, 38(7):523–535, 2021.

[6] Lu Y C, Pilla S, and Warrendale S. Design of automotive composite. *SAE International*, 2014.

[7] Strong A. *Fundamentals of Composites Manufacturing*. Society of Manufacturing Engineers,southfield,Mi., 1989.

[8] Syed F. Future of manufacturing - additive manufacturing. *International Journal of Modern Engineering Research*, 5:1–7, 2015.

[9] Kamble P, Khoje S, and Lele A. Recent developments in 3d printing technologies: Review. *Second International Conference on Intelligent Computing and Control Systems*, 2018.

[10] Baily M and Boworth B. Us manufacturing: Understanding its past and its potential future. *Journal of Economic Perspectives*, 28:3–26, 2014.

[11] Huang S, Liu P, Mokasdar A, and Hou L. Additive manufacturing and its societal impact: A literature review. *International Journal of Advanced Manufacturing Technology*, 67:667–668, 2013.

[12] Thomas Campbell, Christopher Williams, Olga Ivanova, and Banning Garrett. Could 3d printing change the world? technologies, potential, and implications of additive manufacturing. *Technology & Innovation*, 2011.

[13] van den Berg Bibi, van der Hof Simone, and Kosta Eleni. *3D Printing Legal, Philosophical and Economic Dimensions*. 1st edition, 2016.

[14] Nadiyapara Hitesh Hirjibhai and Sarang Pande. A review of variable slicing in fused deposition modeling. *Journal of The Institution of Engineers (India) Series C*, 98(3):387–393, 2016.

[15] Vito Borreli. Kinematic and dynamic analysis of a machine for additive manufacturing. 2018.

[16] Lechowicz P, Koszalka L, Pozniak-Koszalka I, and Kasprzak A. Path optimization in 3d printer: Algorithms and experimentation system. *4th International Symposium on Computational and Business Intelligence*, 2016.

[17] Koda S and Tanaka H. Direct g-code manipulation for 3d material weaving. *Biosensors, Info-Tech Sensors and 3D Systems*, 10167, 2017.

[18] Marlon Cunico, MAchado Wesley, and De Carvalho Jonas. New additive manufacturing technology based on. *2nd Intl. Conf. on Progress in Additive Manufacturing*, 2016.

[19] Ivey Marcus, W. Melenka Garrett, and Ayranci Jason, P. Carey & Cagri. Characterizing short-fiber-reinforced composites produced using additive manufacturing. *Advanced Manufacturing: Polymer & Composites Science*, 3(3), 2012.

[20] Jae-Won Choi, Francisco Medina, Chiyen Kim, David Espalin, David Rodriguez, Brent Stucker, and Ryan Wicker. Development of a mobile fused deposition modeling system with enhanced manufacturing flexibility. *Journal of Materials Processing Technology*, 211(3):424–432, 2011.

[21] Hitesh Hirjibhai Nadiyapara and Sarang Pande. A Review of Variable Slicing in Fused Deposition Modeling. *Journal of The Institution of Engineers (India): Series C*, 98(3):387–393, June 2017.

[22] Zhenzhen Quan, Amanda Wu, Michael Keefe, Xiaohong Qin, Jianyong Yu, Jonghwan Suhr, Joon-Hyung Byun, Byung-Sun Kim, and Tsu-Wei Chou. Additive manufacturing of multi-directional preforms for composites: opportunities and challenges. *Materials Today*, 18(9):503–512, 2015.

[23] J.W Gooch. *Encyclopedic Dictionary of Polymers*. Springer New York, 2011.

[24] P.J. Bartolo and E. Lenz. Computer simulation of stereolithographic curing reactions: Phenomenological versus mechanistic approaches. *CIRP Annals - Manufacturing Technology*, 55:221–225, 12 2006.

[25] Lan Li, Xinchang Zhang, and Frank Liou. Experimental and numerical investigation in directed energy deposition for component repair. *Materials*, 14(6), 2021.

[26] S M Fijul Kabir, Kavita Mathur, and Abdel-Fattah M. Seyam. A critical review on 3d printed continuous fiber-reinforced composites: History, mechanism, materials and properties. *Composite Structures*, 232:111476, 2020.

[27] Elasto-plastic finite element modeling of short carbon fiber reinforced 3d printed acrylonitrile butadiene styrene composites. *ICME-Based Design and Optimization for Additive Manufacturing*, 72:475–484, 2020.

[28] Zengguang Liu, Yanqing Wang, Beicheng Wu, Chunzhi Cui, Yu Guo, and Cheng Yan. A critical review of fused deposition modeling 3d printing technology in manufacturing polylactic acid parts. *The International Journal of Advanced Manufacturing Technology*, 102:2877–2889, 2019.

[29] Editor. *The history of 3D printing.* Uncategorised 2013 [cited 2019 January 27]; Available from: https://www.redorbit.com/reference/the-history-of-3d-printing/, 2019.

[30] Zhanghao Hou, Xiaoyong Tian, Ziqi Zheng, Junkang Zhang, Lu Zhe, Dichen Li, Andrei V Malakhov, and Alexander N Polilov. A constitutive model for 3d printed continuous fiber reinforced composite structures with variable fiber content. *Composites Part B: Engineering*, 189:107893, 2020.

[31] Ismail Fidan, Astrit Imeri, Ankit Gupta, Seymur Hasanov, Aslan Nasirov, Amy Elliott, Frank Alifui-Segbaya, and Norimichi Nanami. The trends and challenges of fiber reinforced additive manufacturing. *The International Journal of Advanced Manufacturing Technology*, 102:1801–1818, 2019.

[32] Madhukar Somireddy and Aleksander Czekanski. Computational modeling of constitutive behaviour of 3d printed composite structures. *Journal of Materials Research and Technology*, 11, 02 2021.

[33] Arthur Sebert, Jared W Nelson, and Gregoire Bertacco. Anisotropic mechanical performance of 3d printed polymers. *Advanced Materials-Tech Connect Briefs*, 2017:170, 2017.

[34] T.G. Yashas Gowda, M.R. Sanjay, K. Subrahmanya Bhat, P. Madhu, P. Senthamaraikannan, and B. Yogesha. Polymer matrix-natural fiber composites: An overview. *Cogent Engineering*, 5(1):1446667, 2018.

[35] Lourens G Blok, Marco L Longana, H Yu, and Ben KS Woods. An investigation into 3d printing of fibre reinforced thermoplastic composites. *Additive Manufacturing*, 22:176–186, 2018.

[36] Cagri Oztan, Ryan Karkkainen, Mauro Fittipaldi, Garrett Nygren, Luke Roberson, Michael Lane, and Emrah Celik. Microstructure and mechanical properties of three dimensional-printed continuous fiber composites. *Journal of Composite Materials*, 53(2):271–280, 2019.

[37] Xiaoyong Tian, Tengfei Liu, Chuncheng Yang, Qingrui Wang, and Dichen Li. Interface and performance of 3d printed continuous carbon fiber reinforced pla composites. *Composites Part A: Applied Science and Manufacturing*, 88:198–205, 2016.

[38] Meng Luo, Xiaoyong Tian, Junfan Shang, Weijun Zhu, Dichen Li, and Yingjie Qin. Impregnation and interlayer bonding behaviours of 3d-printed continuous carbon-fiber-reinforced poly-ether-ether-ketone composites. *Composites Part A: Applied Science and Manufacturing*, 121:130–138, 2019.

[39] Madhukar Somireddy and Aleksander Czekanski. Anisotropic material behavior of 3d printed composite structures – material extrusion additive manufacturing. *Materials Design*, 195:108953, 07 2020.

[40] Juan Naranjo-Lozada, Horacio Ahuett-Garza, Pedro Orta-Castañón, Wilco MH Verbeeten, and Daniel Sáiz-González. Tensile properties and failure behavior of

chopped and continuous carbon fiber composites produced by additive manufacturing. *Additive Manufacturing*, 26:227–241, 2019.

[41] Nekoda van de Werken, Joel Hurley, Pouria Khanbolouki, Ali N Sarvestani, Ali Y Tamijani, and Mehran Tehrani. Design considerations and modeling of fiber reinforced 3d printed parts. *Composites Part B: Engineering*, 160:684–692, 2019.

[42] Haider Al Abadi, Huu-Tai Thai, Vidal Paton-Cole, and VI Patel. Elastic properties of 3d printed fibre-reinforced structures. *Composite Structures*, 193:8–18, 2018.

[43] M. Somireddy and A. Czekanski. Anisotropic material behavior of 3d printed composite structures – material extrusion additive manufacturing. *Materials Design*, 195:108953, 2020.

[44] Odel l & S Roundy & P.K Wright S.H, Ahn & M. Montero & D. Anisotropic material properties of fused deposition modeling abs. *Rapid Prototyping Journal*, 8, 2002.

[45] Torrado A and Roberson D. Failure analysis and anisotropy evaluation of 3d-printed tensile test specimens of different geometries and print raster patterns. *Journal of Failure Analysis and Prevention*, 16, 2016.

[46] Said O, Foyos J, Noorani R, Mandelson M, Marloth R, and Pregger B. Effect of layer orientation on mechanical properties of rapid prototyped samples. *Materials and Manufacturing Processes*, 15, 2000.

[47] Li L, Bellehumeur Q, Sunand C, and Gu P. Composite modeling and analysis for fabrication of fdm prototypes with locally controlled properties. *Journal of Manufacturing Processes*, 4, 2002.

[48] Gao W, Zhang Y, Ramanujana D, Ramania K, Chen Y, Williams C, Wang L, Charlie C, Yung S, Zhang S, and Pablo Z.D. The status, challenges, and future of additive manufacturing in engineering. *Computer-Aided Design*, 69, 2015.

[49] Baumann F, Bugdayci H, Grunert J, Keller F, and Roller D. Influence of slicing tools on quality of 3d printed parts. *Computer-Aided Design and Applications*, 13, 2016.

[50] Sukindar N, Baharudin B, Jaafer C, and Ismail M. Slicer method comparison using open-source 3d printer. *IOP conference series*, 114, 2018.

[51] Grzegorz Ćwikła, Cezary Grabowik, Krzysztof Kalinowski, Iwona Paprocka, and Piotr Ociepka. The influence of printing parameters on selected mechanical properties of fdm/fff 3d-printed parts. In *IOP conference series: materials science and engineering*, volume 227, page 012033. IOP Publishing, 2017.

[52] Hassan Rezayat, W Zhou, Akawut Siriruk, D Penumadu, and SS Babu. Structure–mechanical property relationship in fused deposition modelling. *Materials Science and Technology*, 31(8):895–903, 2015.

[53] Christian Lubombo and Michel A Huneault. Effect of infill patterns on the mechanical performance of lightweight 3d-printed cellular pla parts. *Materials Today Communications*, 17:214–228, 2018.

[54] Mohammad Azeeb Mazlan, Mohamad Azizi Anas, Nor Aiman Nor Izmin, and Abdul Halim Abdullah. Effects of infill density, wall perimeter and layer height in fabricating 3d printing products. *Materials*, 16(2):695, 2023.

[55] Garcia Jordan. Design and process of 3d-printed parts using composite theory. Master's thesis, University of Kentucky, 2019.

[56] Samson Dare Oguntuyi, Kasongo Nyembwe, Mxolisi Brendon Shongwe, and Tajudeen Mojisola. Challenges and recent progress on the application of rapid

sand casting for part production: a review. *The International Journal of Advanced Manufacturing Technology*, pages 1–16, 2023.

[57] Roberson David A. Torrado, Angel R. Failure analysis and anisotropy evaluation of 3d-printed tensile test specimens of different geometries and print raster patterns. *Journal of Failure Analysis and Prevention*, 16:154–164, 2016.

[58] Dan Odell Shad Roundy Paul K. Wright Sung-Hoon Ahn, Michael Montero. Anisotropic material properties of fused deposition modeling abs. *Rapid Prototyping Journal*, 8:248–257, 2002.

[59] K. Gnanasekaran, T. Heijmans, S. van Bennekom, H. Woldhuis, S. Wijnia, G. de With, and H. Friedrich. 3d printing of cnt- and graphene-based conductive polymer nanocomposites by fused deposition modeling. *Applied Materials Today*, 9:21–28, 2017.

[60] Piotr Lechowicz, Leszek Koszalka, Iwona Pozniak-Koszalka, and Andrzej Kasprzak. Path optimization in 3d printer: Algorithms and experimentation system. *2016 4th International Symposium on Computational and Business Intelligence (ISCBI)*, pages 137–142, 2016.

[61] J-M Friedt and E Carry. Introduction to the quartz tuning fork. *American Journal of Physics*, 75(5):415–422, 2007.

[62] I.M. Daniel and O. Ishai. *Engineering Mechanics of Composite Materials*. Engineering Mechanics of Composite Materials. Oxford University Press, 1994.

[63] J-M Friedt and E Carry. Introduction to the quartz tuning fork. *American Journal of Physics*, 75(5):415–422, 2007.

[64] Chuncheng Yang, Xiaoyong Tian, Tengfei Liu, Yi Cao, and Dichen Li. 3d printing for continuous fiber reinforced thermoplastic composites: mechanism and performance. *Rapid Prototyping Journal*, 23(1):209–215, 2017.

[65] Nashat Nawafleh and Emrah Celik. Additive manufacturing of short fiber reinforced thermoset composites with unprecedented mechanical performance. *Additive Manufacturing*, 33:101109, 2020.

[66] Peter J Hine, Hans Rudolf Lusti, and Andrei A Gusev. Numerical simulation of the effects of volume fraction, aspect ratio and fibre length distribution on the elastic and thermoelastic properties of short fibre composites. *Composites science and technology*, 62(10-11):1445–1453, 2002.

[67] B. Möginger and P. Eyerer. Determination of the weighting function g(i,r,vf) for fibre orientation analysis of short fibre-reinforced composites. *Composites*, 22(5):394–399, 1991.

[68] C Pascual-González, M Iragi, A Fernández, JP Fernández-Blázquez, L Aretxabaleta, and CS Lopes. An approach to analyse the factors behind the micromechanical response of 3d-printed composites. *Composites Part B: Engineering*, 186:107820, 2020.

[69] S.H. Masood. Advances in fused deposition modeling in comprehensive materials processing. In *Comprehensive Materials Processing*, pages 69–91. Elsevier, 2014.

[70] Carbonx abs+cf high-performance carbon fiber reinforced abs filament. `https://www.3dxtech.com/product/carbonx-abs-cf/`. Accessed: 2022-12-12.

[71] Francis I. Baratta, William T. Matthews, George D. Quinn, Charles L. Tucker, III, and Erwin Liang. Errors associated with flexure testing of brittle. Technical report, Army Lab Command, Watertown, MA Material Technology Lab.

[72] G Chabaud, M Castro, C Denoual, and A Le Duigou. Hygromechanical properties of 3d printed continuous carbon and glass fibre reinforced polyamide composite for outdoor structural applications. *Additive Manufacturing*, 26:94–105, 2019.

[73] G.P. Carman and K.L. Reifsnider. Micromechanics of short-fiber composites. *Composites Science and Technology*, 43(2):137–146.

[74] R Pemberton, D Edser, and M Gower. Optimisation of acid digestion conditions for volume fraction measurements of hard to digest fibre-reinforced polymer composites. Technical Report MN 12, National Physical Laboratory, 2020.

[75] MAA Mohsin, Lorenzo Iannucci, and ES Greenhalgh. Fibre-volume-fraction measurement of carbon fibre reinforced thermoplastic composites using thermogravimetric analysis. *Heliyon*, 5(1):e01132, 2019.

[76] G.D. Sims and W.R. Broughton. Glass fiber reinforced plastics—properties. In Anthony Kelly and Carl Zweben, editors, *Comprehensive Composite Materials*, chapter 2.05. Pergamon.

[77] P Kulkarni and D Dutta. Deposition strategies and resulting part stiffnesses in fused deposition modeling. *ASME Journal of Manufacturing Science Engineering*, 121(1):93–103, 1999.

[78] Brett G Compton and Jennifer A Lewis. 3d-printing of lightweight cellular composites. *Advanced materials*, 26(34):5930–5935, 2014.

[79] M. Samykano, S.K. Selvamani, and K. Kadirgama. Mechanical property of fdm printed abs: influence of printing parameters. *Int. J. Adv. Manuf. Tech.*, 102:2779–2796.

[80] Ke Chen, Liguo Yu, Yonghui Cui, Mingyin Jia, and Kai Pan. Optimization of printing parameters of 3d-printed continuous glass fiber reinforced polylactic acid composites. *Thin-Walled Structures*, 164(107717).

[81] Ahmed El Moumen, Mostapha Tarfaoui, and Khalid Lafdi. Modelling of the temperature and residual stress fields during 3d printing of polymer composites. *The International Journal of Advanced Manufacturing Technology*, 104:1661–1676, 2019.

[82] Refractory glass and ohter ceramic materials. In *Annual book of ASTM standards*, chapter 17. American Society for Testing and Materials, 1979.

[83] JC Halpin Affdl and JL Kardos. The halpin-tsai equations: a review. *Polymer Engineering & Science*, 16(5):344–352, 1976.

[84] Charles L Tucker III and Erwin Liang. Stiffness predictions for unidirectional short-fiber composites: review and evaluation. *Composites science and technology*, 59(5):655–671, 1999.

[85] Continuous carbon fiber - high strength 3d printing material by markforged. `https://markforged.com/materials/continuous-fibers/continuous-carbon-fiber/`. Accessed: 2023-01-08.

Curriculum Vitae

JORDAN GARCIA

WORK EXPERIENCE

Engineering Technology Instructor
Murray State University
January 2022 – Present | Murray, Ky

Teaching Assistant
University of Kentucky First Year Engineering
August 2019 – January 2022 | Lexington, KY

Graduate Research Assistant
University of Kentucky Paducah Campus
July 2022 – August 2022 | Paducah, KY

EDUCATION

Ph.D. Mechanical Engineering
University of Kentucky
(In Progress)

Dissertation title: Laminar Composite Theory Applied to 3D Printed Composites using Customizable Carbon Ratios
Y. Charles Lu, research advisor

M.S. Mechanical Engineering
University of Kentucky
August 2018 – September 2019

Thesis title: Design and Process of 3D Printed Parts using Composite Theory

B.S. Mechanical Engineering
University of Kentucky Paducah Campus
August 2014 – May 2018

Certificate in Exploratory Machining
West Kentucky Community and Technical College
Sept 2012 – May 2016

PUBLICATIONS

Journal Articles

- Garcia, J., Harper, R., & Lu, Y. (2022). Anisotropic material behaviors of three-dimensional printed carbon-fiber polymer composites with open-source printers. *ASME Journal of Manufacturing Science and Engineering*, *144*, 031014:1–6.
- Garcia, J., & Lu, Y. (2022). Anisotropic dynamic mechanical properties of 3d printed carbon-fiber composites. *SAE International Journal of Advances and Current Practices in Mobility-V131-99EJ*, *4*, 1610–1618.
- Garcia, J., Harper, R., Bradely, C., Schmidt, J., & Lu, Y. (2020). Evaluations of mechanical properties of ABS parts from open-source 3d printers and conventional manufacturing. *SAE International Journal of Advances and Current Practices in Mobility*, *2*, 1314–1321.